NASA TM X-758

TECHNICAL MEMORANDUM

X-758

STABILITY AND CONTROL CHARACTERISTICS OF A 0.0667-SCALE MODEL OF THE FINAL VERSION OF THE NORTH AMERICAN X-15 RESEARCH AIRPLANE (CONFIGURATION 3) AT TRANSONIC SPEEDS

By Robert S. Osborne

Langley Research Center
Langley Station, Hampton, Va.

NATIONAL AERONAUTICS AND SPACE ADMINISTRATION
WASHINGTON
April 1963

NATIONAL AERONAUTICS AND SPACE ADMINISTRATION

TECHNICAL MEMORANDUM X-758

STABILITY AND CONTROL CHARACTERISTICS OF A 0.0667-SCALE MODEL OF THE FINAL VERSION OF THE NORTH AMERICAN X-15 RESEARCH AIRPLANE (CONFIGURATION 3) AT TRANSONIC SPEEDS

By Robert S. Osborne

SUMMARY

In order to determine its static longitudinal and lateral-directional stability and control characteristics at transonic speeds, a 0.0667-scale force model of configuration 3 of the North American X-15 research airplane has been tested in the Langley 8-foot transonic pressure tunnel. The test range included Mach numbers from 0.60 to 1.18, angles of attack from -20° to 20°, and angles of sideslip of -5.1° and 0°. The results of the investigation including a summary of some of the important stability and control parameters are presented without analysis.

INTRODUCTION

As part of the wind-tunnel program required for the development of the North American X-15 research airplane, a 0.0667-scale force model of the final version of the X-15 (configuration 3) has been tested in the Langley 8-foot transonic pressure tunnel in order to determine its static stability and control characteristics at transonic speeds. Tests of this model at Mach numbers from 2.29 to 4.65 are reported in reference 1. The results of pressure-distribution tests of a model of a configuration nearly identical to that of configuration 3 at Mach numbers from 0.60 to 4.65 are presented in references 2 and 3. Other tests of force models approximating configuration 3 are reported in references 4 to 7. Tests of a force model of an earlier version of the X-15 (configuration 1) in the Langley 8-foot transonic pressure tunnel are reported in reference 8.

The model was tested at Mach numbers from 0.60 to 1.18, at angles of attack from -20° to 20°, and at angles of sideslip of -5.1° and 0°. Drag, static longitudinal stability, and static lateral-directional stability were determined; the effectiveness of the horizontal tail as a pitch and roll control and the vertical tails as a yaw control was measured; and the effects of opening the speed brakes on drag and static stability were obtained. The results of this

investigation including a summary of some of the important stability and control parameters are presented herein without analysis.

SYMBOLS

Longitudinal data are presented about the stability axes and lateral-directional data are presented about the body axes for a center-of-gravity location of 20 percent of the wing mean aerodynamic chord.

b	wing span, in.
C_D	drag coefficient, D/qS
$C_{D,o}$	drag coefficient at zero lift
C_L	lift coefficient, L/qS
$C_{L(L/D)_{max}}$	lift coefficient for maximum lift-drag ratio
$C_{L,t}$	trim lift coefficient
$\frac{\partial C_{L,t}}{\partial \delta_e}$	trim lift effectiveness parameter, per deg
C_{L_α}	lift-curve slope, per deg
C_l	rolling-moment coefficient, M_X/qSb
C_{l_β}	effective dihedral parameter, $\frac{\partial C_l}{\partial \beta}$, per deg
$C_{l_{\delta_a}}$	rolling moment due to differential deflection of horizontal tail, $\frac{\partial C_l}{\partial \delta_a}$, per deg
$C_{l_{\delta_v}}$	rolling moment due to vertical-tail deflection, $\frac{\partial C_l}{\partial \delta_v}$, per deg
C_m	pitching-moment coefficient, $M_Y/qS\bar{c}$
$C_{m_{C_L}}$	static longitudinal stability parameter, $\frac{\partial C_m}{\partial C_L}$

$C_{m_{\delta_e}}$ pitch effectiveness parameter at constant lift coefficient, $\frac{\partial C_m}{\partial \delta_e}$, per deg

C_n yawing-moment coefficient, M_Z/qSb

C_{n_β} static directional stability parameter, $\frac{\partial C_n}{\partial \beta}$, per deg

$C_{n_{\delta_a}}$ yawing moment due to differential deflection of horizontal tail, $\frac{\partial C_n}{\partial \delta_a}$, per deg

$C_{n_{\delta_v}}$ yawing moment due to vertical-tail deflection, $\frac{\partial C_n}{\partial \delta_v}$, per deg

$C_{p,b}$ base pressure coefficient, $\frac{p_b - p}{q}$

C_Y lateral-force coefficient, Y/qS

$\bar{c}$ wing mean aerodynamic chord, in.

D force along X_S-axis, positive rearward, lb

F_Y lateral force, lb

L lift, lb

$(L/D)_{max}$ maximum lift-drag ratio

M free-stream Mach number

M_X moment about X-axis, in-lb

M_Y moment about Y-axis, in-lb

M_Z moment about Z-axis, in-lb

p_b static pressure at model base, lb/sq ft

p free-stream static pressure, lb/sq ft

q free-stream dynamic pressure, lb/sq ft

R	Reynolds number
S	total wing area, sq ft
X,Y,Z	body axes
X_S,Y_S,Z_S	stability axes
α	angle of attack of fuselage center line, deg
β	angle of sideslip, deg
δ_a	differential deflection of horizontal tail when used as roll control, positive when left-hand surface has more positive deflection, (trailing edge down), deg
δ_e	deflection of horizontal tail when used as pitch control (taken as average of left- and right-hand surface deflections and positive when trailing edge is down), deg
δ_v	deflection of upper and lower vertical-tail surfaces, positive when trailing edge is to left, deg

APPARATUS AND TESTS

Model

The X-15 is a rocket-powered research airplane designed for hypersonic speeds at very high altitudes. It employs a 5-percent-thick low-aspect-ratio trapezoidal wing mounted in the midposition on a fuselage consisting of a body of revolution with large side fairings. The horizontal tail which has 45° sweepback of the quarter-chord line is all movable for pitch control and is deflected differentially for roll control. The outboard panels of the upper and lower vertical-tail surfaces are deflected for directional control; the inboard panels are fixed and contain the speed brakes.

The 0.0667-scale force model of the North American X-15 research airplane used in this investigation was supplied by the contractor and was of stainless-steel construction. Photographs of the model are presented in figure 1, and dimensional details are shown in figure 2 and table I.

The model represented configuration 3 of the X-15. Features that distinguish this configuration from configuration 1 (ref. 8) include an increased fuselage diameter, shortened fuselage side fairings, increased leading-edge radii on wing and horizontal tail, wing shifted forward 3.6 inches (full scale), horizontal tail shifted rearward 5.4 inches (full scale), a larger vertical tail having 10° full-wedge airfoil sections with the total exposed area distributed

about 55 percent above the fuselage and 45 percent below, and reduced speed-brake area. The contractor's code designation for the model tested was $B_4W_2X_{14}H_9V_{U_5}J_{U_2}V_{L_7}J_{L_2}$.

The movable portions of the upper and lower vertical tails and both horizontal-tail panels could be actuated remotely while the wind tunnel was in operation. The speed brakes were maintained in the closed position or were opened 35° relative to the closed position as indicated in figure 2. The speed-brake hinge lines were located at the speed-brake leading edges and had 0° sweepback.

Tunnel and Model Support

The tests were conducted in the Langley 8-foot transonic pressure tunnel which is a single-return rectangular slotted-throat wind tunnel having controls that allowed for the independent variation of Mach number, stagnation pressure, temperature, and humidity.

The model was attached to a sting support by an electrical strain-gage balance located inside the fuselage. The sting support was cylindrical for 2.4 base diameters downstream of the model base and had a diameter of 0.55 base diameter. At its downstream end, the sting was attached to an arc-shaped support strut which spanned the tunnel vertically. This support strut was rotated to obtain changes in angle of attack; the center of rotation of the system was near the model in order to minimize overall vertical motion of the model. Variations in angle of sideslip were obtained by insertion of properly angled couplings in the model support system.

Measurements and Accuracy

Model forces and moments were measured by a six-component internal strain-gage balance. They were converted by automatic electrical computing equipment to lift, drag, and pitching moment about the stability axes and to lateral force, yawing moment, and rolling moment about the body axes. (See fig. 3.) The center of gravity was located at 20 percent of the mean aerodynamic chord based on the total wing area. (See fig. 2.) At a Mach number of 1.0 and a dynamic pressure of 784 pounds per square foot, accuracies of the coefficients are estimated to be:

C_L	±0.01
C_D	±0.002
C_m	±0.002
C_l	±0.0005
C_n	±0.0005
C_Y	±0.005

The angle of attack was set to within ±0.1° by means of a pendulum-type attitude indicator located in the nose of the model. The angles of sideslip were determined to within ±0.2° by means of a calibration of sting and balance deflection with respect to model lateral force and yawing moment. Horizontal- and vertical-tail deflections were measured remotely by means of differential transformers attached to the control-surface linkages and are estimated to be accurate within ±0.2°. Speed-brake deflections are estimated to be accurate within ±0.1°.

The Mach number was determined within ±0.003 from a calibration with respect to the pressure in the chamber surrounding the slotted test section. Base pressure coefficients were determined from an average of measurements taken on the upper and lower portions of the base and are estimated to be accurate within ±0.005.

Tests

The complete model was tested with horizontal-tail deflections for pitch and roll control, with vertical-tail deflections for yaw control, and with the speed brakes open and closed. The model was also tested with the horizontal tail removed, with the lower vertical tail removed, and with both vertical tails removed. The detailed test program is indicated in table II.

The test range included Mach numbers from 0.60 to 1.18, angles of attack from -20° to 20°, and angles of sideslip of -5.1° and 0°. The tests were conducted at a tunnel stagnation pressure of approximately 1 atmosphere. The average test Reynolds number based on the wing mean aerodynamic chord varied from approximately 2.2×10^6 to 2.8×10^6 over the Mach number range. (See fig. 4.) For all tests, 0.1-inch-wide boundary-layer transition strips consisting of No. 120 carborundum grains were installed along the 10-percent-chord lines of the wing and tail surfaces and at 10 percent of the fuselage length.

Corrections

Tunnel-boundary interference at subsonic speeds is minimized by the slotted test section, and no corrections for this interference have been applied. No corrections are necessary for the effects of supersonic boundary-reflected disturbances since they are negligible for Mach numbers up to approximately 1.03 (ref. 9), and the reflected disturbances pass well downstream of the base of the model at a Mach number of 1.18.

With the use of the measured base pressure coefficients (shown for three configurations in fig. 5), the data presented have been adjusted to an assumed condition of free-stream static pressure acting over the base of the fuselage. No sting-interference corrections have been applied. However, as indicated from the results of reference 10, errors in the drag data due to the presence of the sting are estimated to be small and errors in the other coefficients are probably negligible.

RESULTS AND CONCLUSIONS

The results of an investigation of the stability and control characteristics of a 0.0667-scale model of the final version of the X-15 research airplane are presented in the following figures:

	Figures
Basic longitudinal data as functions of C_L	6 to 15
Basic lateral-directional data as functions of α	16 to 24
Longitudinal stability and control parameters	25 to 27
Drag and maximum lift-drag-ratio parameters	28
Lateral-directional stability and control parameters	29 to 33

A more detailed index of the results presented is shown in table II.

The data indicate that the configuration investigated has generally satisfactory static stability and control characteristics at the Mach numbers and angles of attack tested. Notable exceptions, however, include a region of neutral longitudinal stability at low negative angles of attack at Mach numbers from 0.60 to 0.95 and excessive positive dihedral at high angles of attack at Mach numbers above 0.60.

Langley Research Center,
National Aeronautics and Space Administration,
Langley Station, Hampton, Va., November 8, 1962.

REFERENCES

1. Franklin, Arthur E., and Lust, Robert M.: Investigation of the Aerodynamic Characteristics of a 0.067-Scale Model of the X-15 Airplane (Configuration 3) at Mach Numbers of 2.29, 2.98, and 4.65. NASA TM X-38, 1959.

2. Osborne, Robert S., and Stafford, Virginia C.: Basic Pressure Measurements On a 0.0667-Scale Model of the North American X-15 Research Airplane at Transonic Speeds. NASA TM X-344, 1960.

3. Hodge, B. Leon, and Burbank, Paige B.: Pressure Distribution of a 0.0667-Scale Model of the X-15 Airplane for an Angle-of-Attack Range of 0° to 28° at Mach Numbers of 2.30, 2.88, and 4.65. NASA TM X-275, 1960.

4. Lopez, Armando E., and Tinling, Bruce E.: The Static and Dynamic-Rotary Stability Derivatives at Subsonic Speeds of a Model of the X-15 Research Airplane. NACA RM A58F09, 1958.

5. Tunnell, Phillips J., and Latham, Eldon A.: The Static and Dynamic-Rotary Stability Derivatives of a Model of the X-15 Research Airplane at Mach Numbers From 1.55 to 3.50. NASA MEMO 12-23-58A, 1959.

6. Dunning, Robert W.: The Control Characteristics of Two Preliminary Models of the X-15 Research Airplane at Mach Numbers of 2.98 and 4.01. NASA TM X-212, 1960.

7. Penland, Jim A., and Fetterman, David E., Jr.: Static Longitudinal, Directional, and Lateral Stability and Control Data at a Mach Number of 6.83 of the Final Configuration of the X-15 Research Airplane. NASA TM X-236, 1960.

8. Osborne, Robert S.: Aerodynamic Characteristics of a 0.0667-Scale Model of the North American X-15 Research Airplane at Transonic Speeds. NASA TM X-24, 1959.

9. Wright, Ray H., Ritchie, Virgil S., and Pearson, Albin O.: Characteristics of the Langley 8-Foot Transonic Tunnel With Slotted Test Section. NACA Rep. 1389, 1958. (Supersedes NACA RM L51H10 by Wright and Ritchie and RM L51K14 by Ritchie and Pearson.)

10. Osborne, Robert S.: High-Speed Wind-Tunnel Investigation of the Longitudinal Stability and Control Characteristics of a $\frac{1}{16}$-Scale Model of the D-558-2 Research Airplane at High Subsonic Mach Numbers and at a Mach Number of 1.2. NACA RM L9C04, 1949.

TABLE I.- DIMENSIONS OF 0.0667-SCALE MODEL OF CONFIGURATION 3 OF NORTH AMERICAN X-15 RESEARCH AIRPLANE

Wing:	
Airfoil section	Modified NACA 66-005
Total area, sq in.	127.728
Exposed area, sq in.	66.816
Total span, in.	17.87
Exposed span, in.	11.968
Total aspect ratio	2.50
Exposed aspect ratio	2.15
Leading-edge sweepback, deg	36.75
Quarter-chord-line sweepback, deg	25.64
Trailing-edge sweepforward, deg	17.75
Root chord at center line, in.	11.914
Exposed root chord, in.	8.8
Tip chord, in.	2.383
Total taper ratio	0.20
Exposed taper ratio	0.27
Mean aerodynamic chord based on total area, in.	8.207
Longitudinal distance from fuselage nose to total wing 0.20$\bar{c}$, in.	22.76
Dihedral, deg	0
Incidence, deg	0
Horizontal tail (in plane of surface):	
Airfoil section	Modified NACA 66-005
Total area, sq in.	73.850
Exposed area, sq in.	32.832
Total span, in.	14.978
Exposed span, in.	9.008
Exposed aspect ratio	2.48
Leading-edge sweepback, deg	50.58
Quarter-chord-line sweepback, deg	45
Trailing-edge sweepback, deg	19.28
Root chord at center line, in.	8.175
Exposed root chord, in.	5.6
Tip chord, in.	1.686
Exposed taper ratio	0.30
Mean aerodynamic chord based on exposed area, in.	3.986
Hinge line, percent exposed $\bar{c}$	25
Longitudinal distance from total wing 0.20$\bar{c}$ to exposed tail 0.25$\bar{c}$, in.	12.461
Dihedral, deg	-15
Upper vertical tail (exposed panel):	
Airfoil section	10° wedge
Area, sq in.	26.075
Span, in.	3.669
Aspect ratio	0.52
Leading-edge sweepback, deg	30
Trailing-edge sweepback, deg	0

TABLE I.- DIMENSIONS OF 0.0667-SCALE MODEL OF CONFIGURATION 3 OF NORTH AMERICAN X-15 RESEARCH AIRPLANE - Concluded

Root chord, in.	8.171
Tip chord, in.	6.053
Taper ratio	0.74
Mean aerodynamic chord, in.	7.153
Longitudinal distance from total wing 0.20$\bar{c}$ to exposed panel 0.25$\bar{c}$, in.	10.309
Movable portion -	
Area, sq in.	16.848
Span, in.	2.482
Root chord, in.	7.49
Tip chord, in.	6.053
Hinge line, percent exposed panel $\bar{c}$	29
Speed brake (one side) -	
Area, sq in.	3.514
Chord, in.	2.678
Average span, in.	1.308
Lower vertical tail (exposed panel):	
Airfoil section	10^{o} wedge
Area, sq in.	22.476
Span, in.	3.085
Aspect ratio	0.42
Leading-edge sweepback, deg	30
Trailing-edge sweepback, deg	0
Root chord, in.	8.171
Tip chord, in.	6.4
Taper ratio	0.78
Mean aerodynamic chord, in.	7.321
Longitudinal distance from total wing 0.20$\bar{c}$ to exposed panel 0.25$\bar{c}$, in.	10.144
Movable portion -	
Area, sq in.	12.6
Span, in.	1.881
Root chord, in.	7.486
Tip chord, in.	6.4
Hinge line, percent exposed panel $\bar{c}$	30
Speed brake (one side) -	
Area, sq in.	3.514
Chord, in.	2.678
Average span, in.	1.308
Fuselage:	
Length, in.	39.36
Maximum depth, in.	3.733
Maximum width with side fairings, in.	5.868
Maximum width without side fairings, in.	3.733
Fineness ratio without side fairings	10.54
Base diameter, in.	3.197

TABLE II.- INDEX OF FIGURES PRESENTING RESULTS

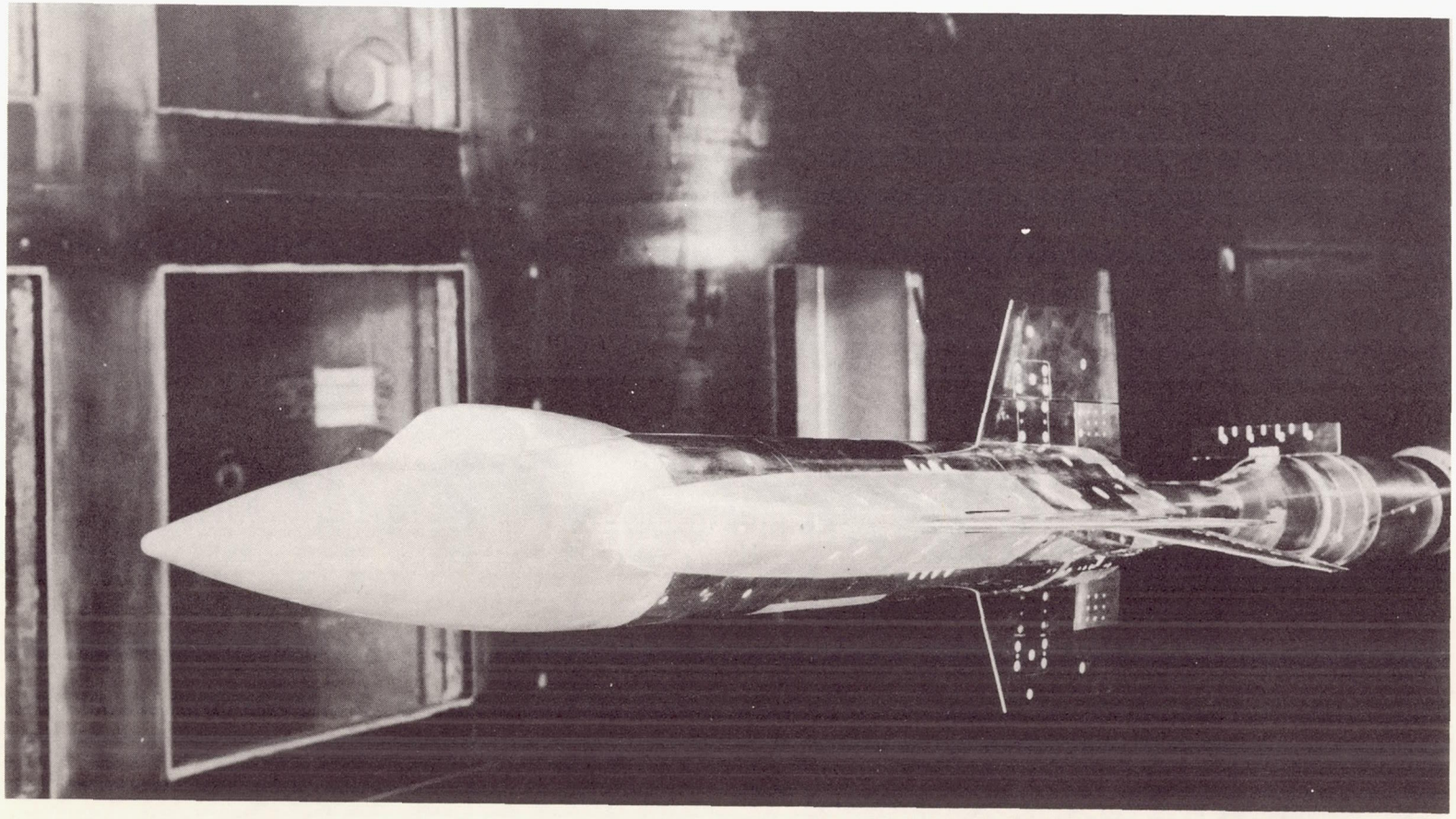

L-57-5411

Figure 1.- Photographs of 0.0667-scale model of X-15 installed in Langley 8-foot transonic pressure tunnel.

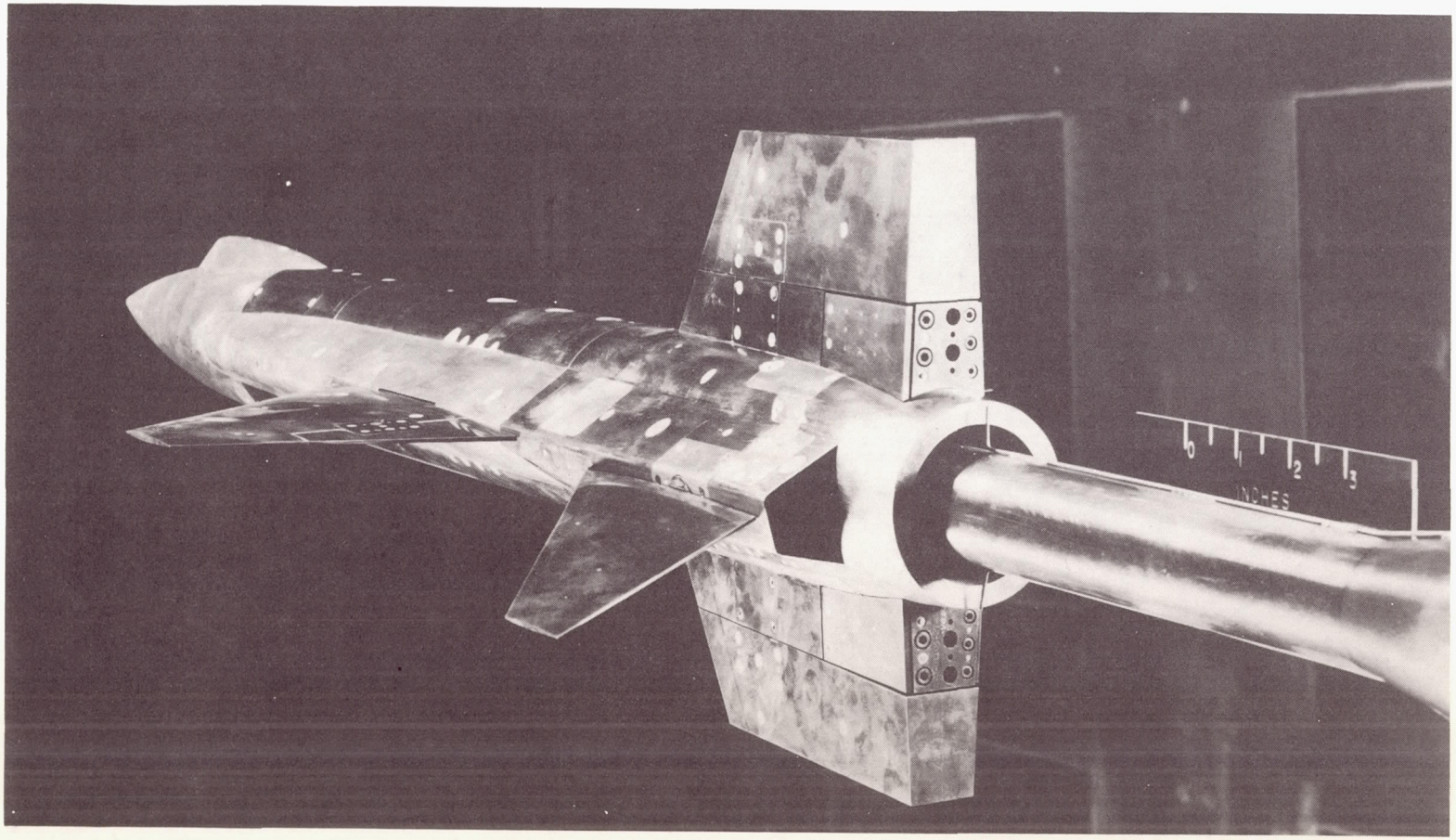

Figure 1.- Concluded. L-57-5412

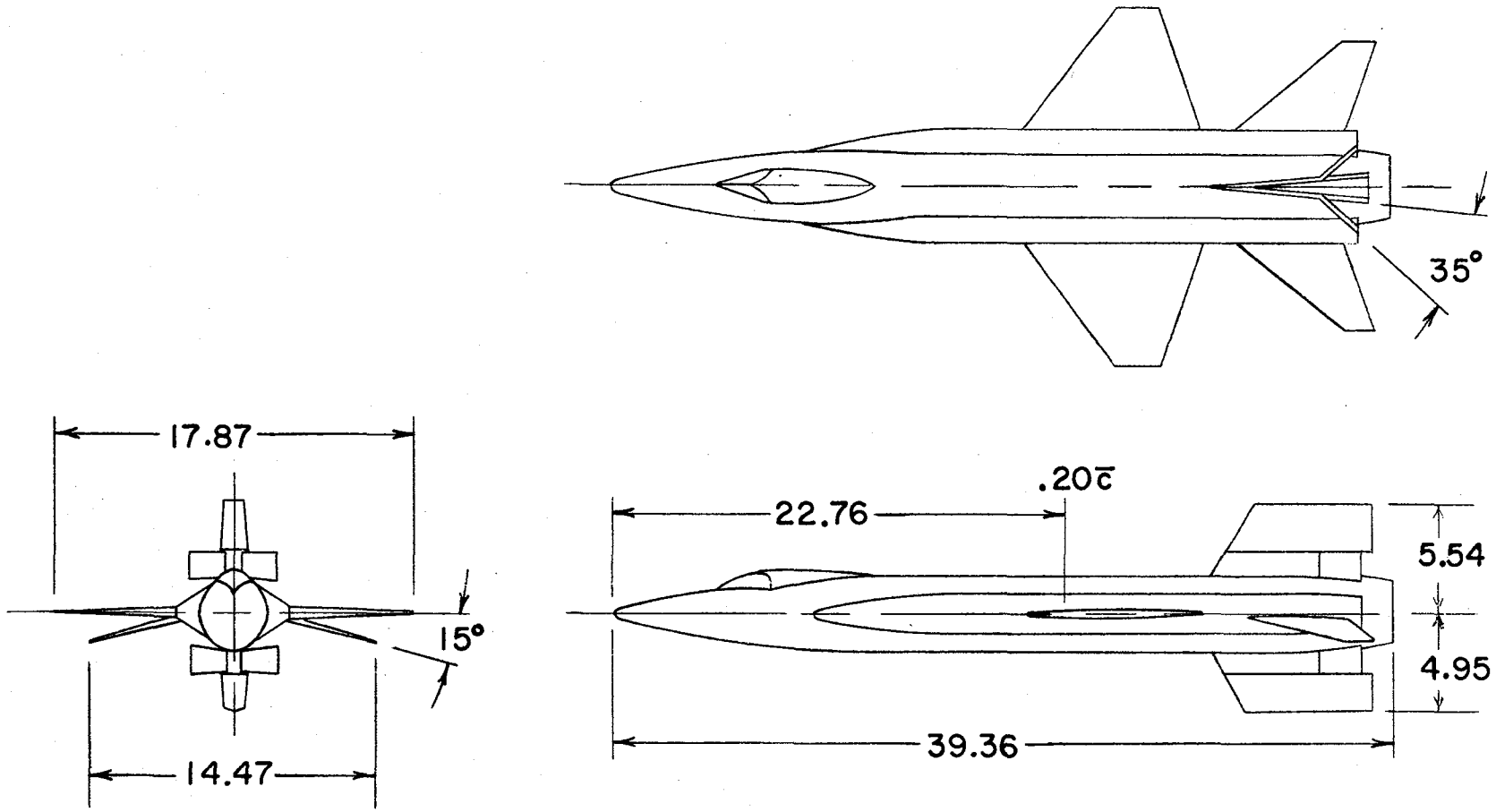

Figure 2.- Drawing of 0.0667-scale model of X-15 with speed brakes open. All dimensions are in inches unless otherwise noted.

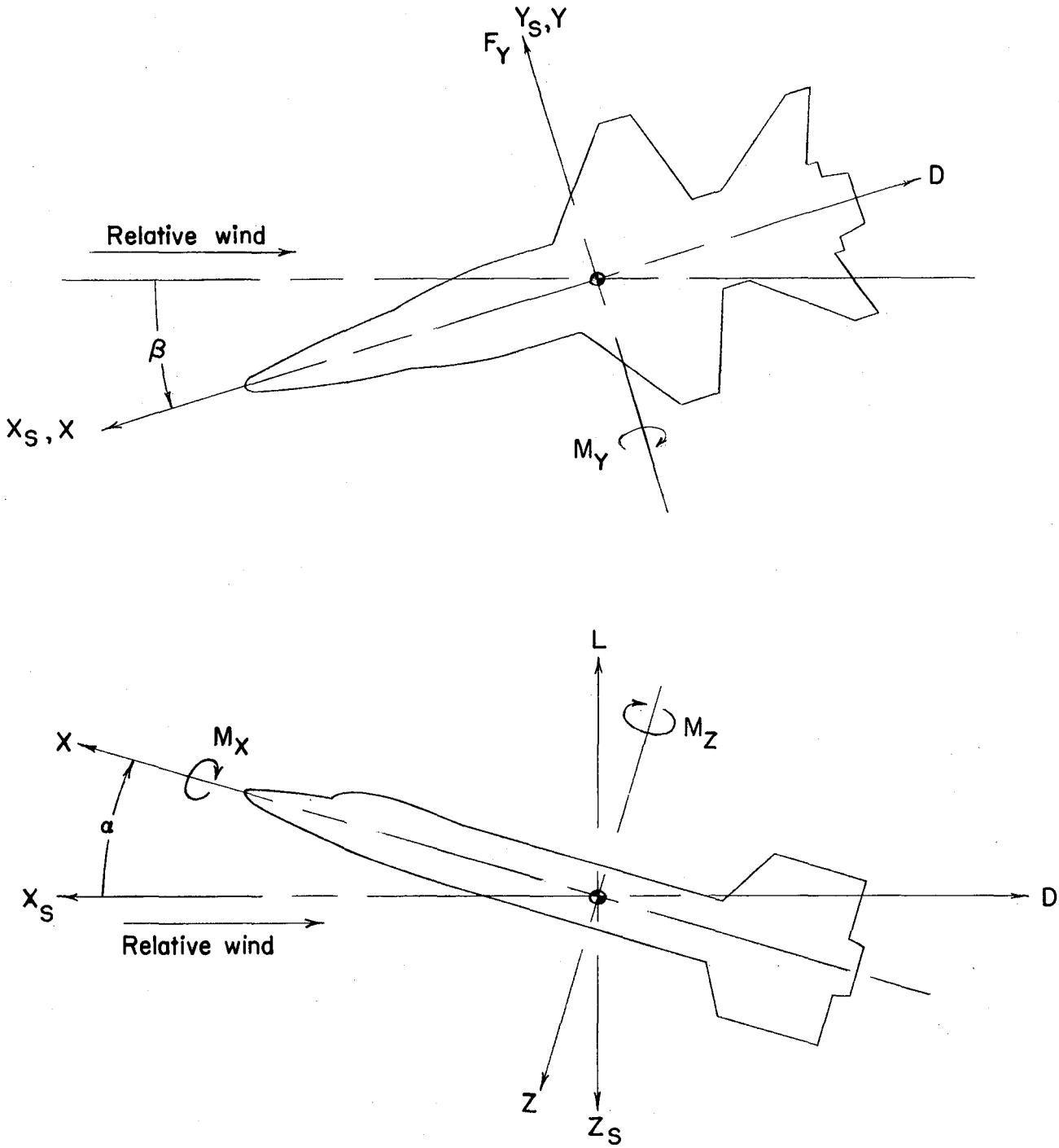

Figure 3.- System of axes. Arrows indicate positive directions.

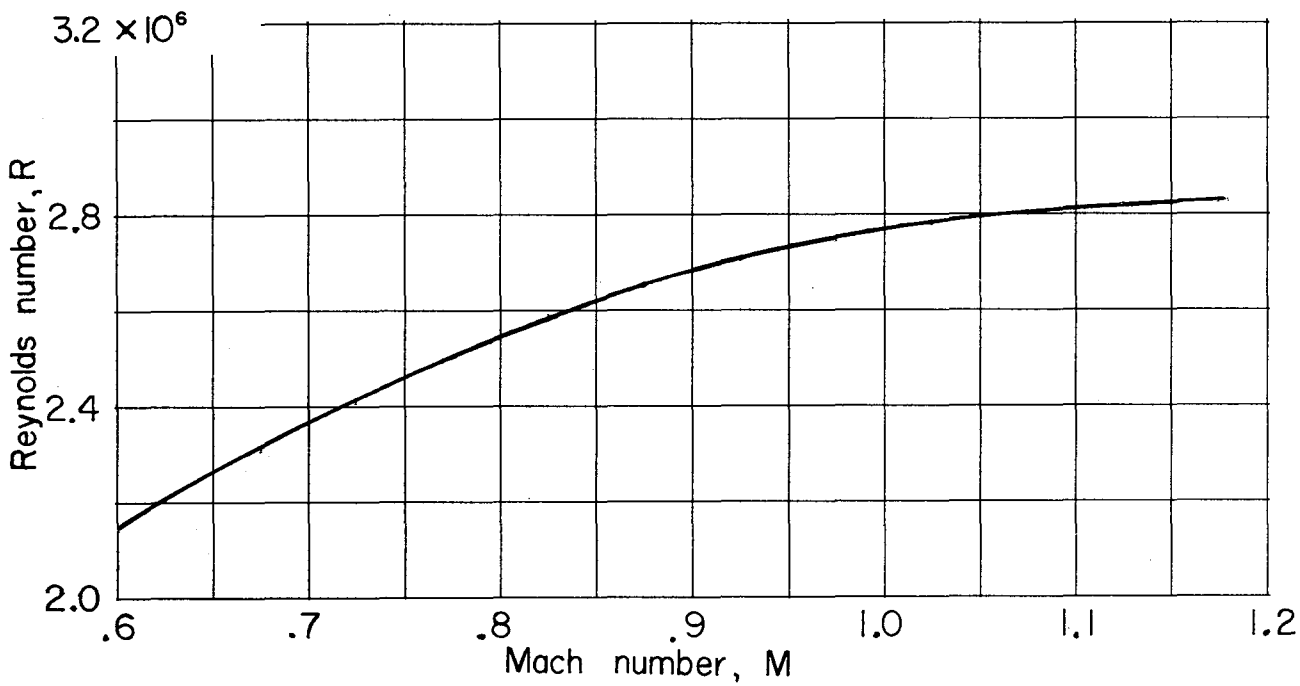

Figure 4.- Variation with Mach number of test Reynolds number based on $\bar{c}$ = 8.207 inches.

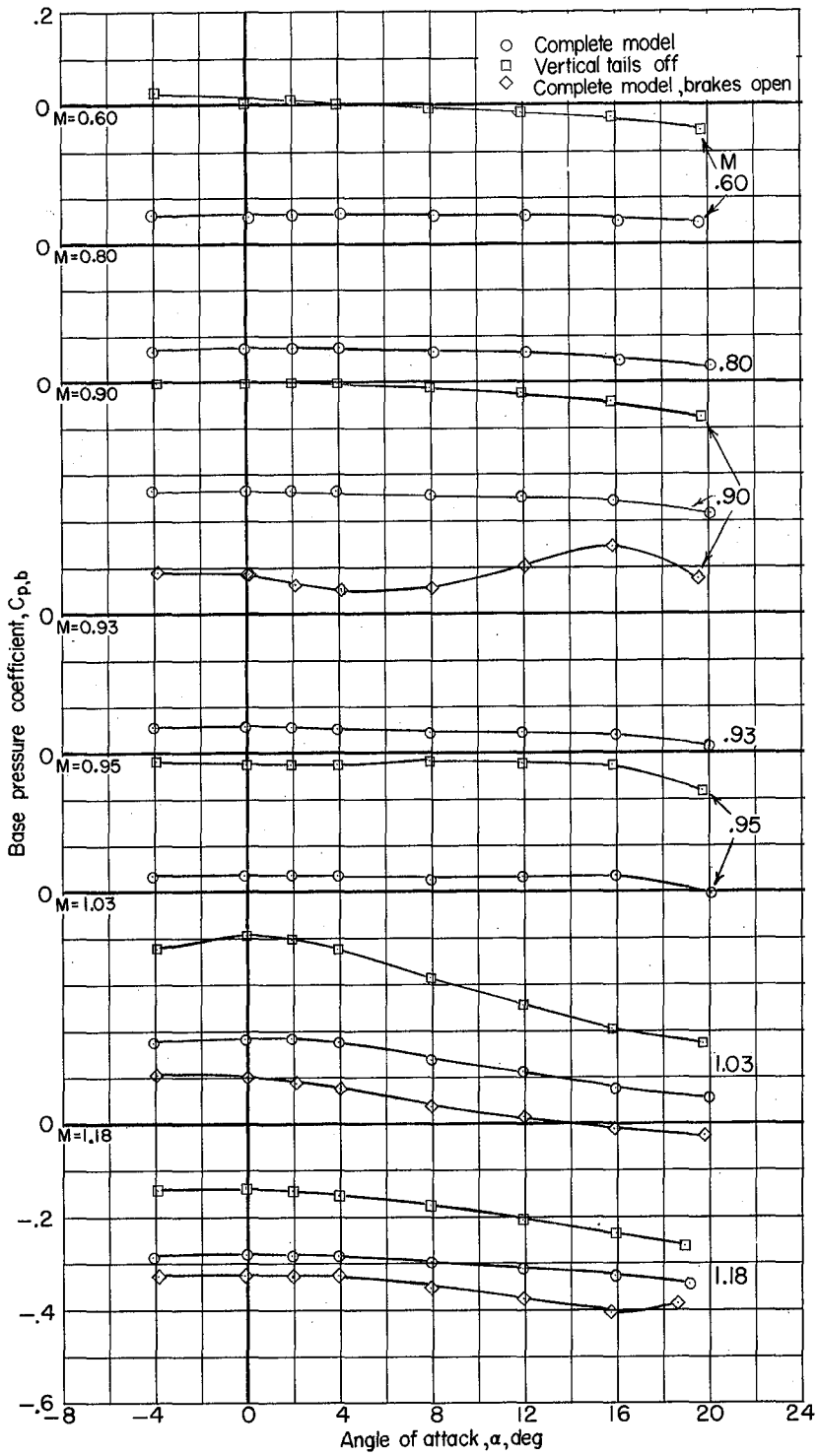

Figure 5.- Base pressure coefficients for complete model and for model without vertical tails. Surfaces undeflected unless otherwise noted. $\beta = 0^{o}$.

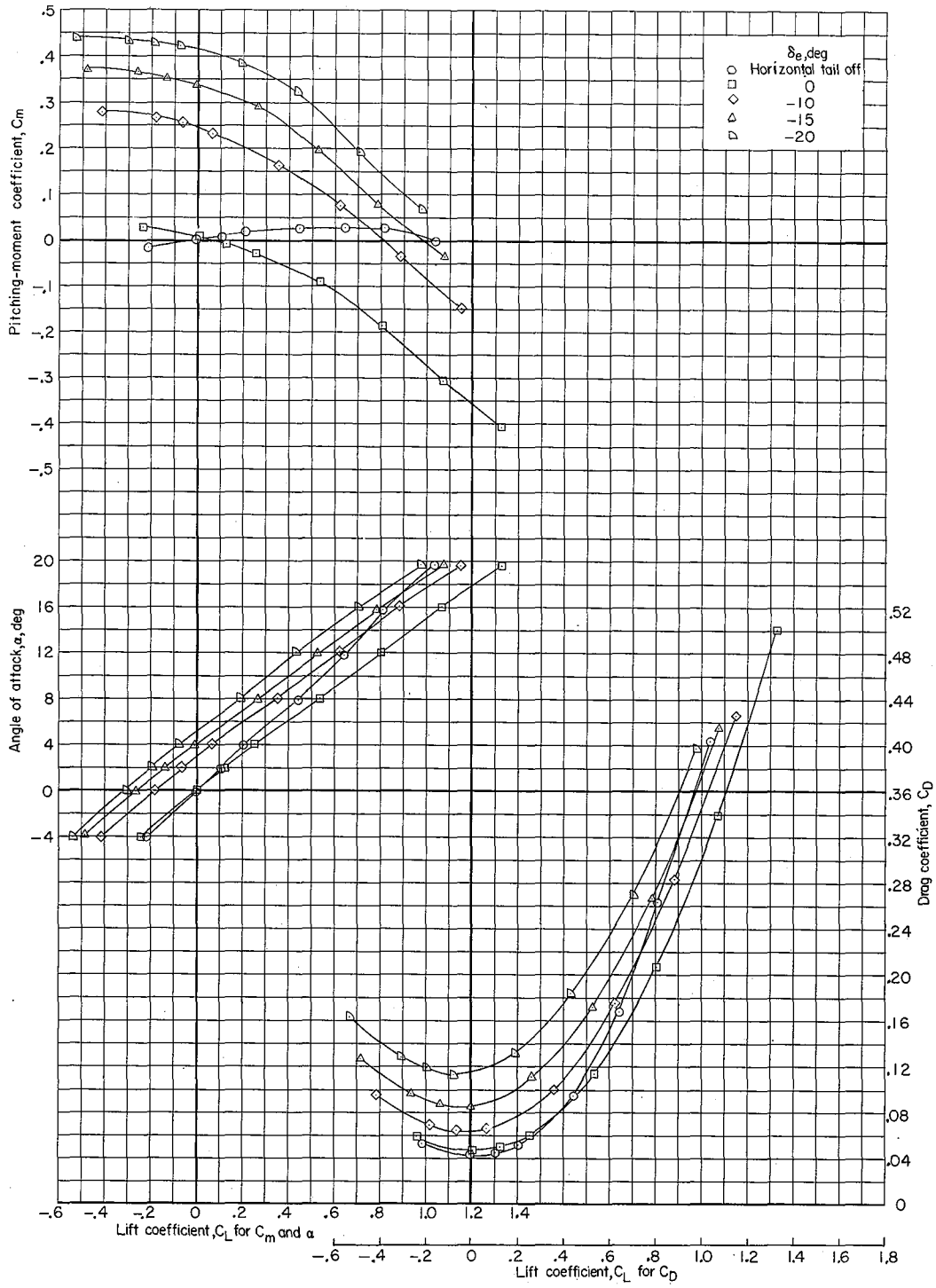

(a) M = 0.60.

Figure 6.- Longitudinal characteristics of model with various δ_e and of model without horizontal tail; other surfaces undeflected. $\beta = 0^o$.

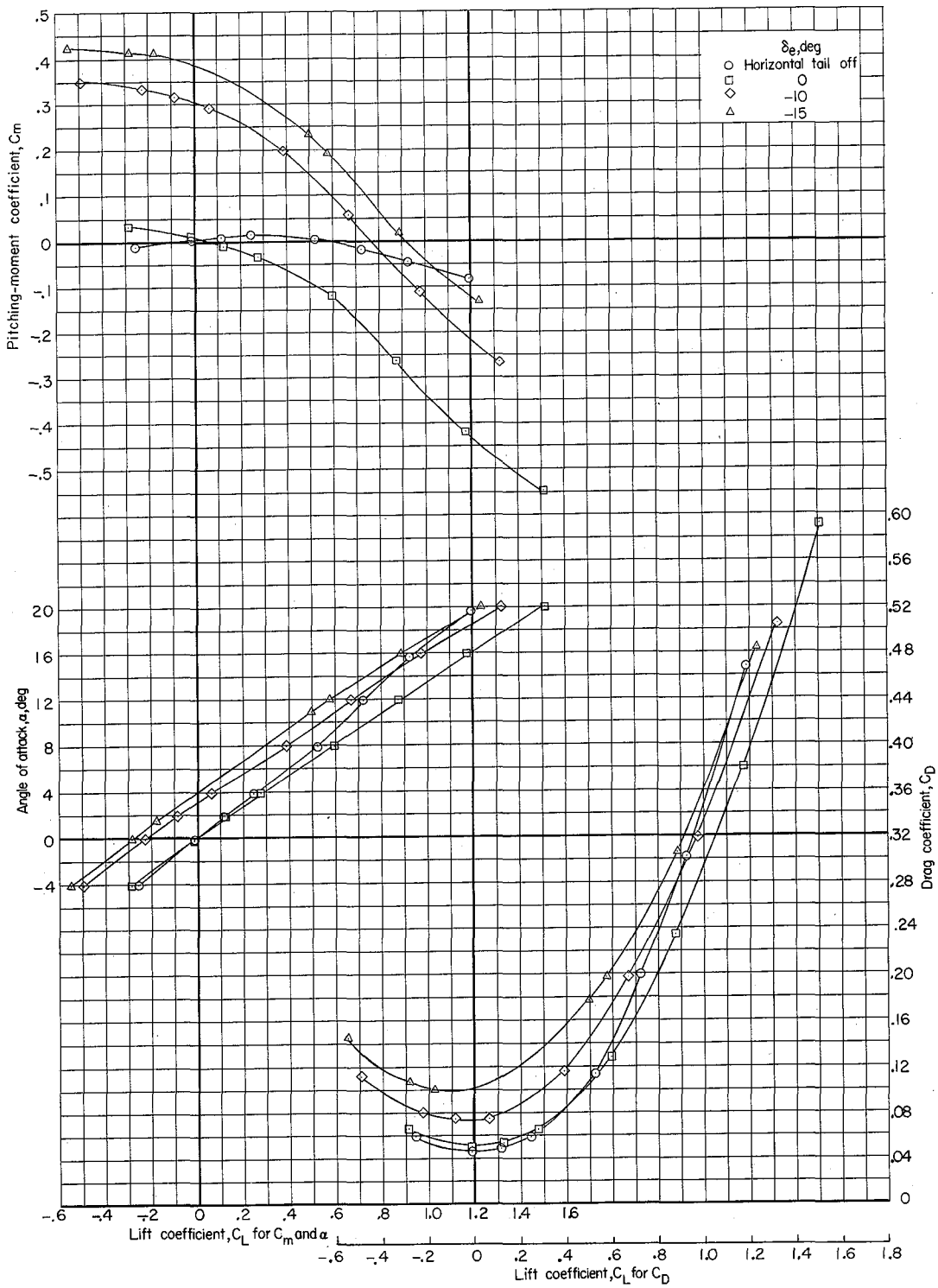

(b) M = 0.90.

Figure 6.- Continued.

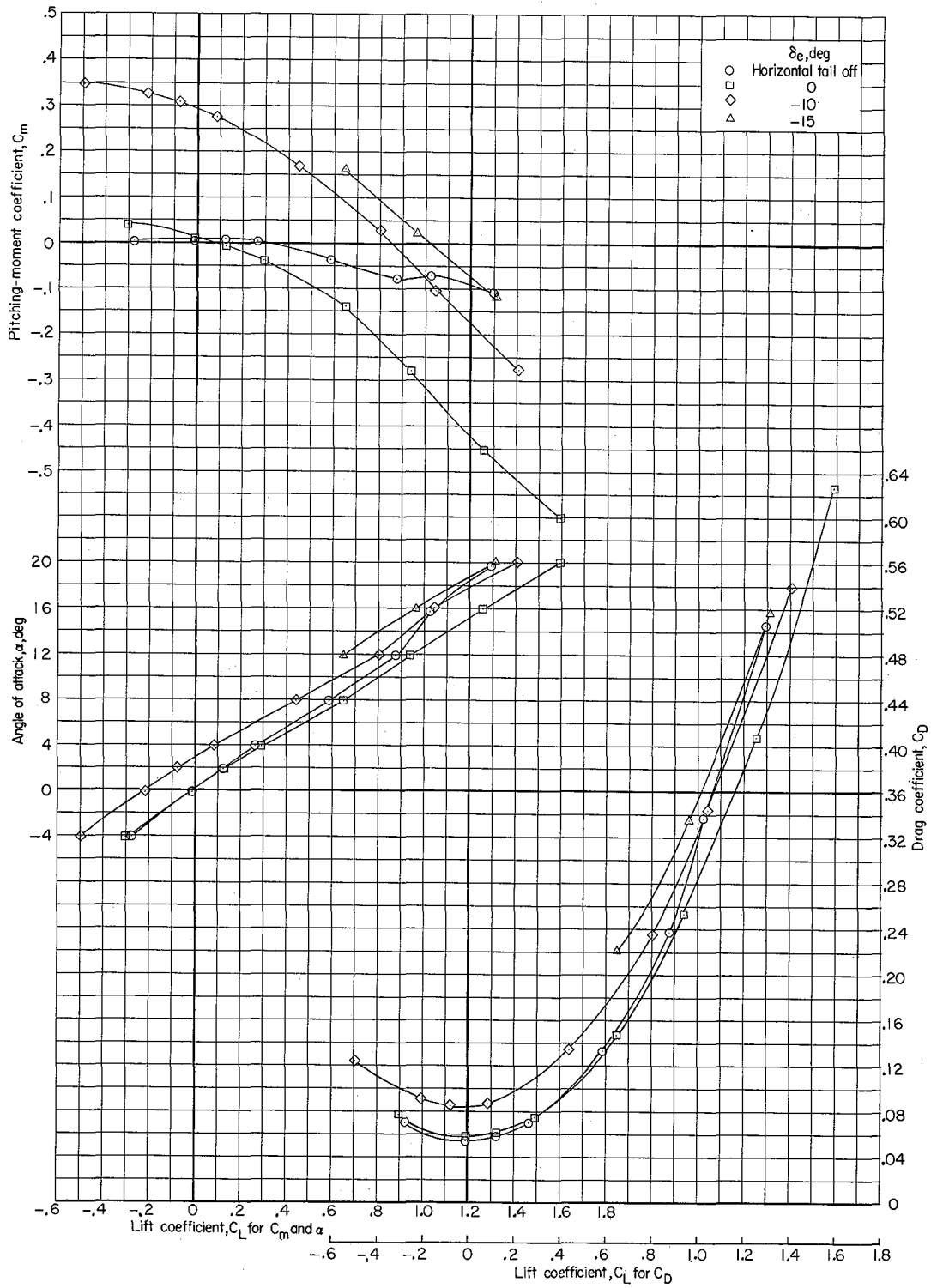

(c) M = 0.95.

Figure 6.- Continued.

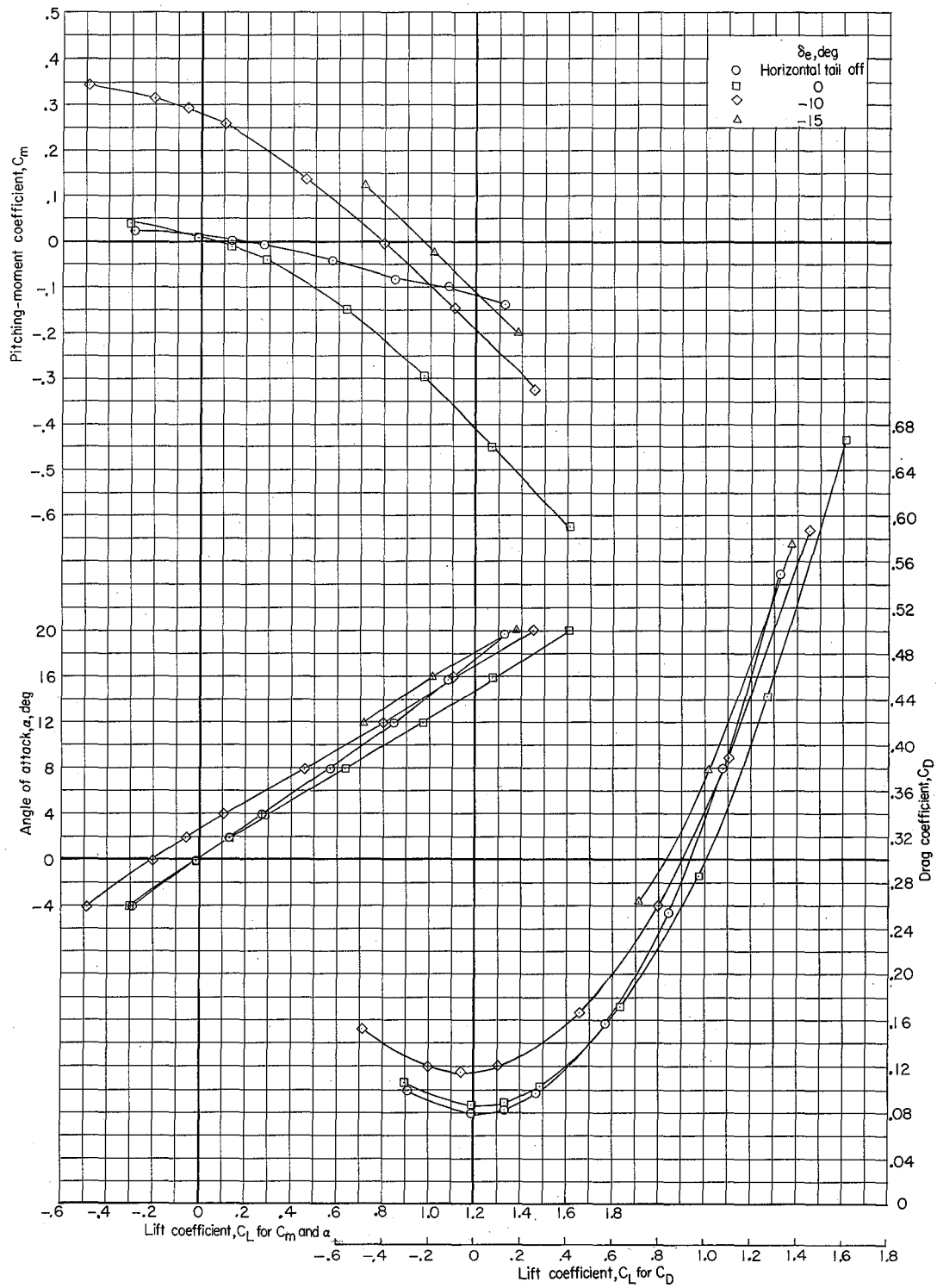

(d) M = 1.03.

Figure 6.- Continued.

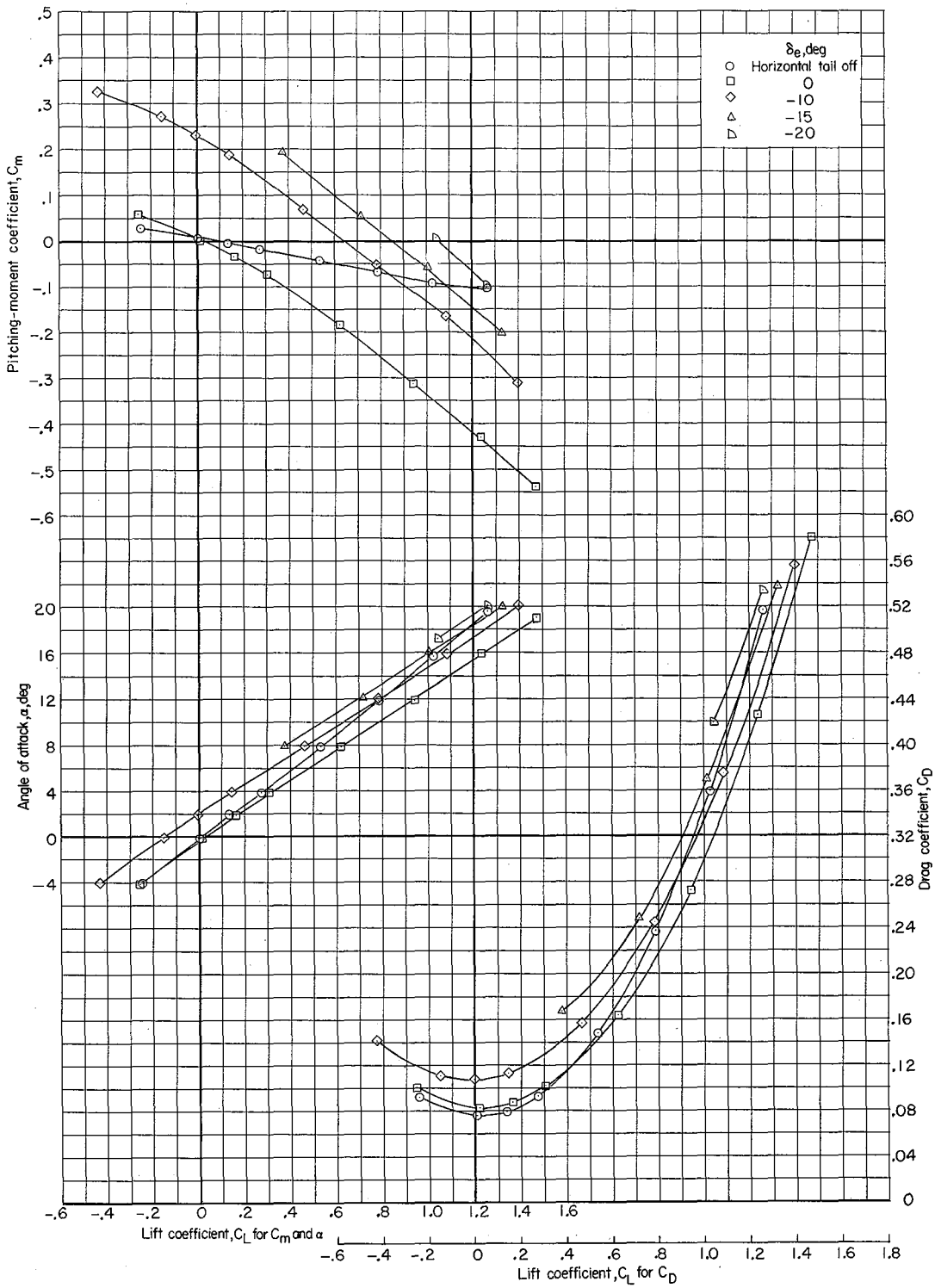

(e) M = 1.18.

Figure 6.- Continued.

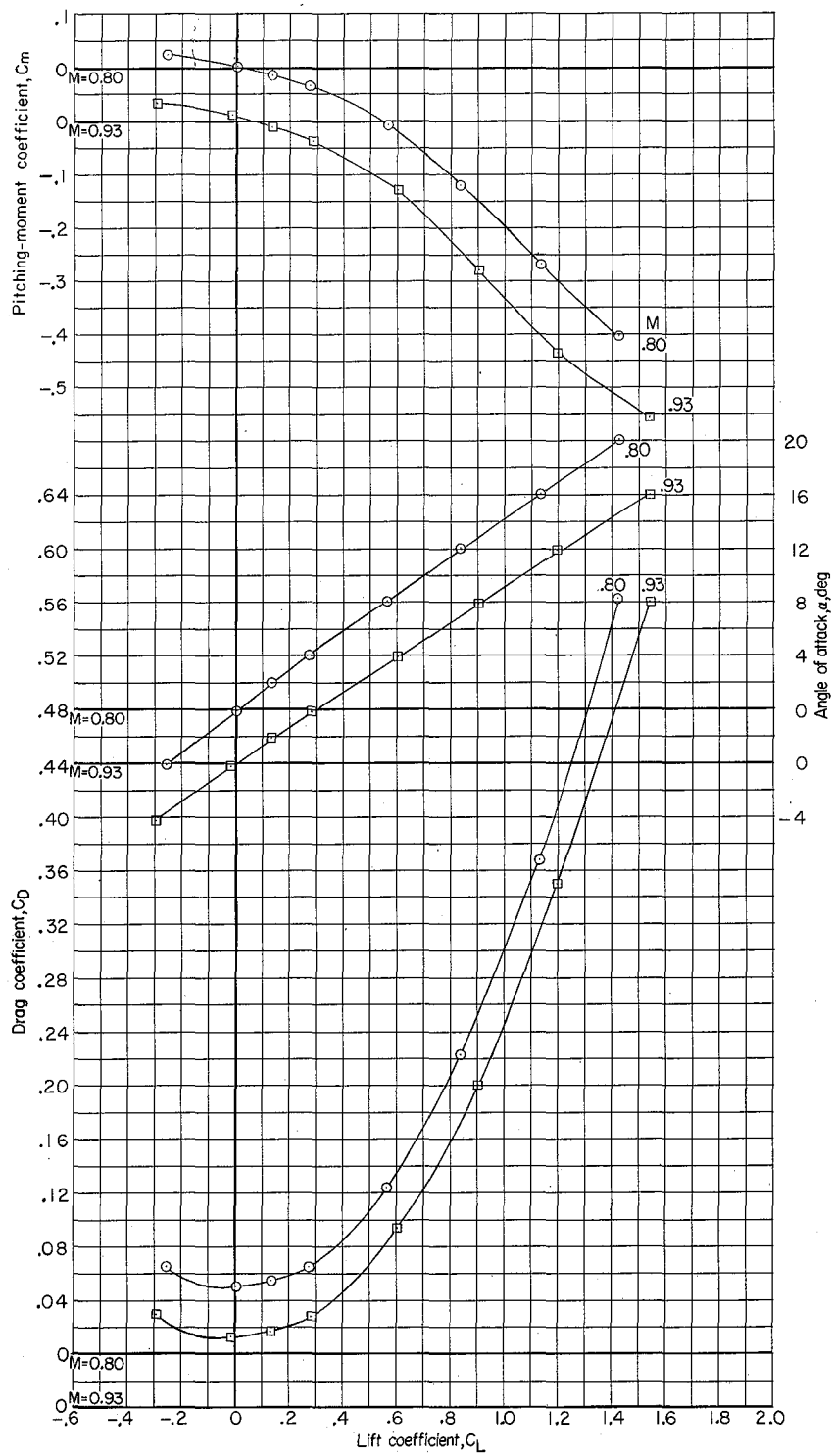

(f) M = 0.80 and 0.93; $\delta_e = 0^o$.

Figure 6.- Concluded.

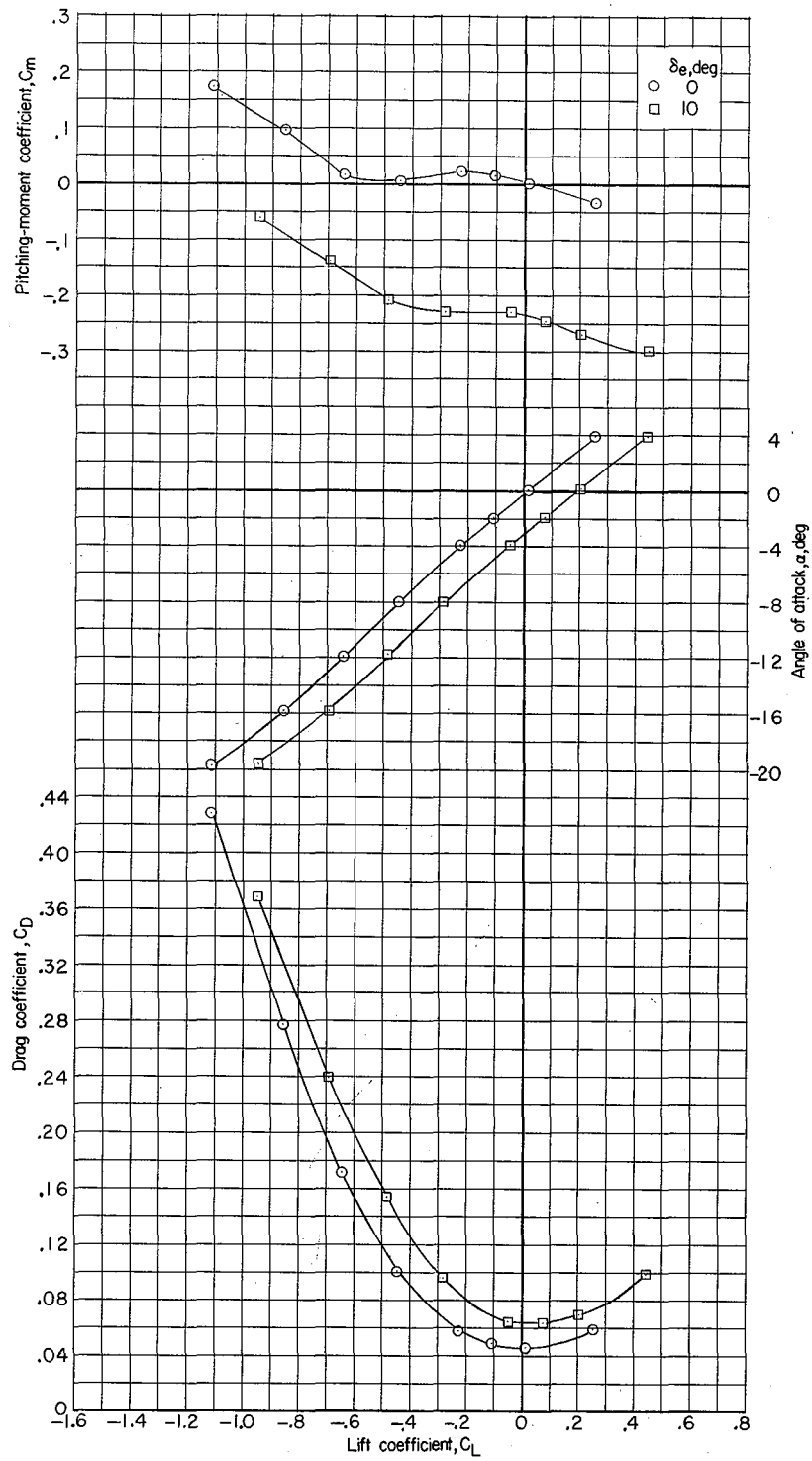

(a) M = 0.60.

Figure 7.- Longitudinal characteristics of model at negative angles of attack. $\beta = 0^\circ$; $\delta_e = 0^\circ$ and 10°; other surfaces undeflected.

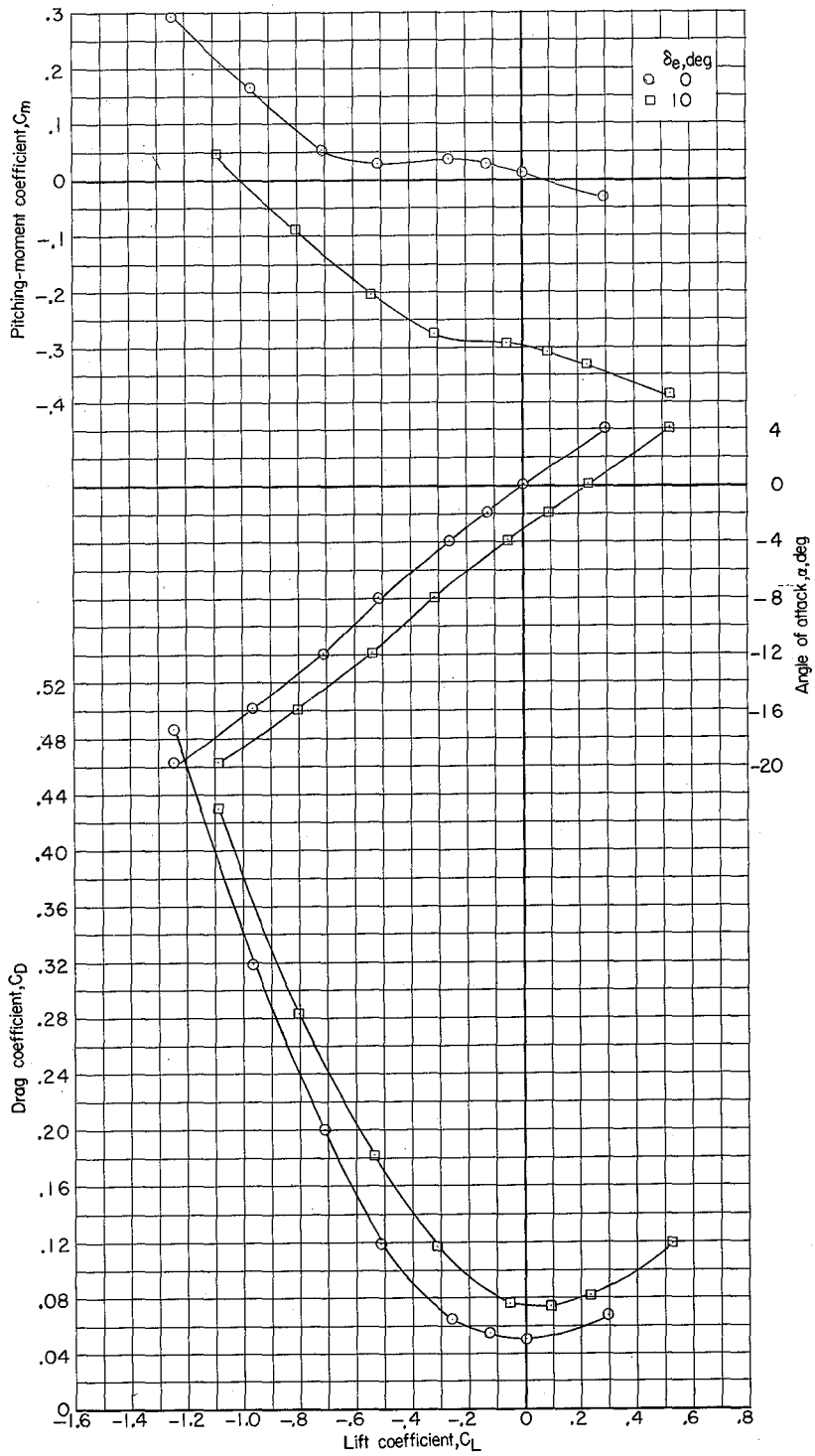

(b) M = 0.90.

Figure 7.- Continued.

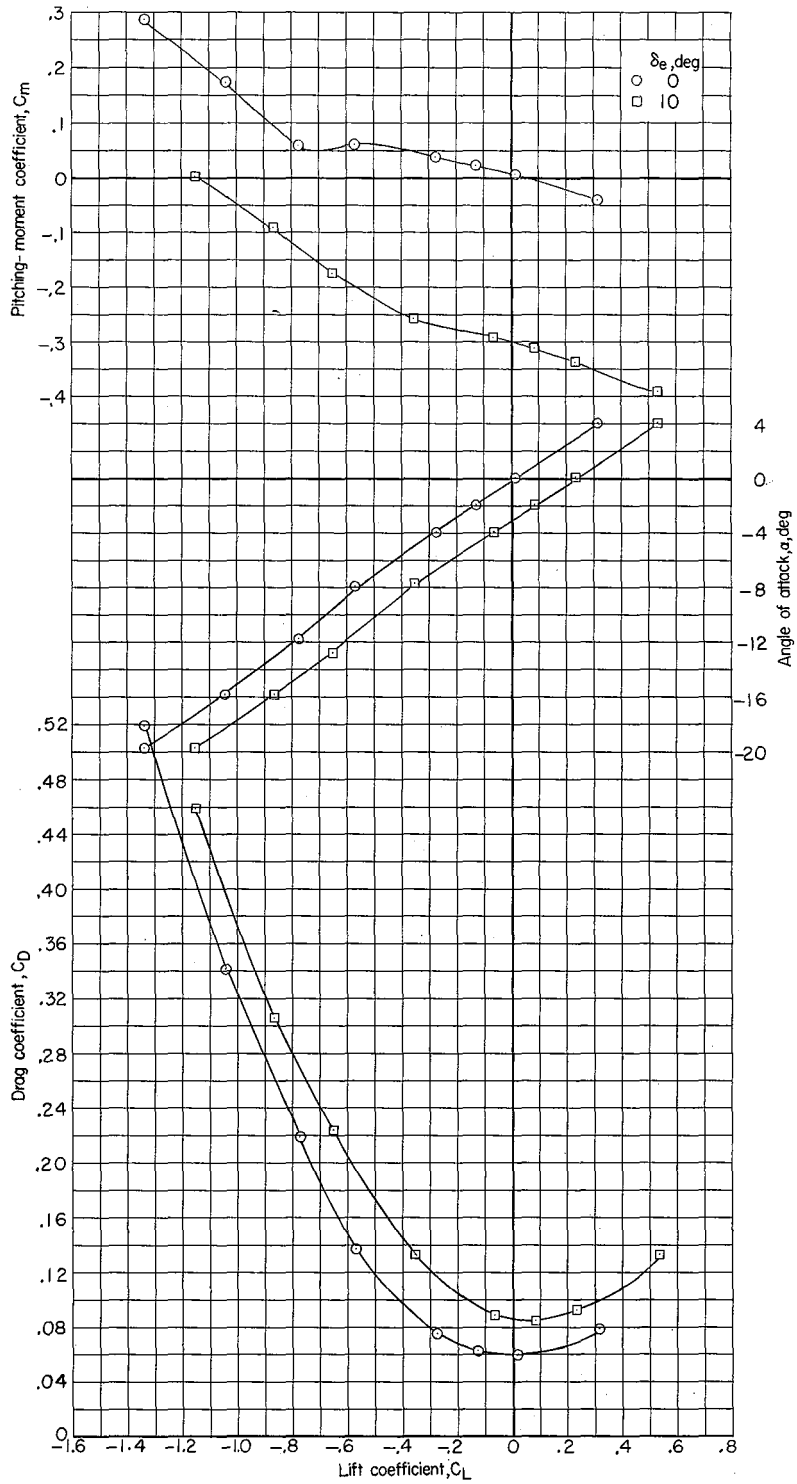

(c) M = 0.95.

Figure 7.- Continued.

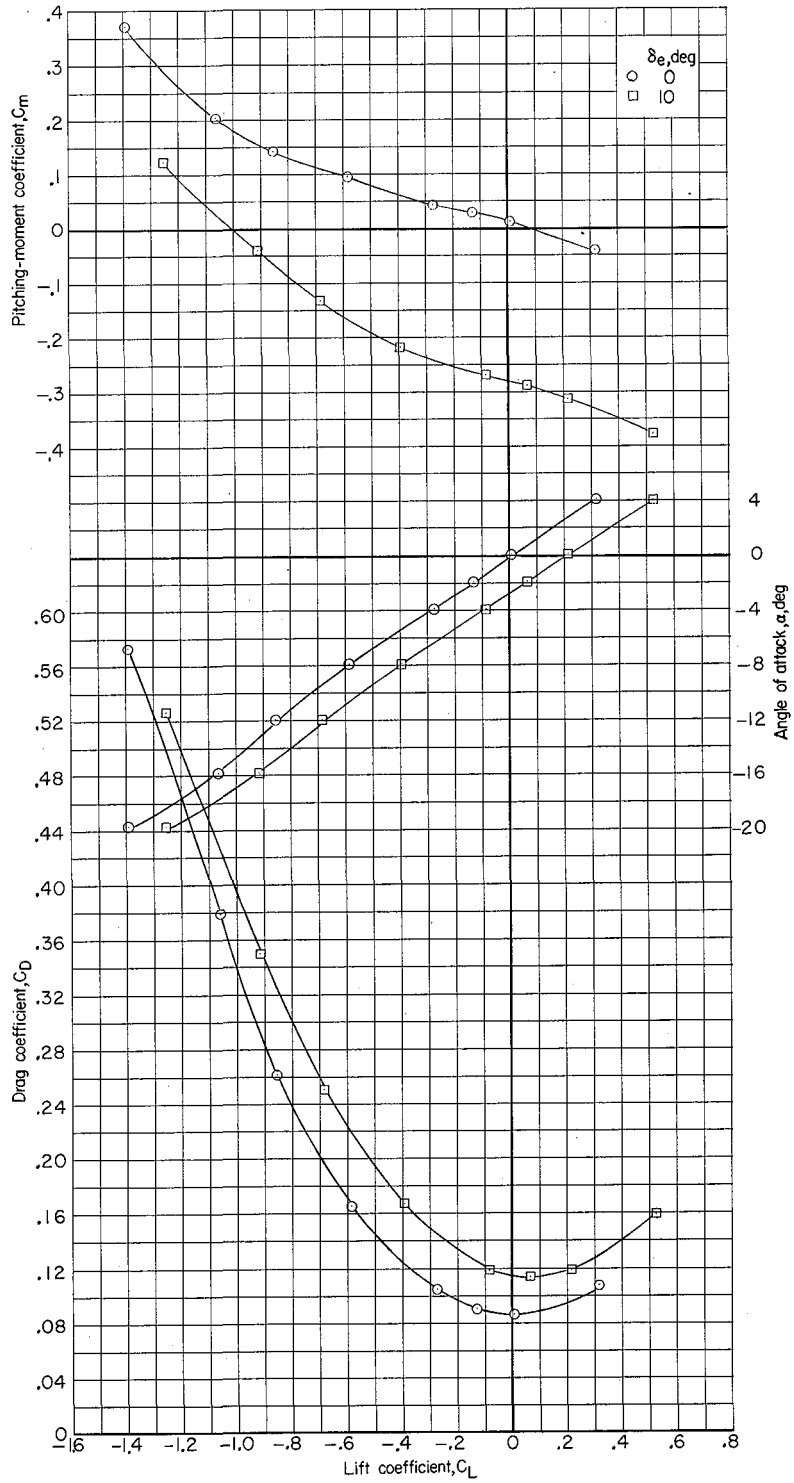

(d) M = 1.03.

Figure 7.- Continued.

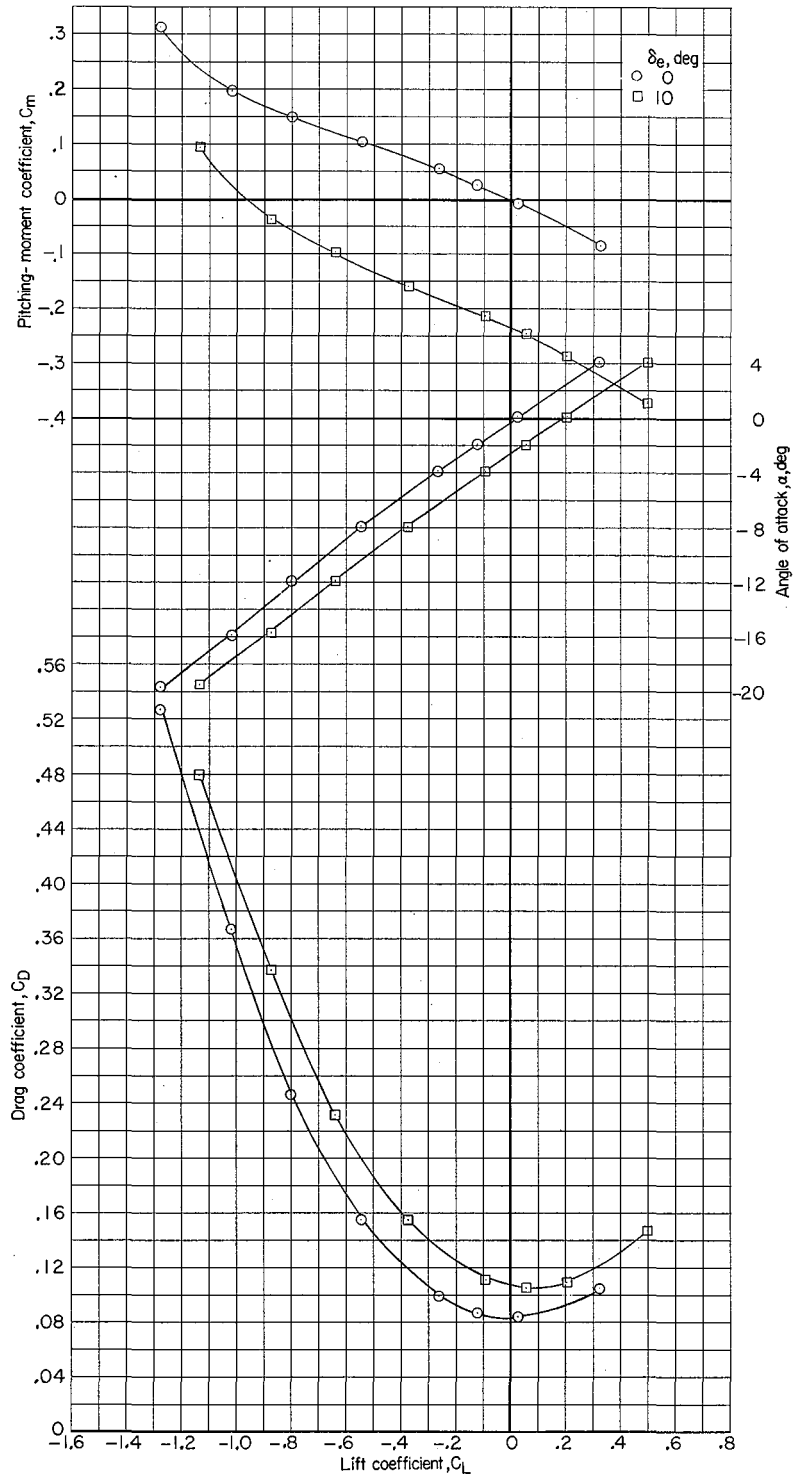

(e) M = 1.18.

Figure 7.- Concluded.

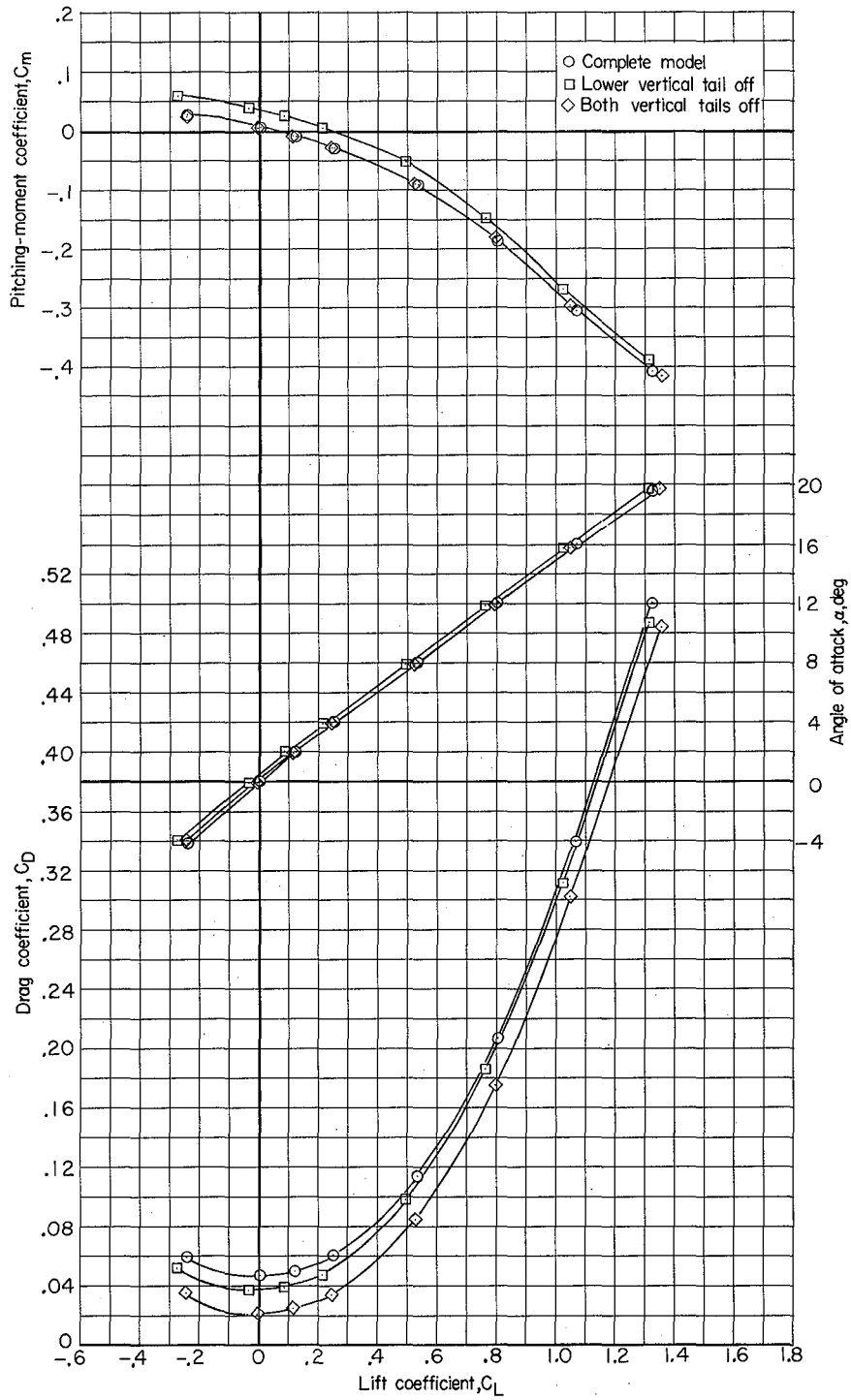

(a) M = 0.60.

Figure 8.- Longitudinal characteristics of model and of model without vertical tails, surfaces undeflected. $\beta = 0^\circ$.

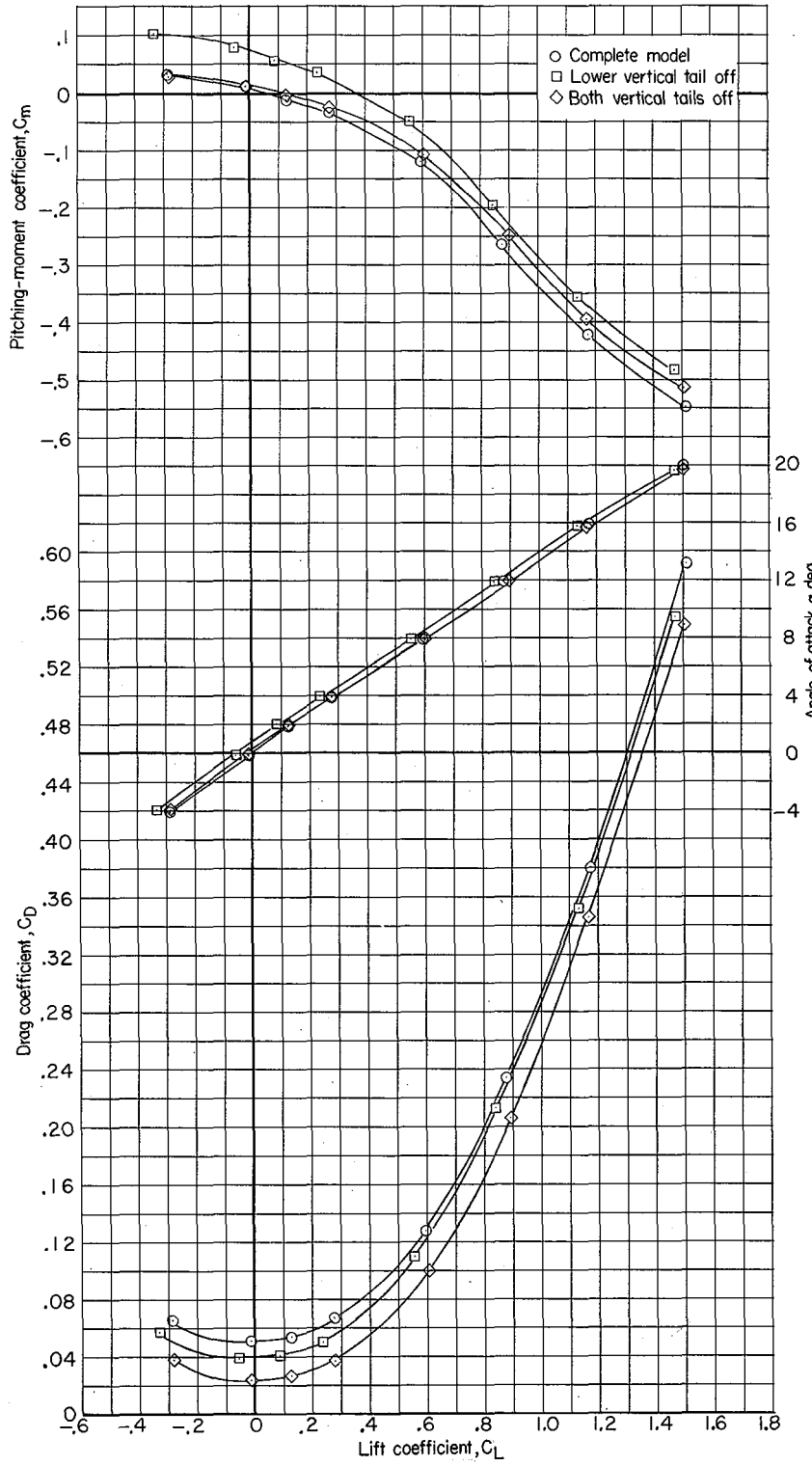

(b) M = 0.90.

Figure 8.- Continued.

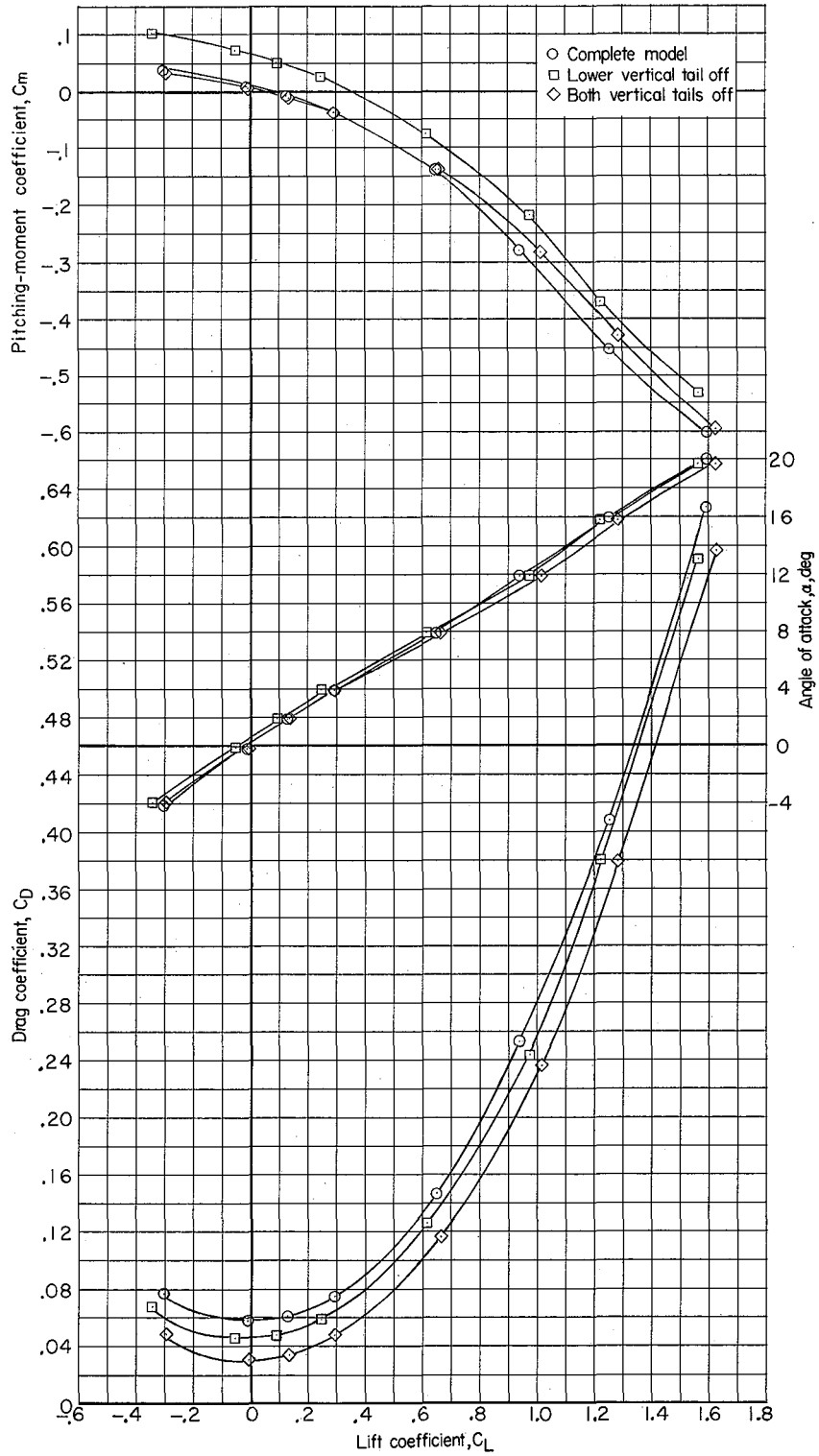

(c) M = 0.95.

Figure 8.- Continued.

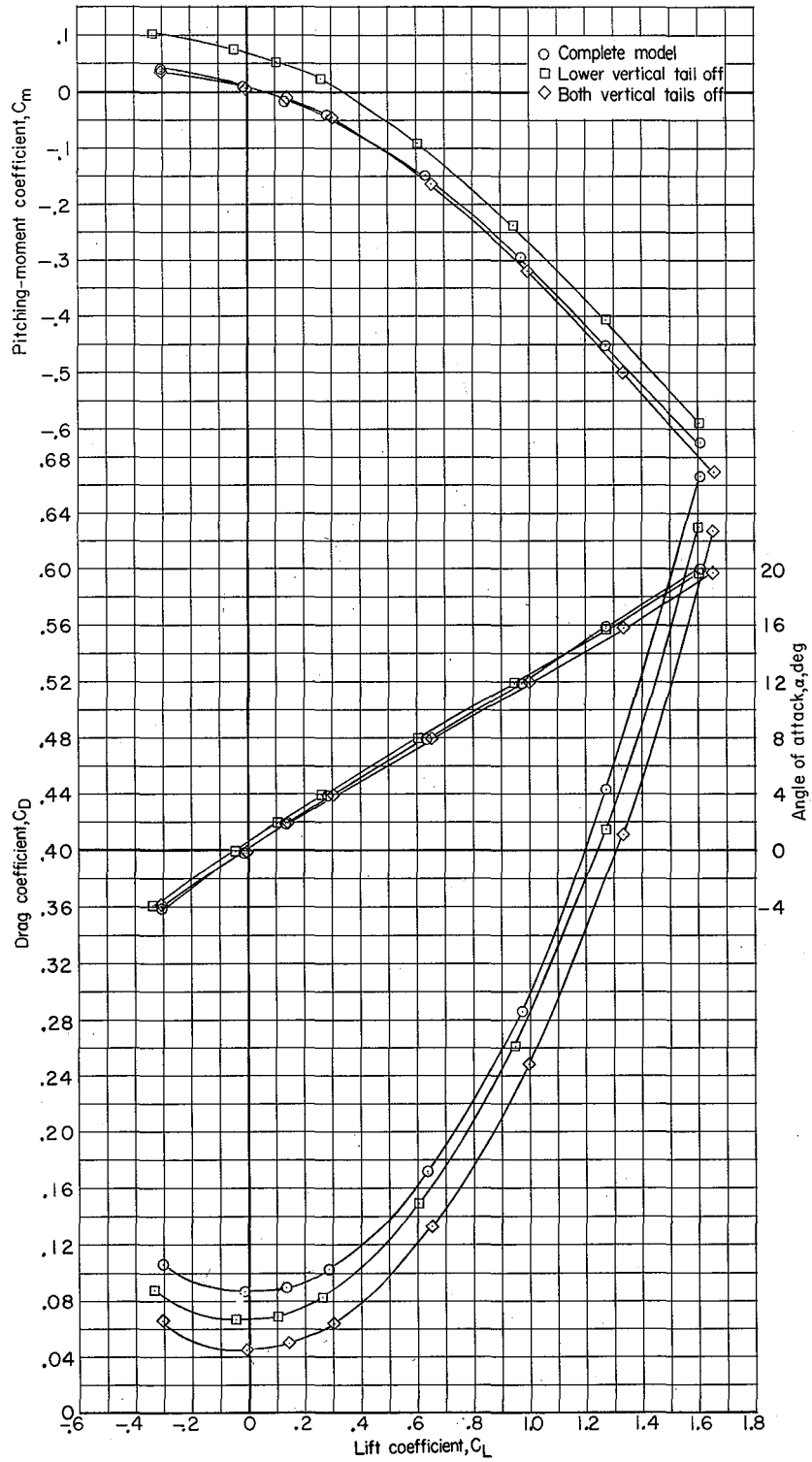

(d) M = 1.03.

Figure 8.- Continued.

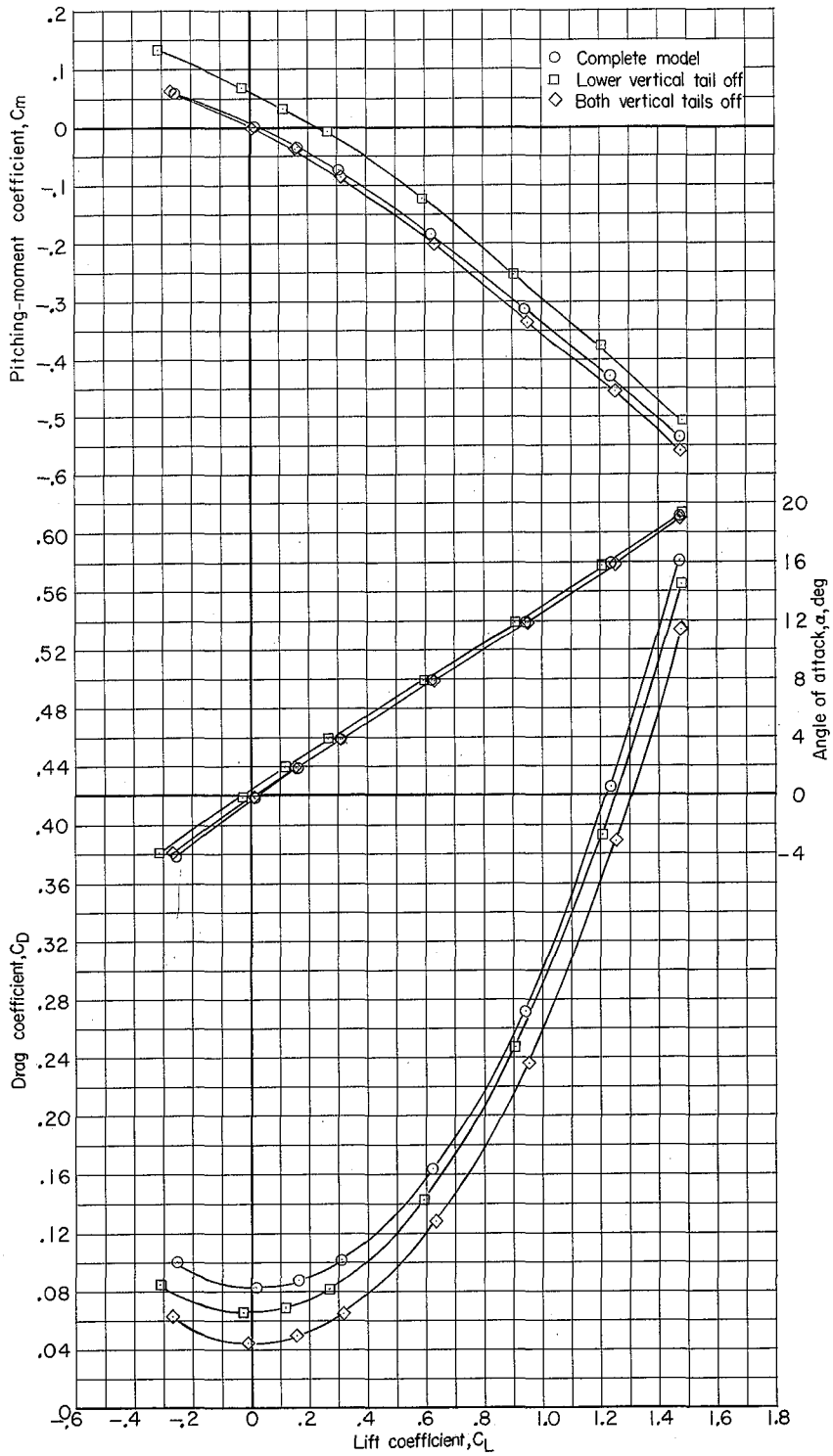

(e) M = 1.18.

Figure 8.- Concluded.

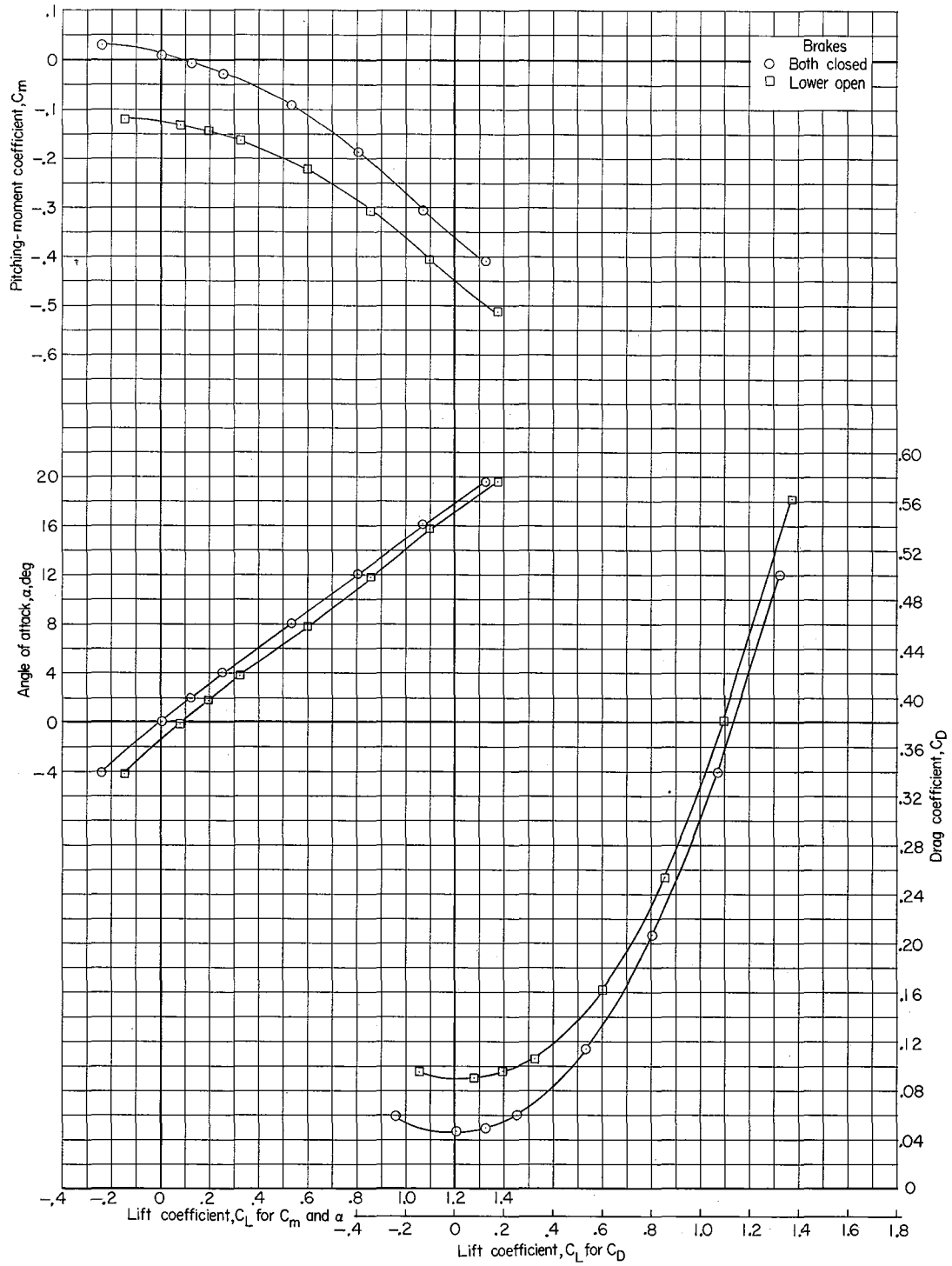

(a) M = 0.60.

Figure 9.- Longitudinal characteristics of model with speed brakes open and closed; other surfaces undeflected. $\beta = 0^{\circ}$.

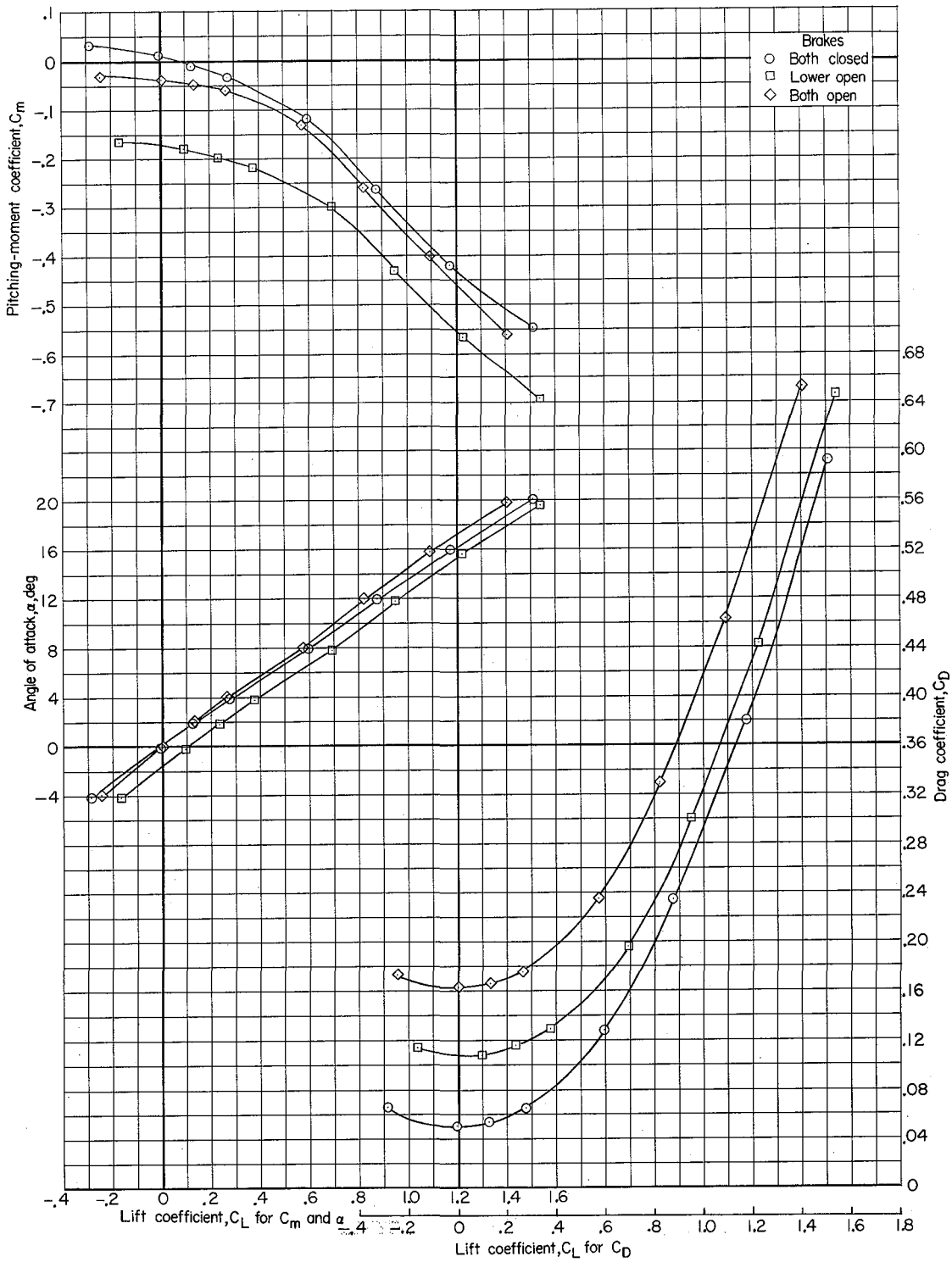

(b) M = 0.90.

Figure 9.- Continued.

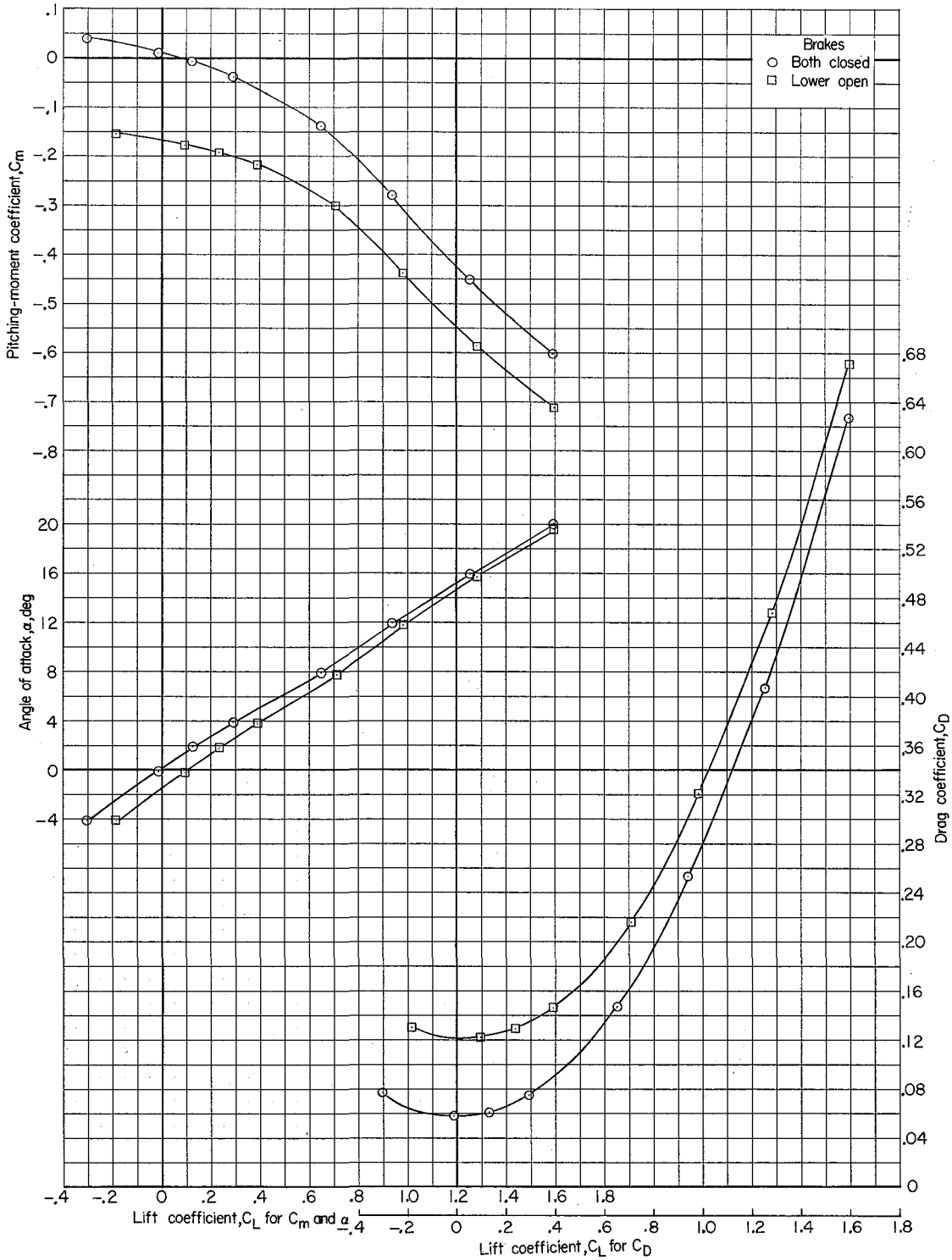

(c) M = 0.95.

Figure 9.- Continued.

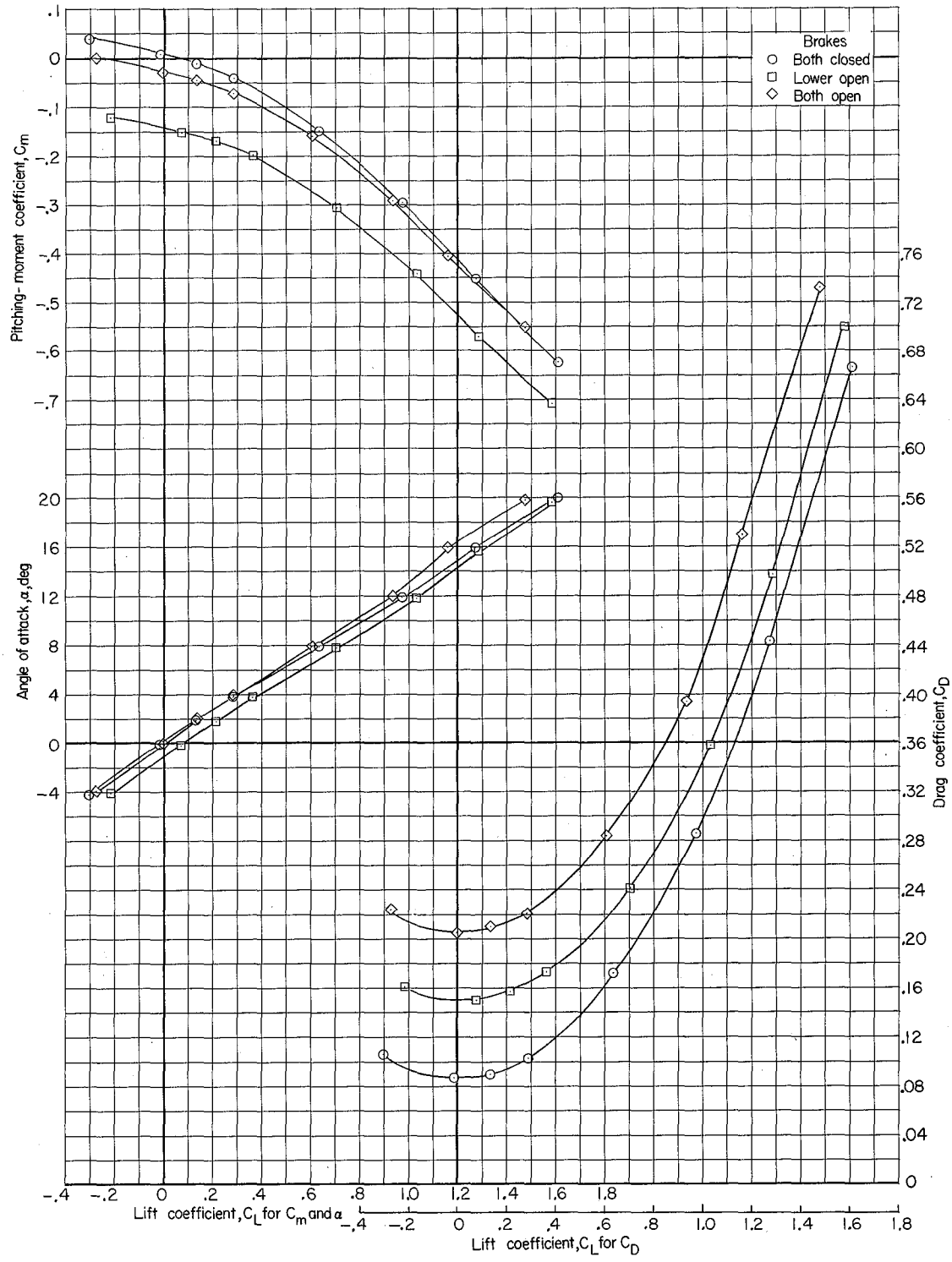

(d) M = 1.03.

Figure 9.- Continued.

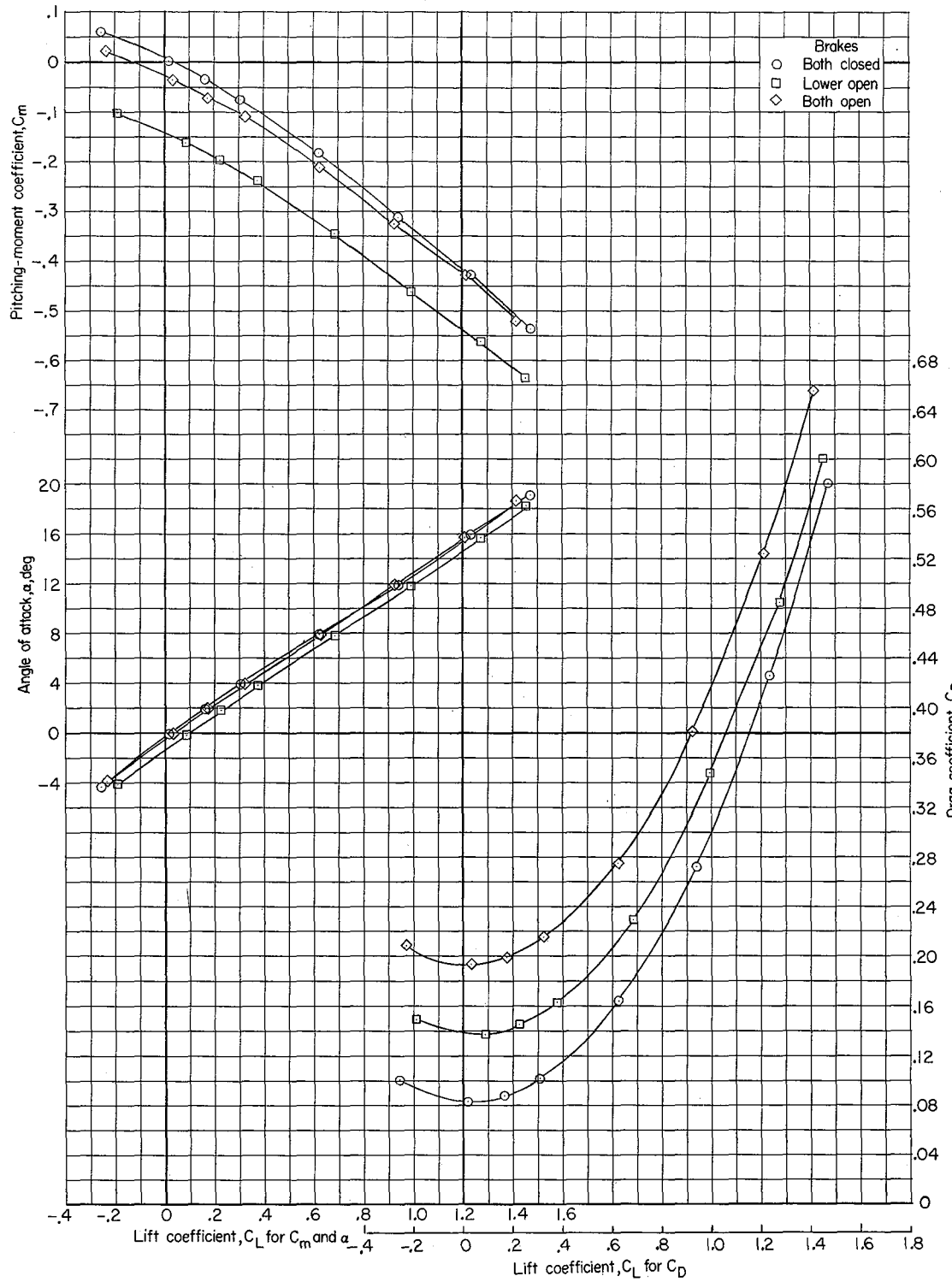

(e) M = 1.18.

Figure 9.- Concluded.

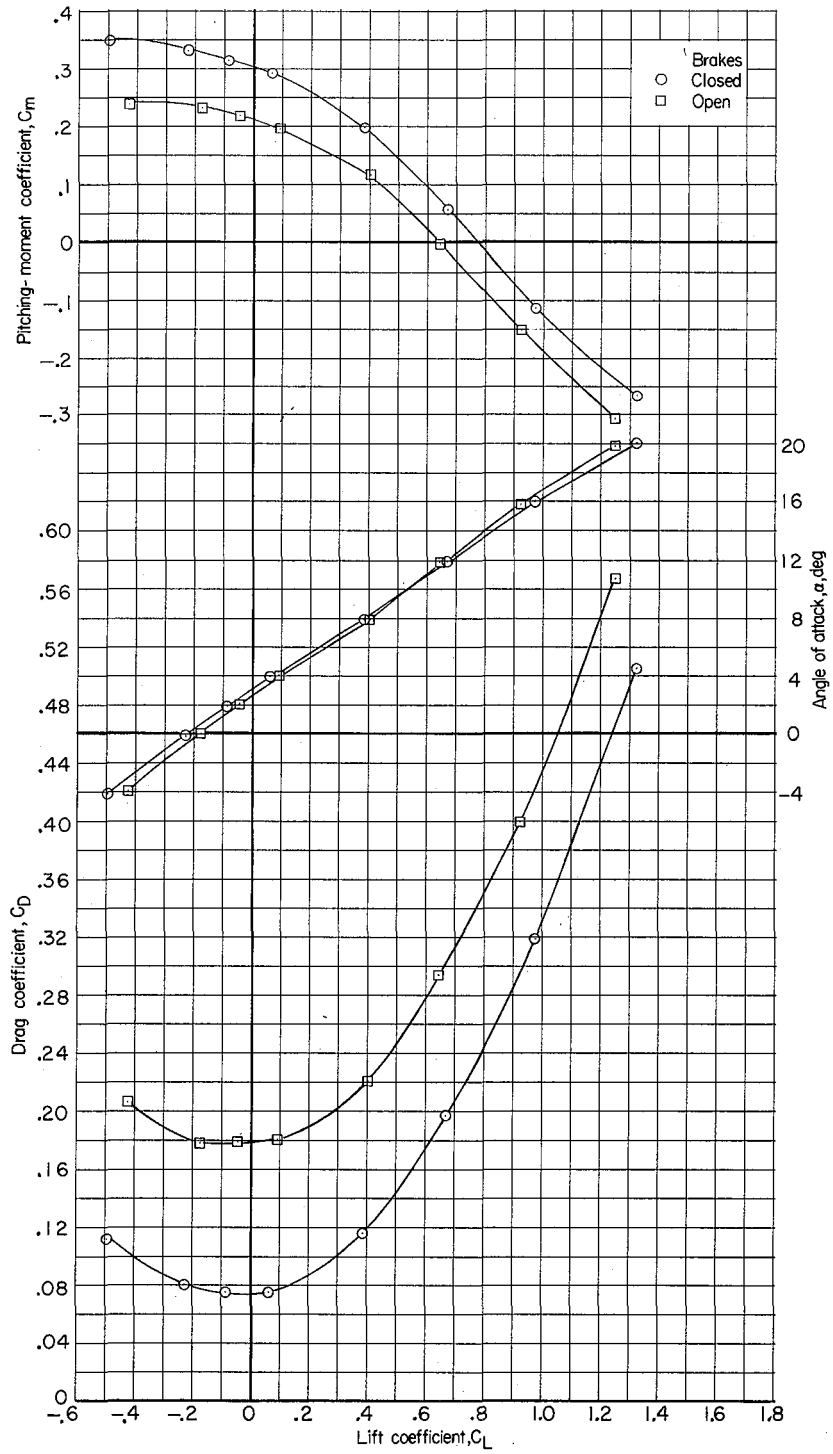

(a) M = 0.90.

Figure 10.- Longitudinal characteristics of model with speed brakes open and closed. $\beta = 0^\circ$; $\delta_e = -10^\circ$; other surfaces undeflected.

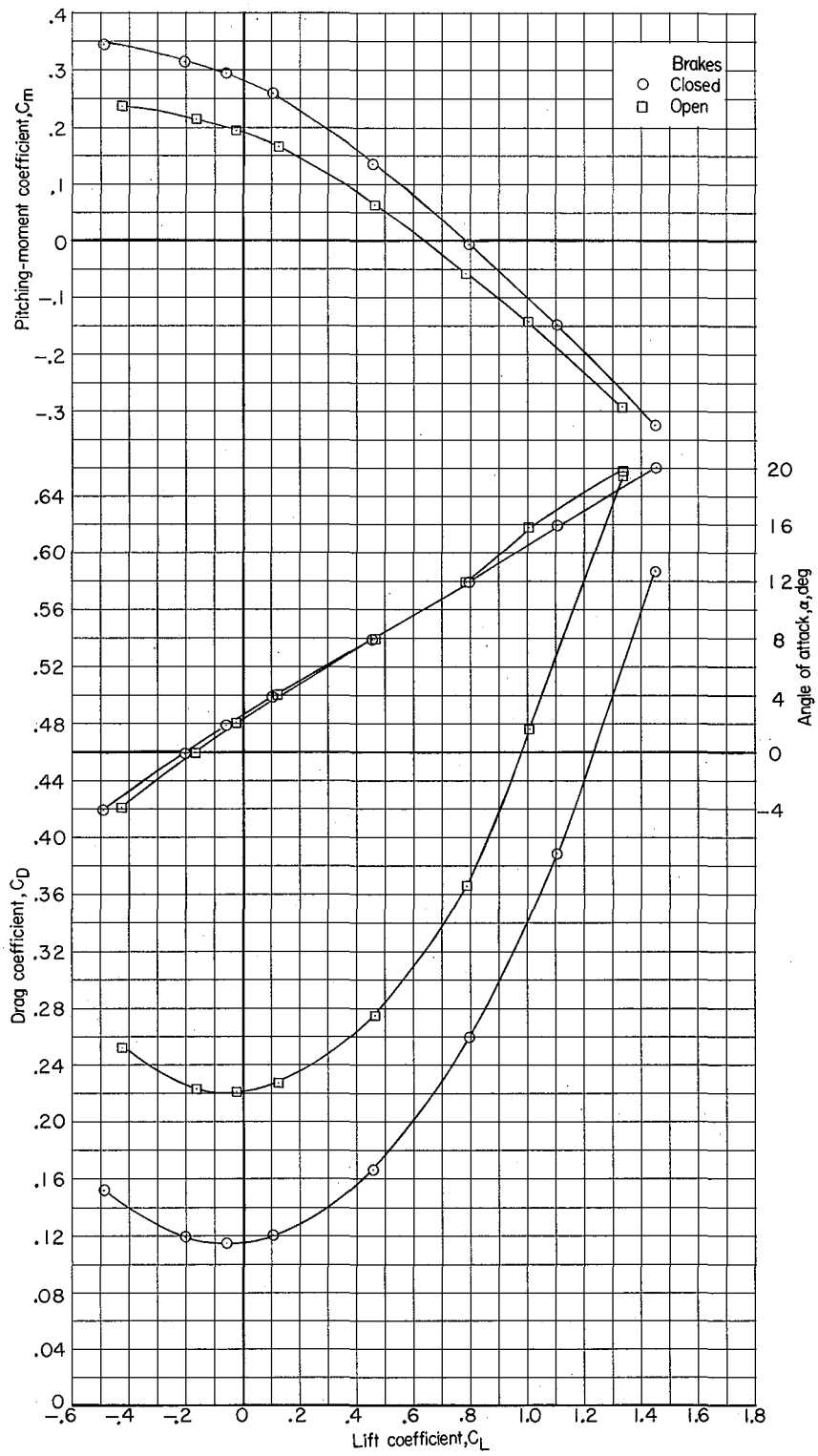

(b) M = 1.03.

Figure 10.- Continued.

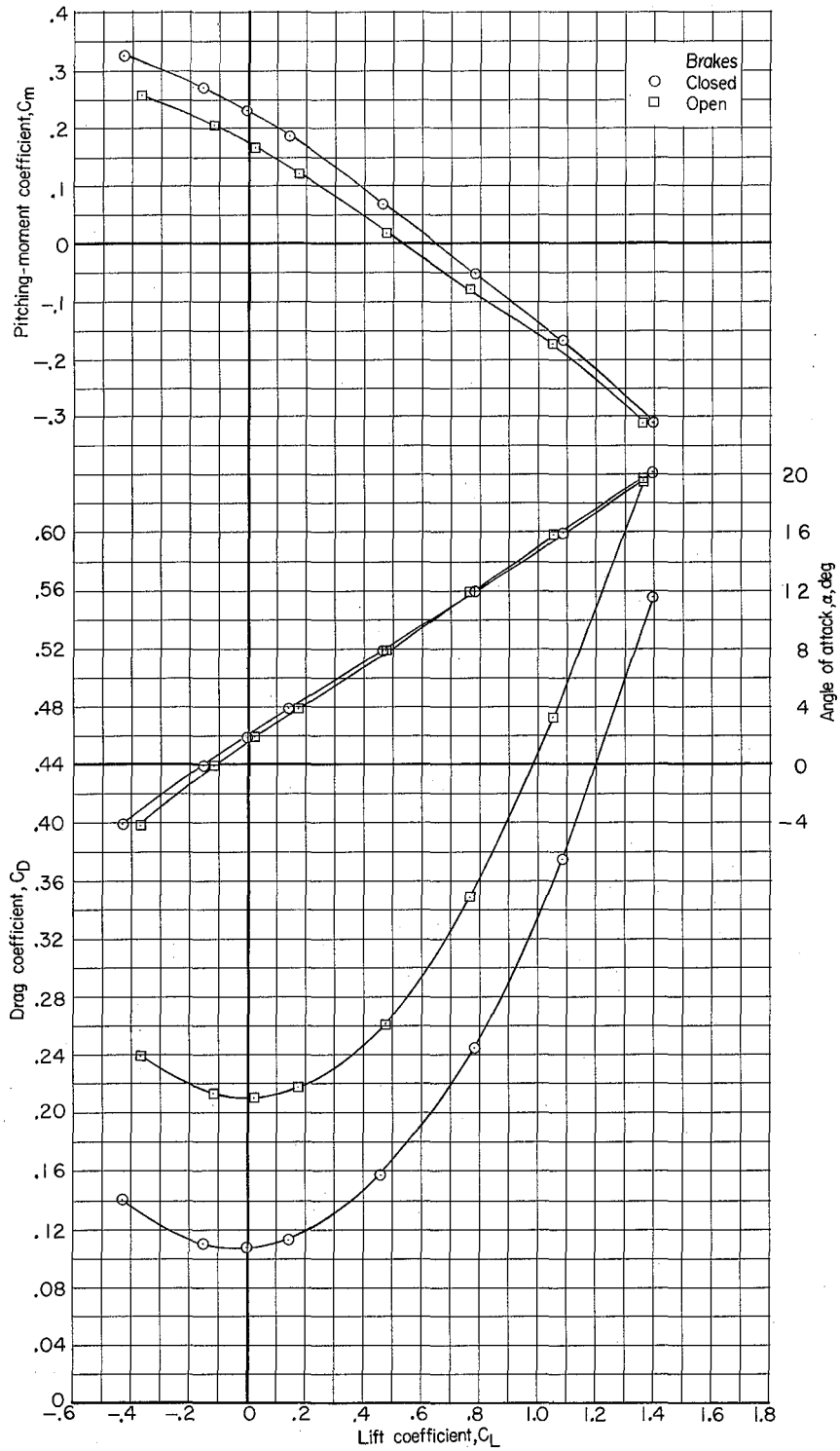

(c) M = 1.18.

Figure 10.- Concluded.

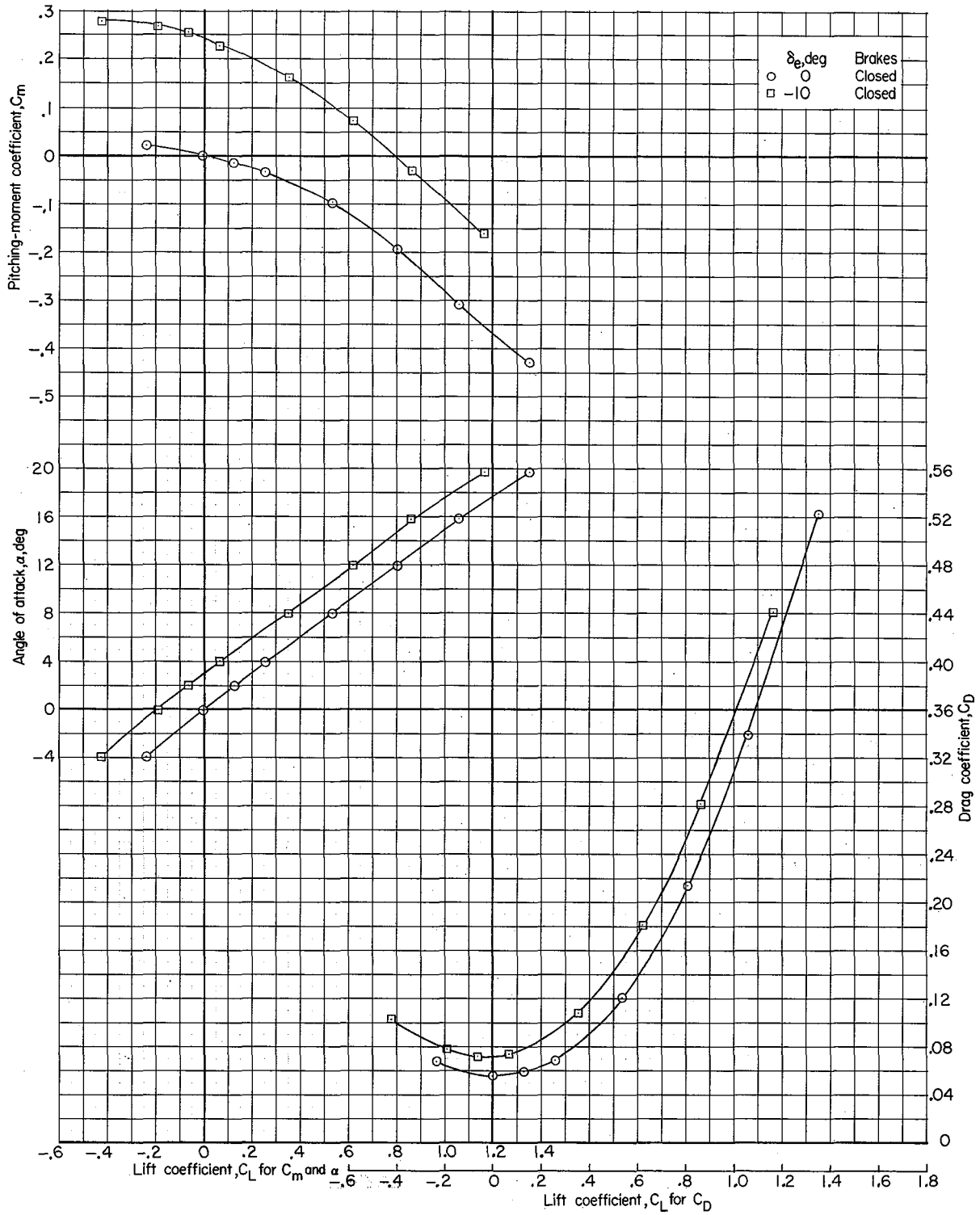

(a) M = 0.60.

Figure 11.- Longitudinal characteristics of model with various δ_e and with speed brakes open and closed. $\beta = 0^o$; $\delta_a = 0^o$; $\delta_r = -7.5^o$.

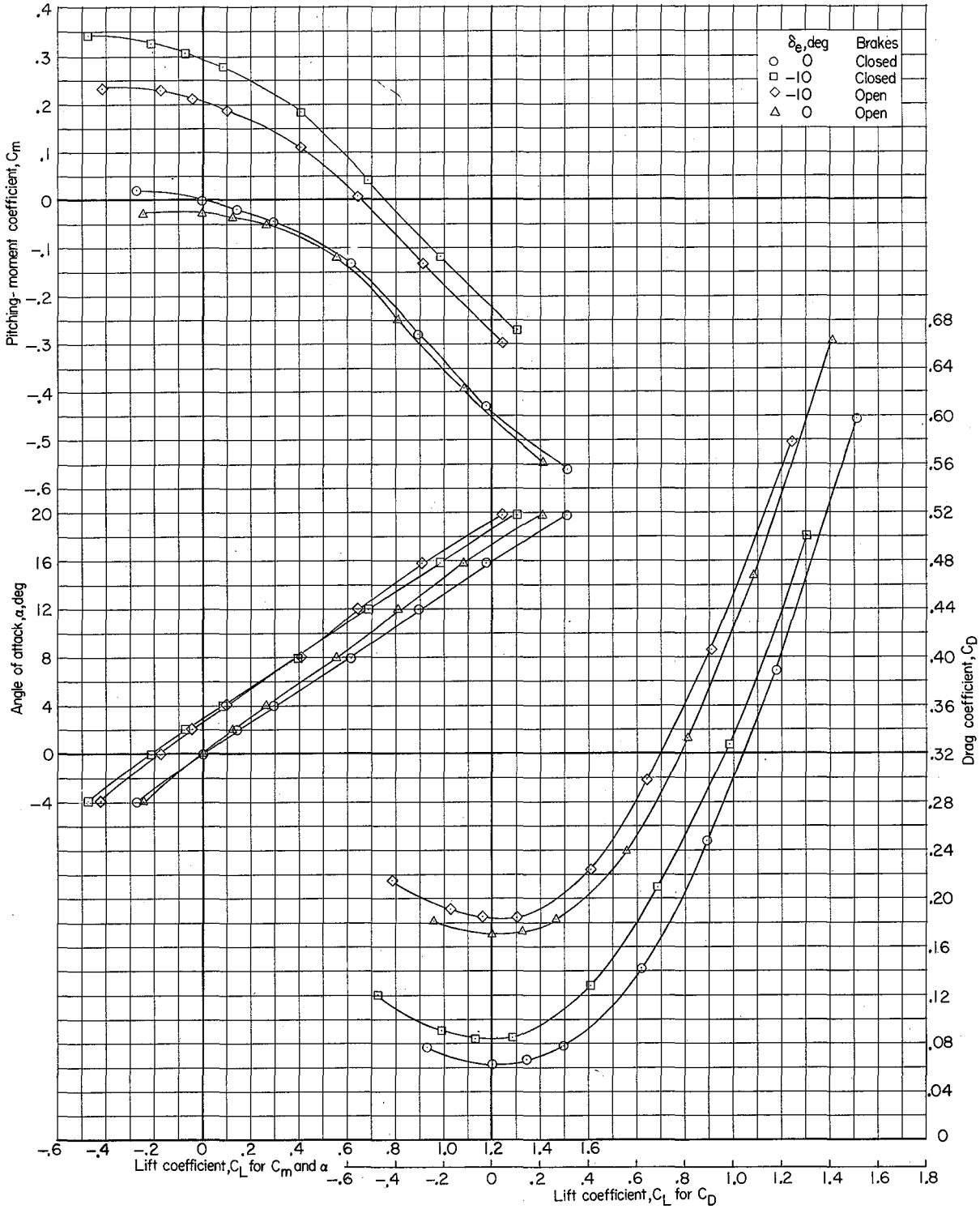

(b) M = 0.90.

Figure 11.- Continued.

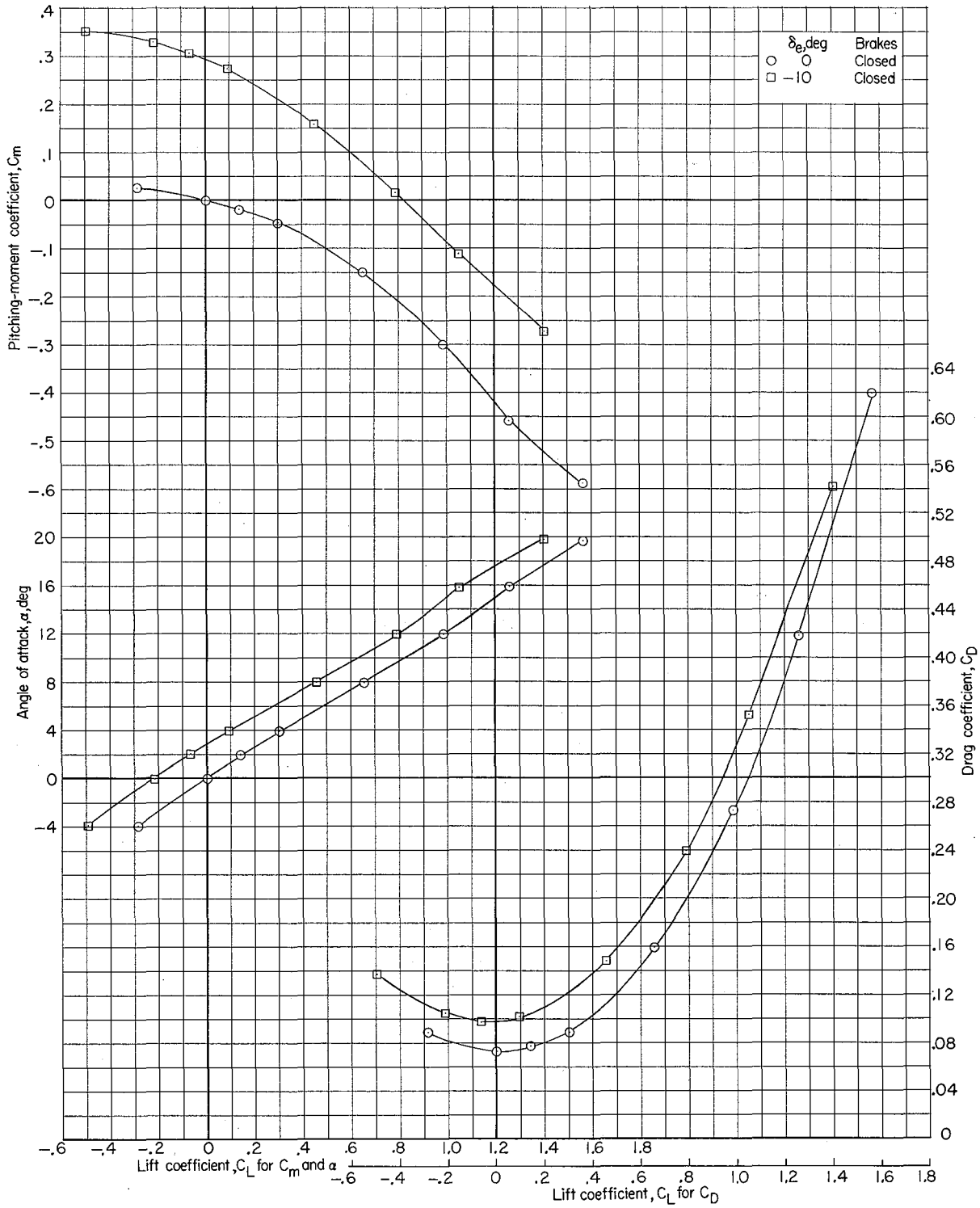

(c) M = 0.95.

Figure 11.- Continued.

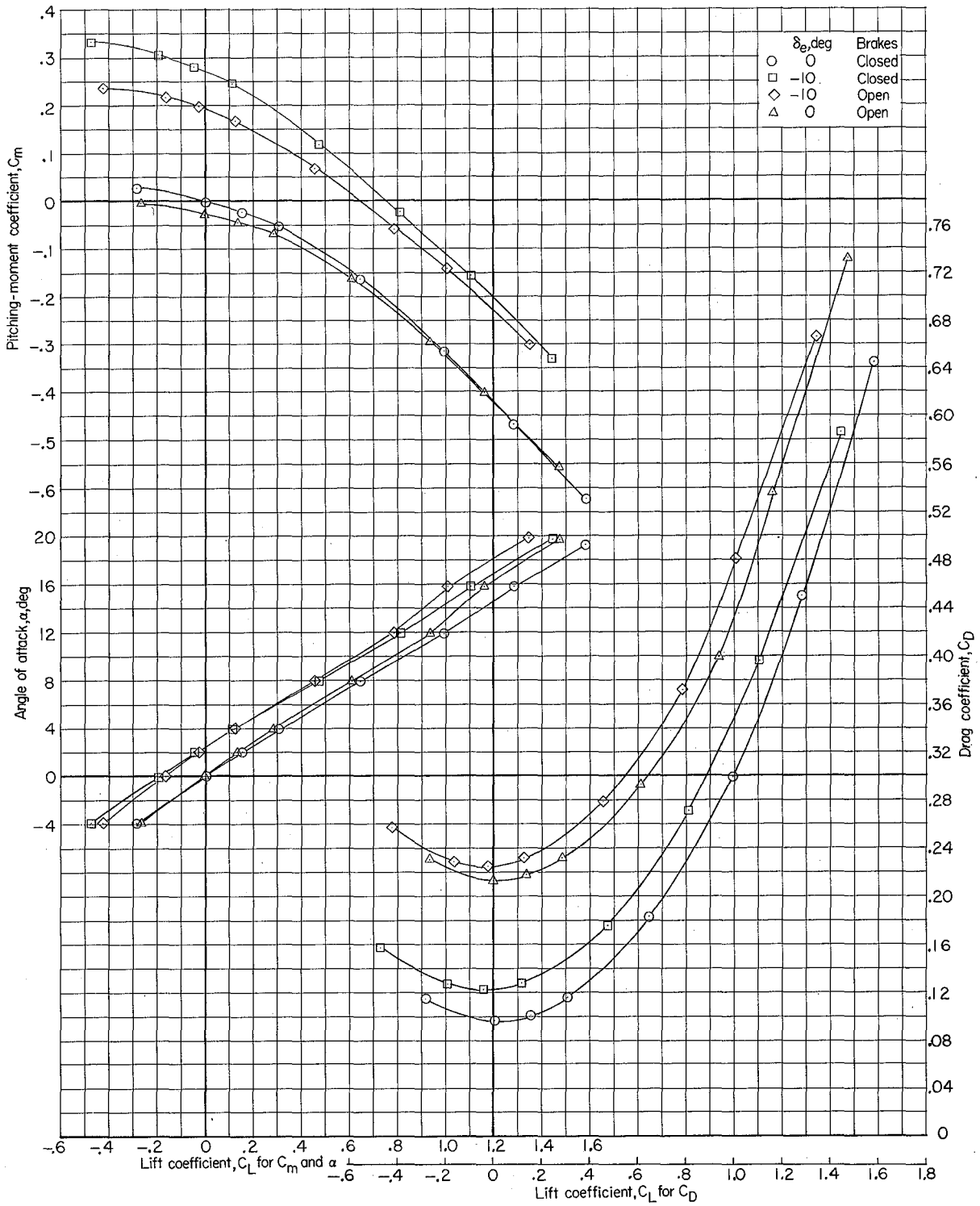

(d) M = 1.03.

Figure 11.- Continued.

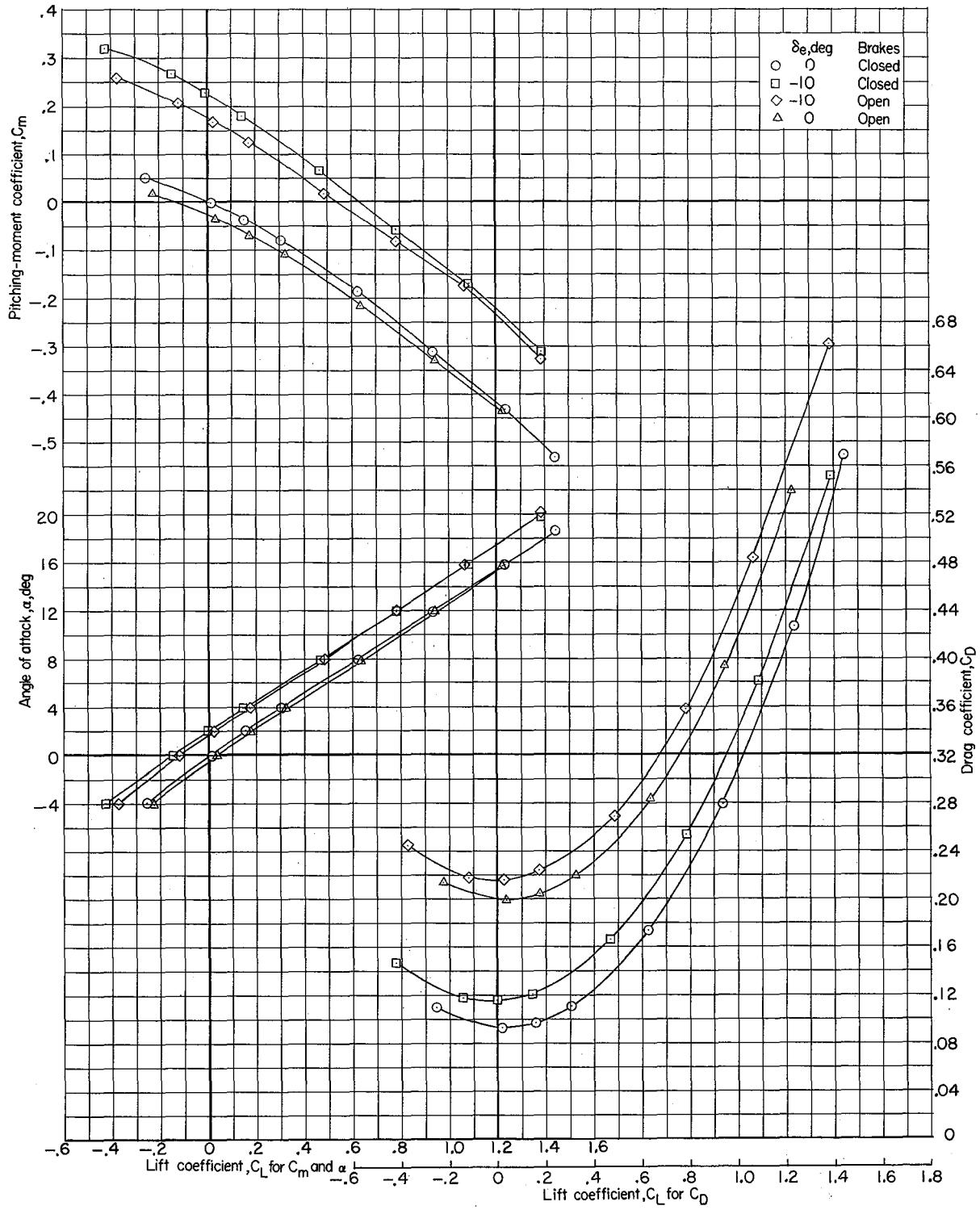

(e) M = 1.18.

Figure 11.- Concluded.

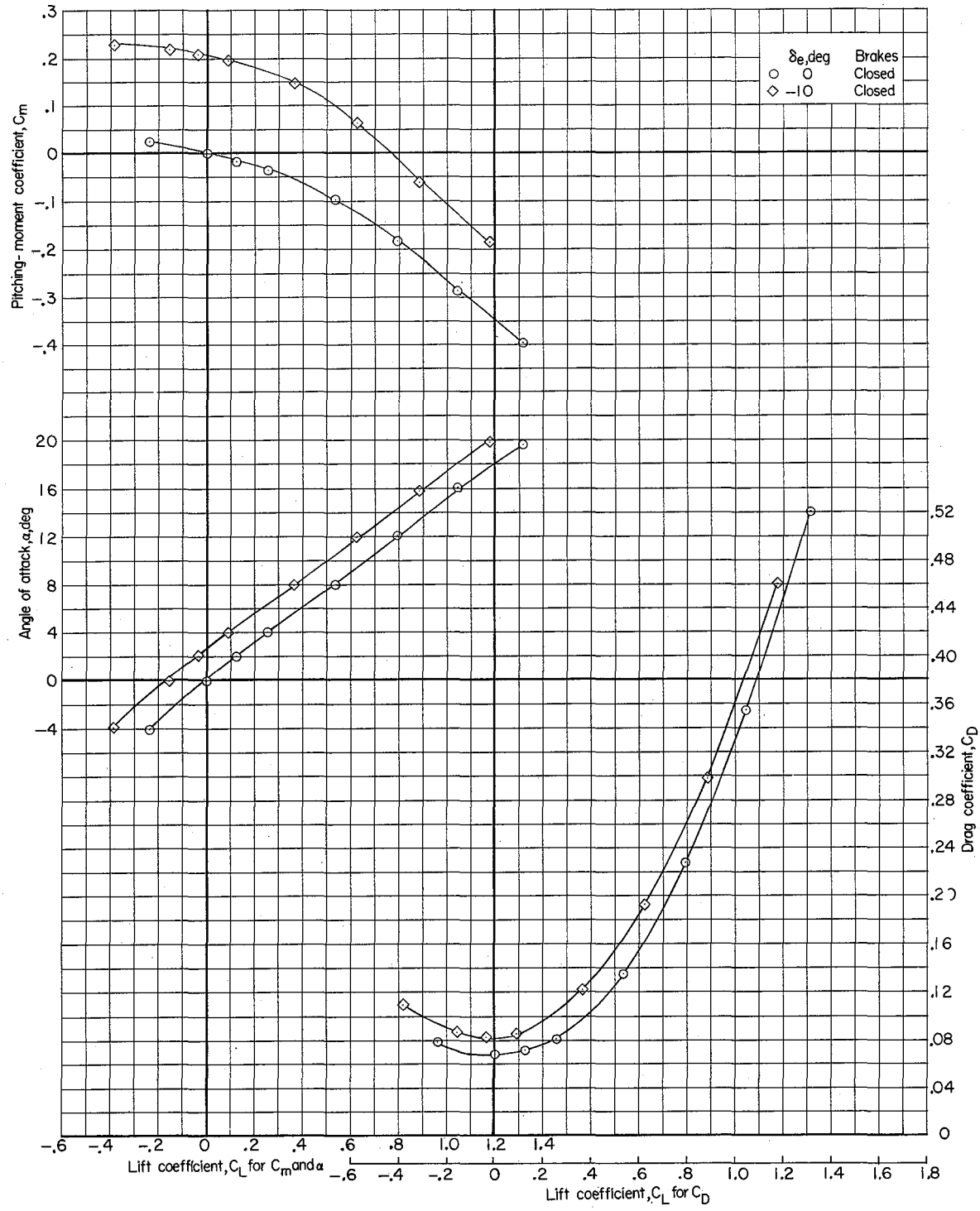

(a) M = 0.60.

Figure 12.- Longitudinal characteristics of model with various δ_e and with speed brakes open and closed. $\beta = 0^\circ$; $\delta_a = 20^\circ$; $\delta_v = 0^\circ$.

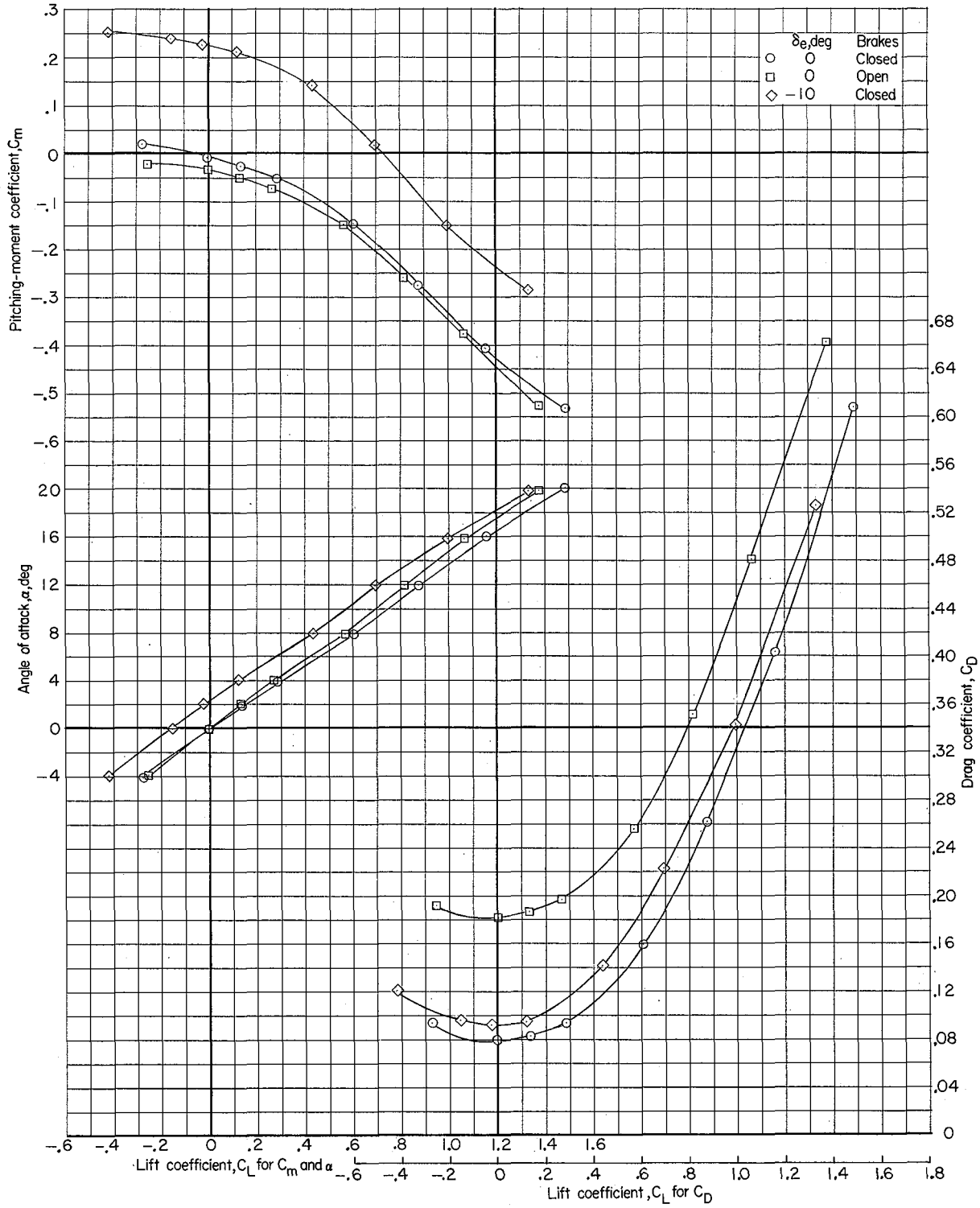

(b) M = 0.90.

Figure 12.- Continued.

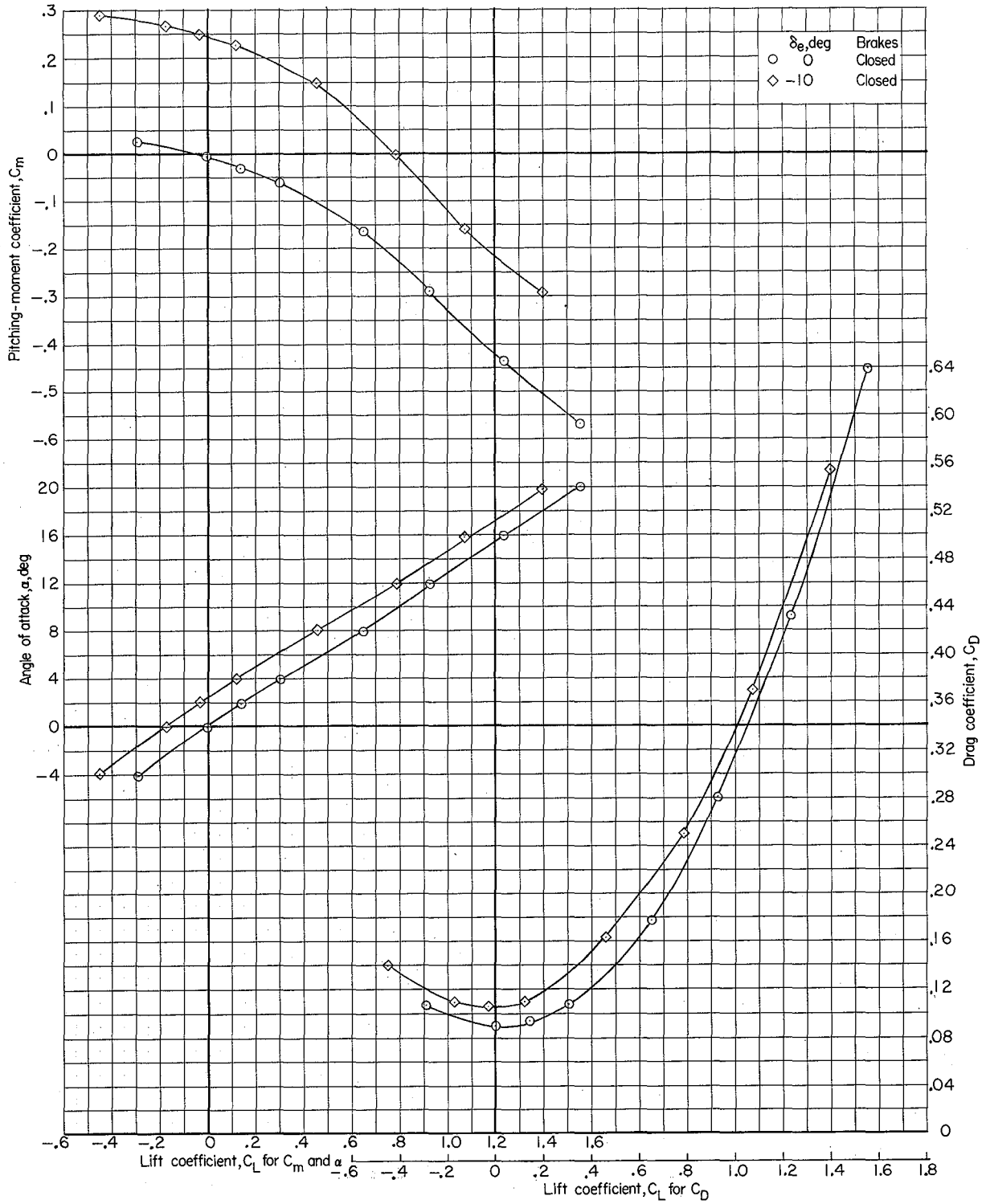

(c) M = 0.95.

Figure 12.- Continued.

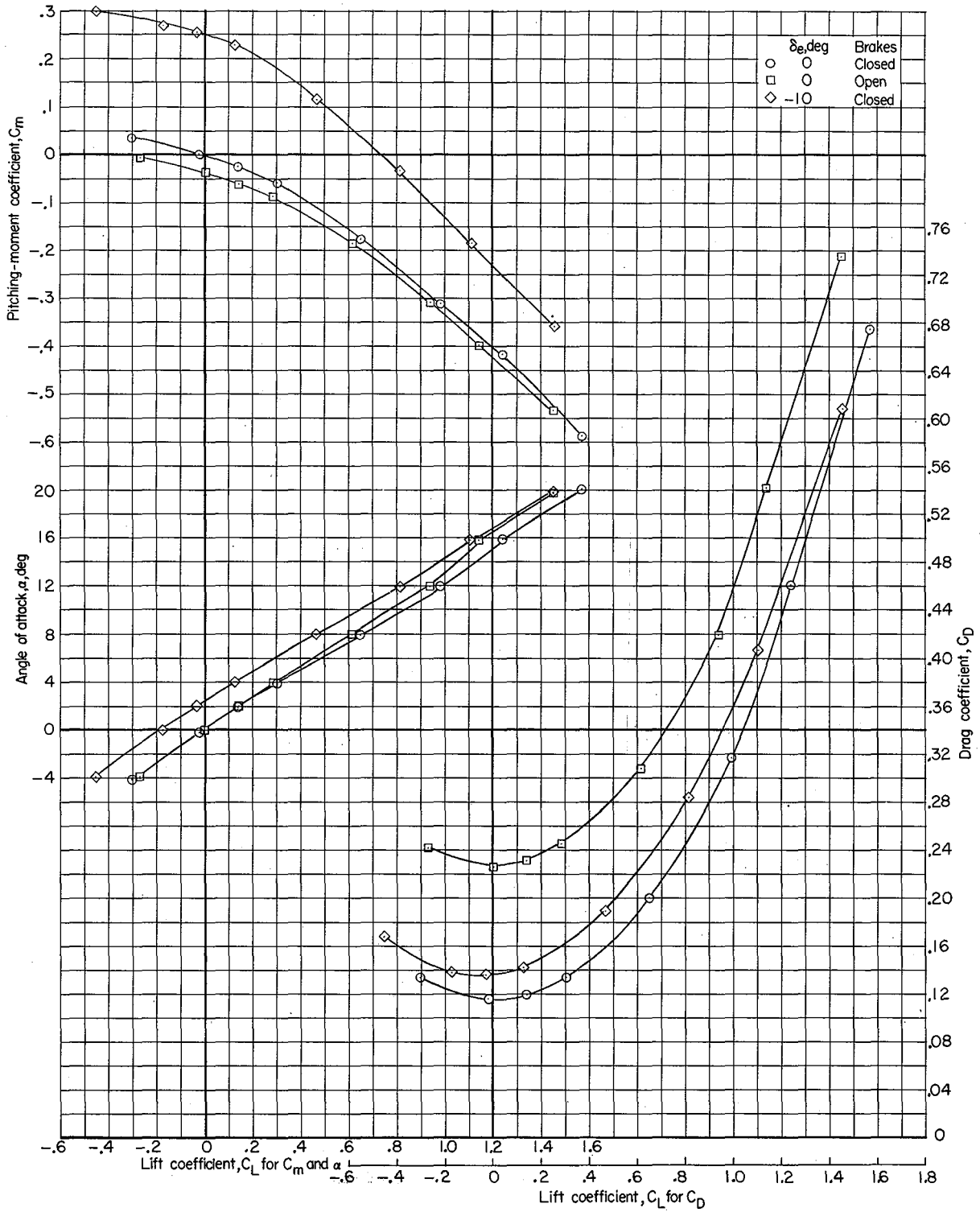

(d) M = 1.03.

Figure 12.- Continued.

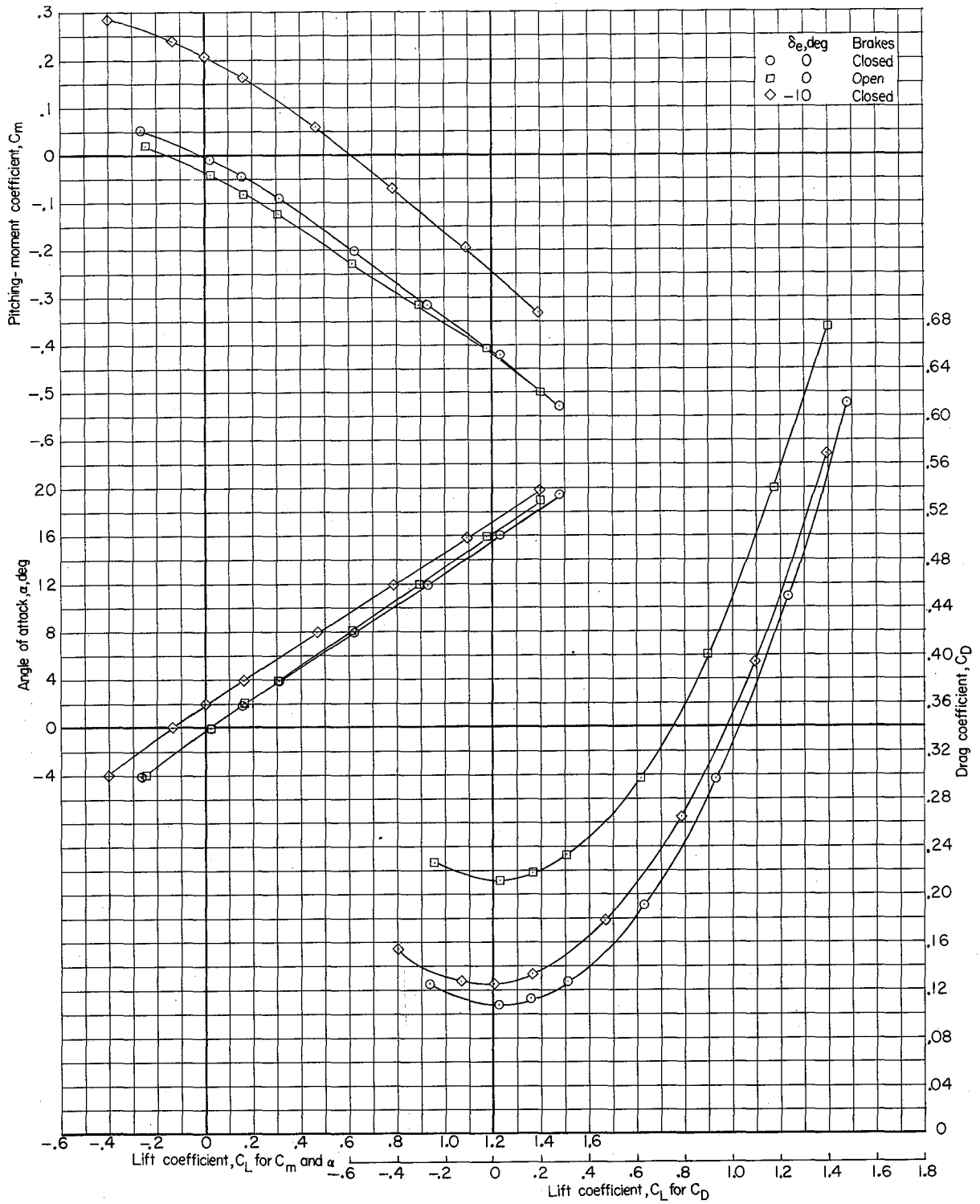

(e) M = 1.18.

Figure 12.- Concluded.

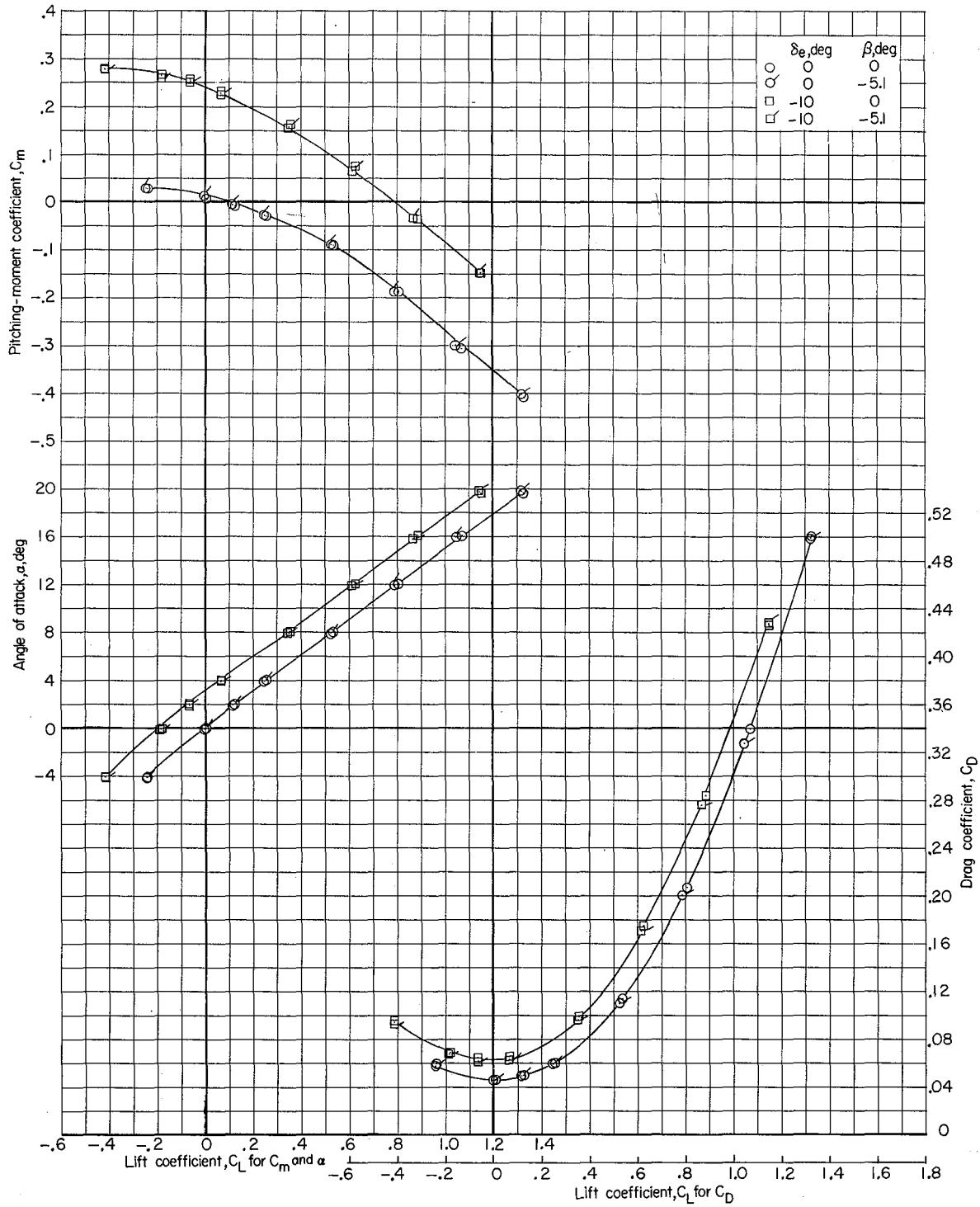

(a) M = 0.60.

Figure 13.- Longitudinal characteristics of complete model at $\beta = 0^\circ$ and -5.1°. $\delta_e = 0^\circ$ and -10°; other surfaces undeflected.

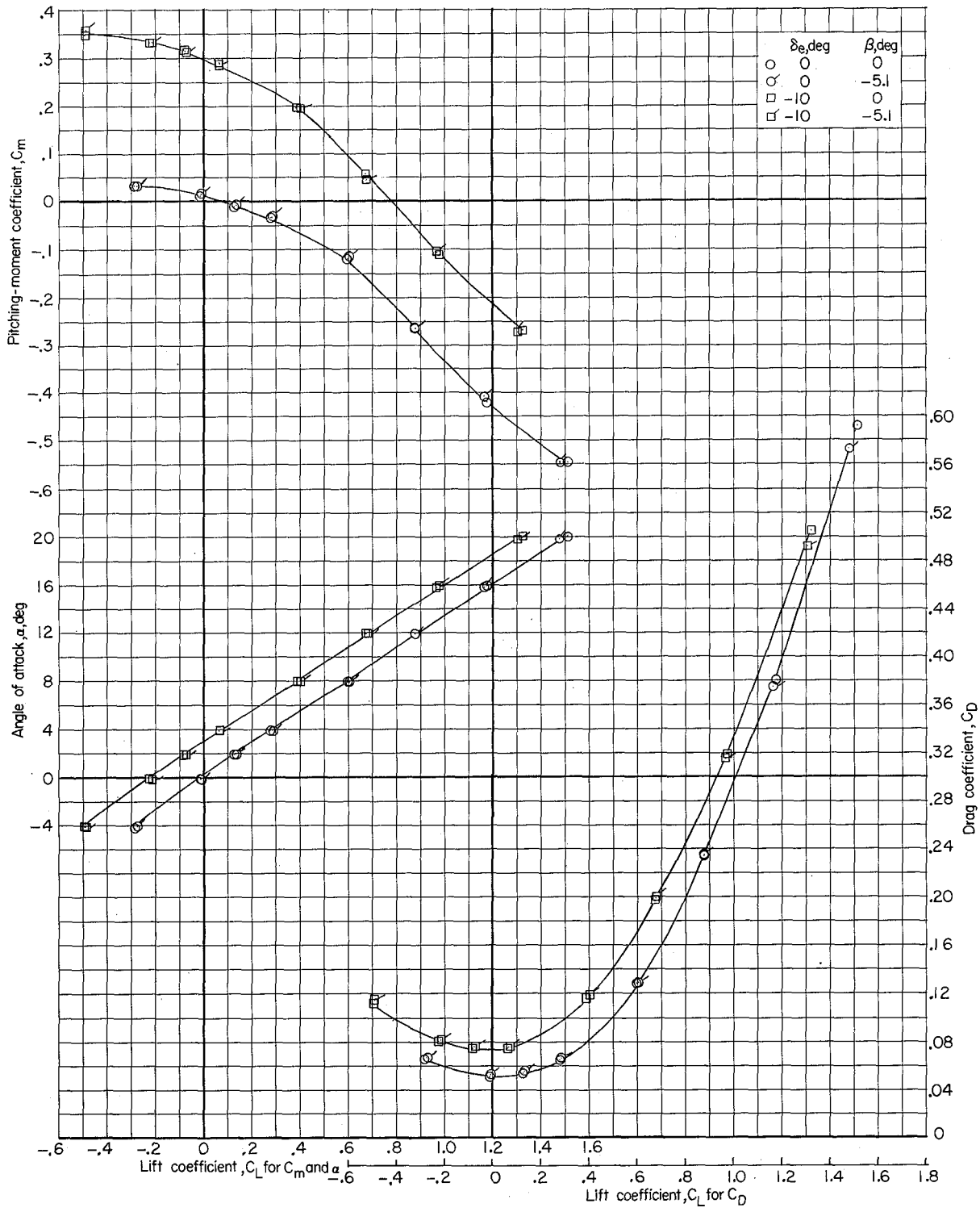

(b) M = 0.90.

Figure 13.- Continued.

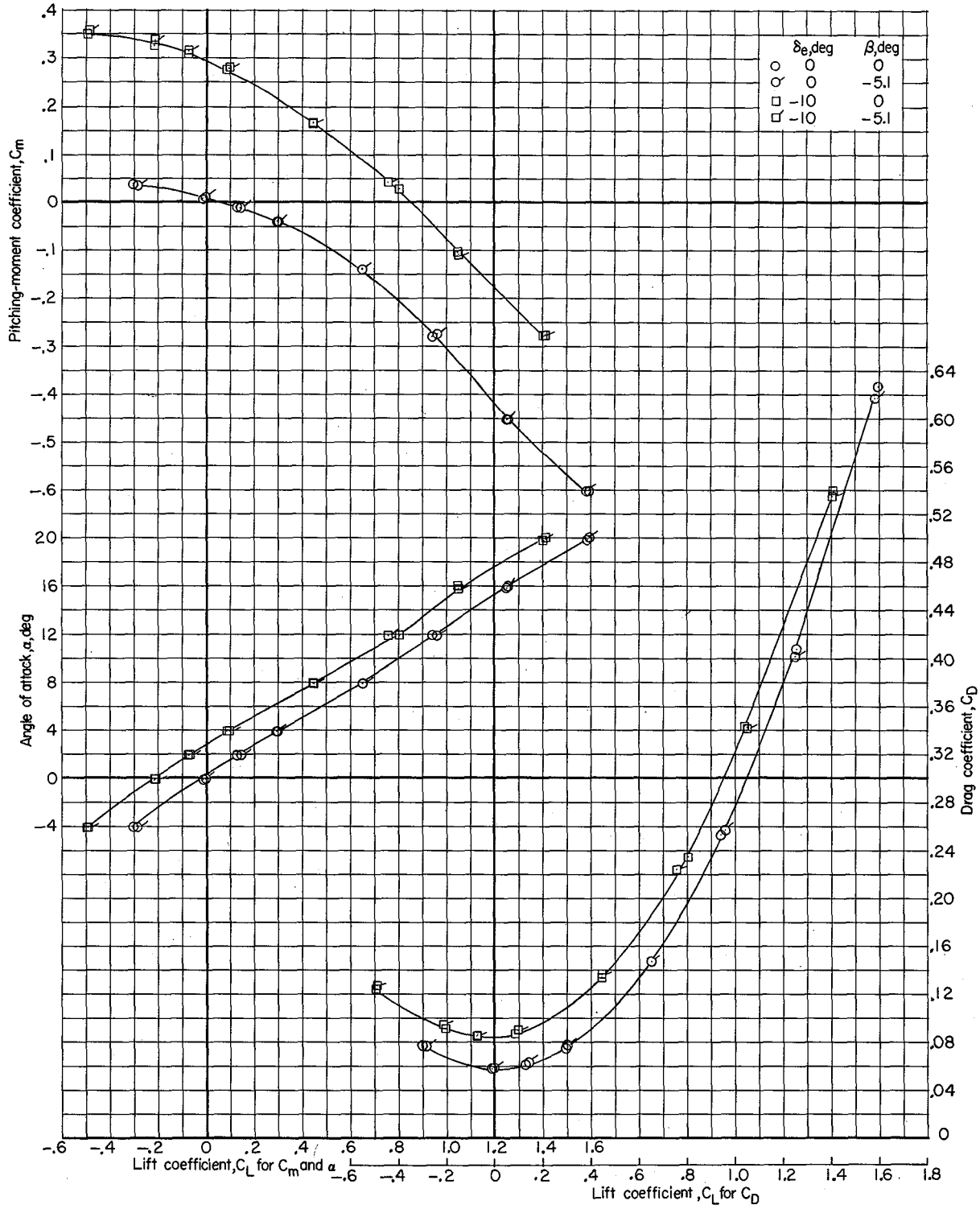

(c) M = 0.95.

Figure 13.- Continued.

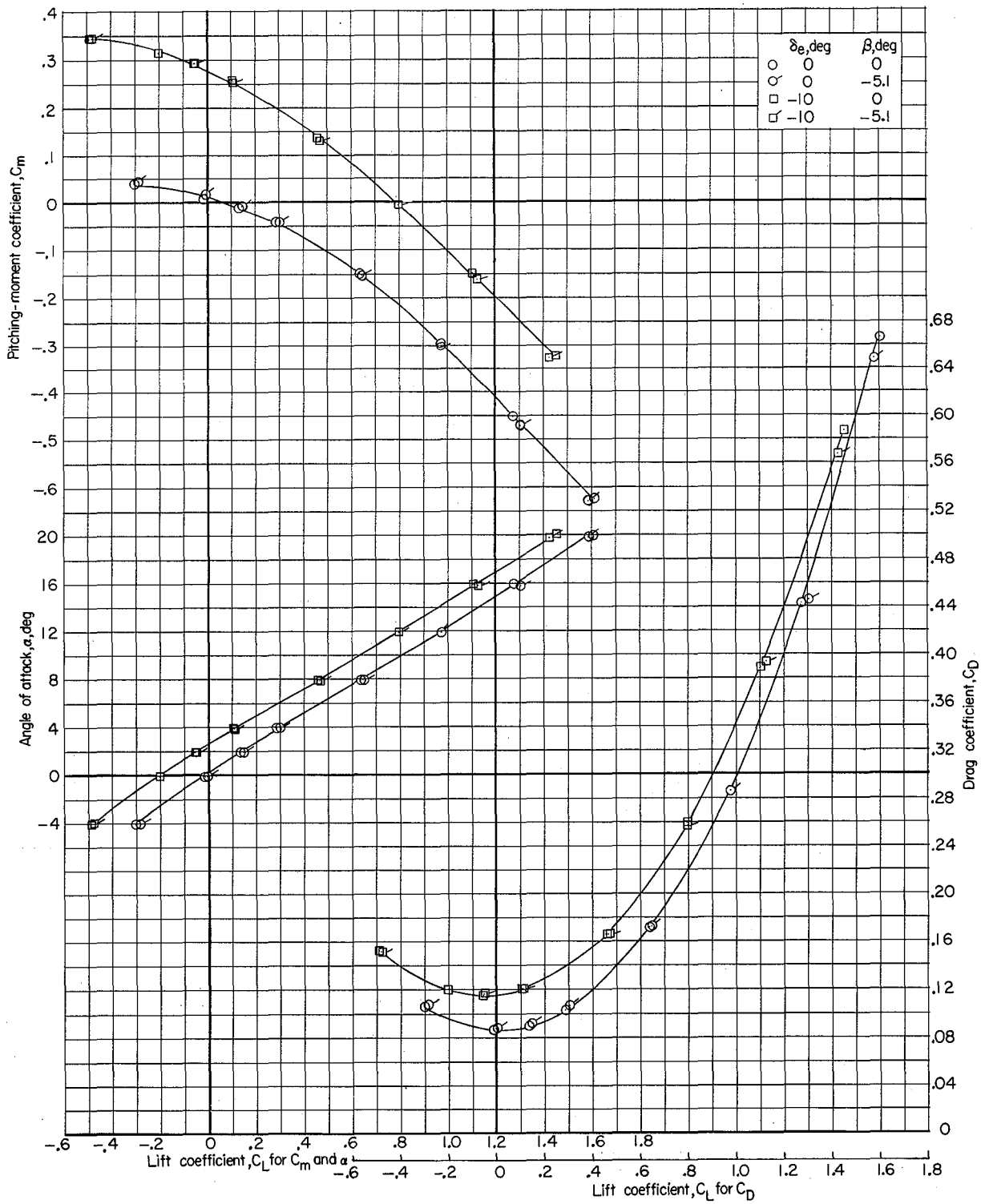

(d) M = 1.03.

Figure 13.- Continued.

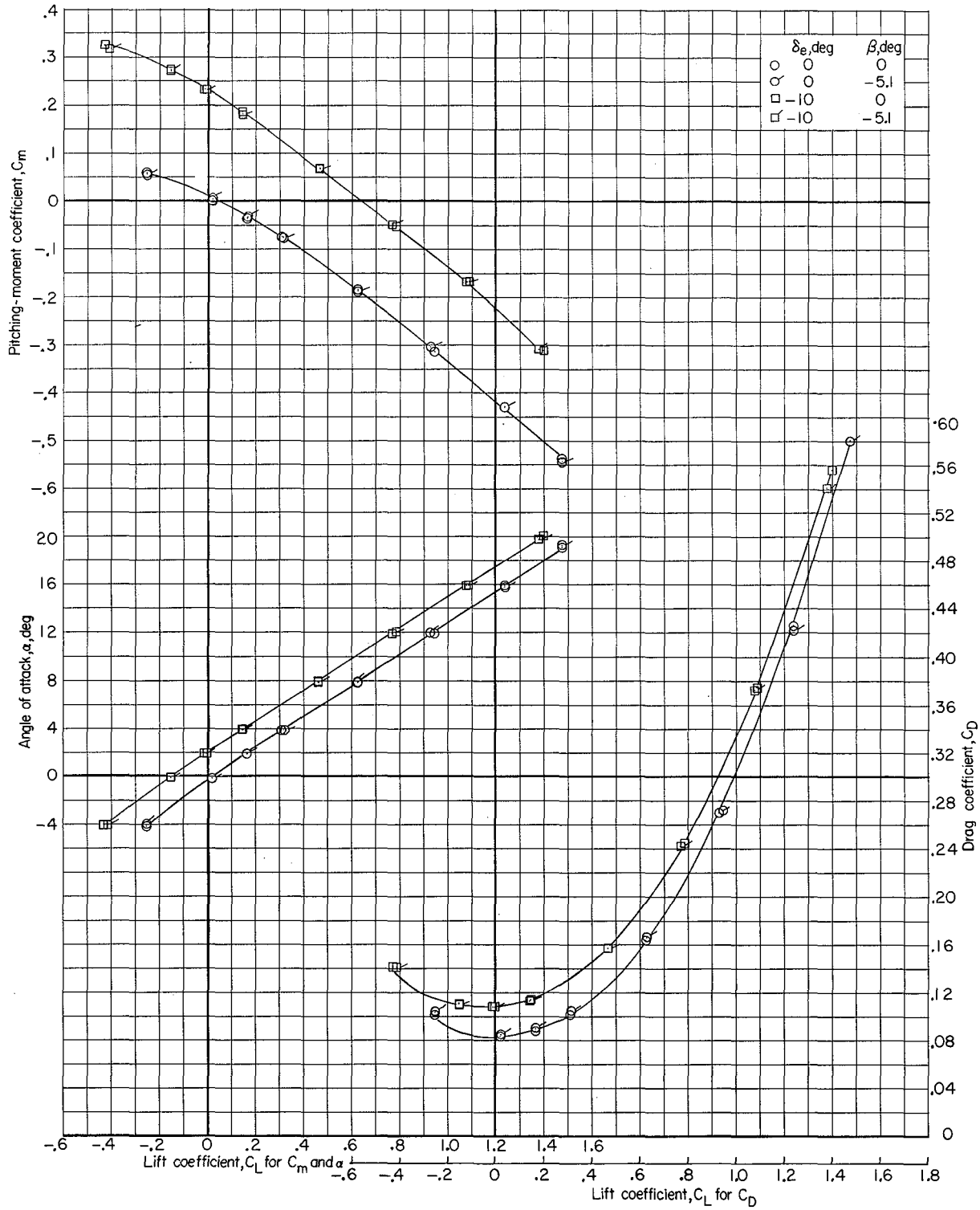

(e) M = 1.18.

Figure 13.- Concluded.

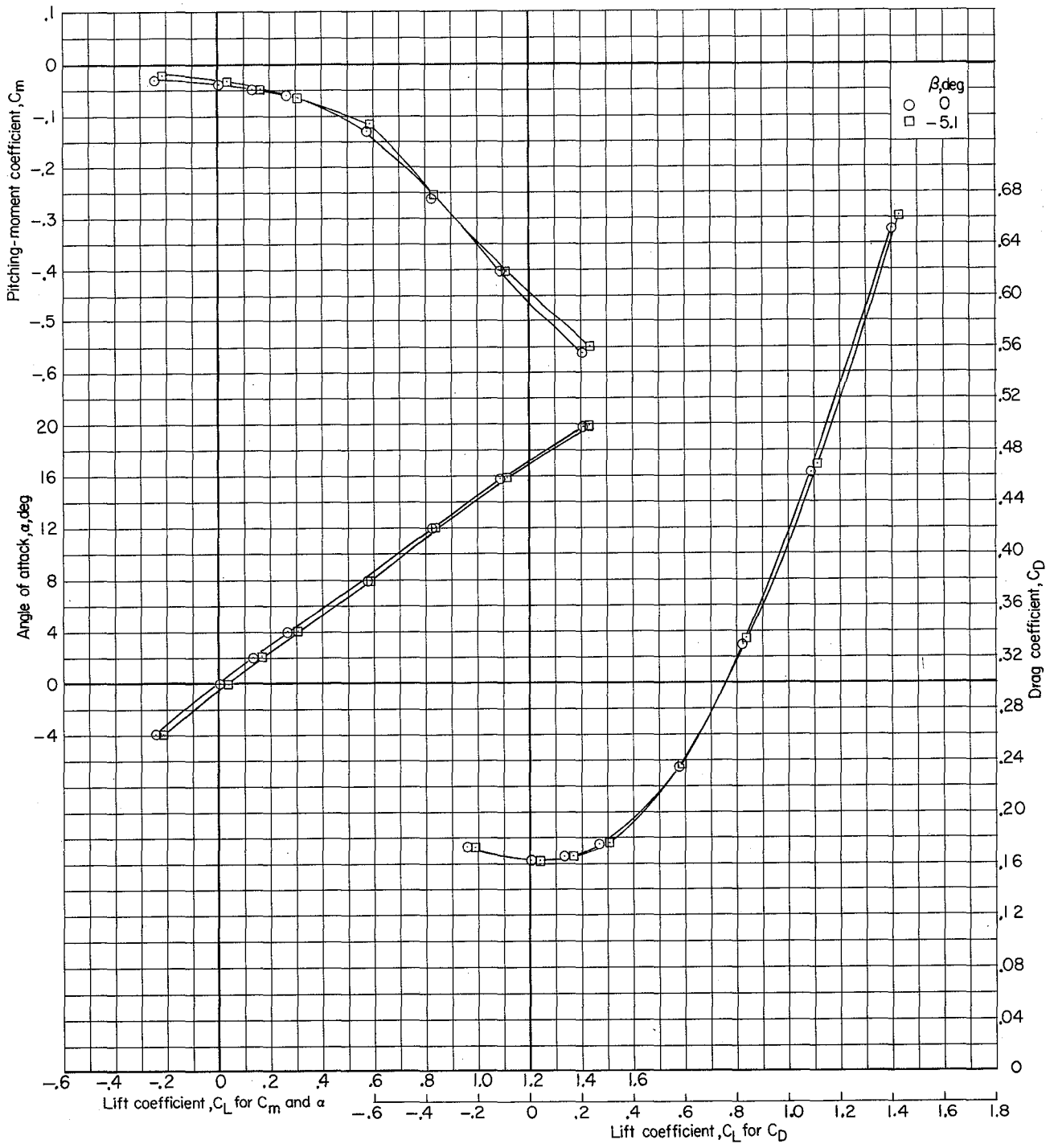

(a) M = 0.90.

Figure 14.- Longitudinal characteristics of complete model with speed brakes open; other surfaces undeflected. $\beta = 0^\circ$ and -5.1°.

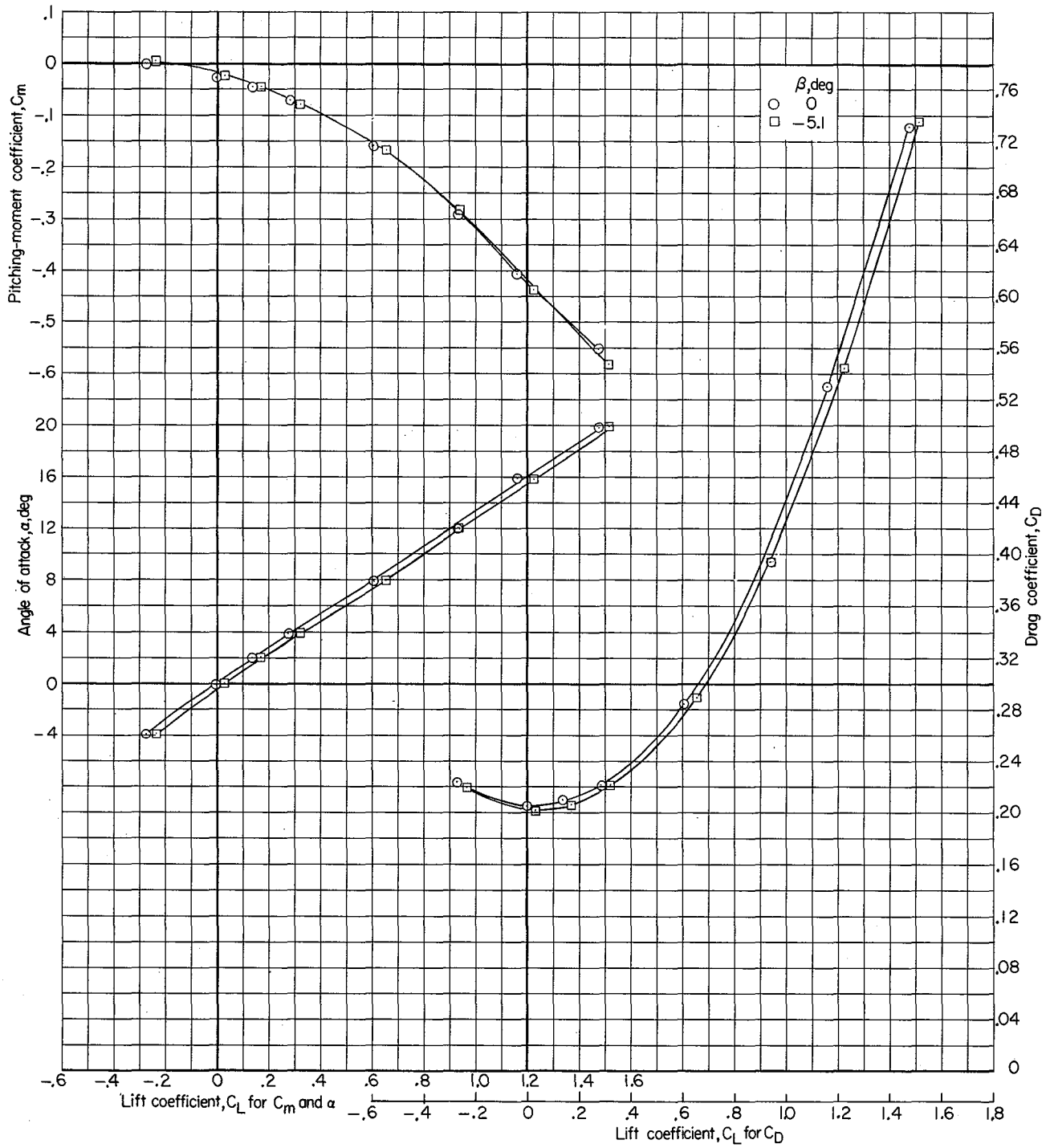

(b) M = 1.03.

Figure 14.- Continued.

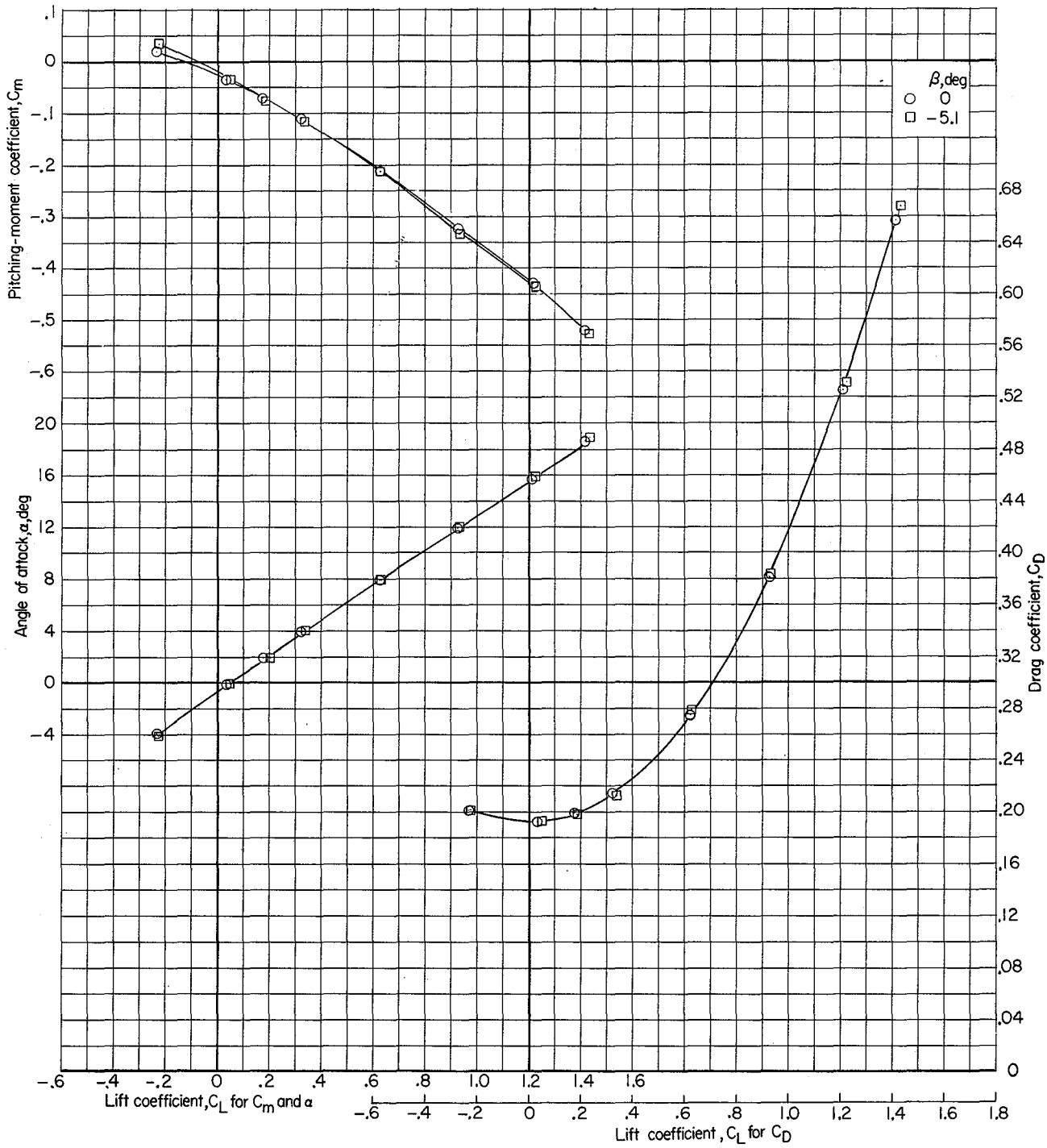

(c) M = 1.18.

Figure 14.- Concluded.

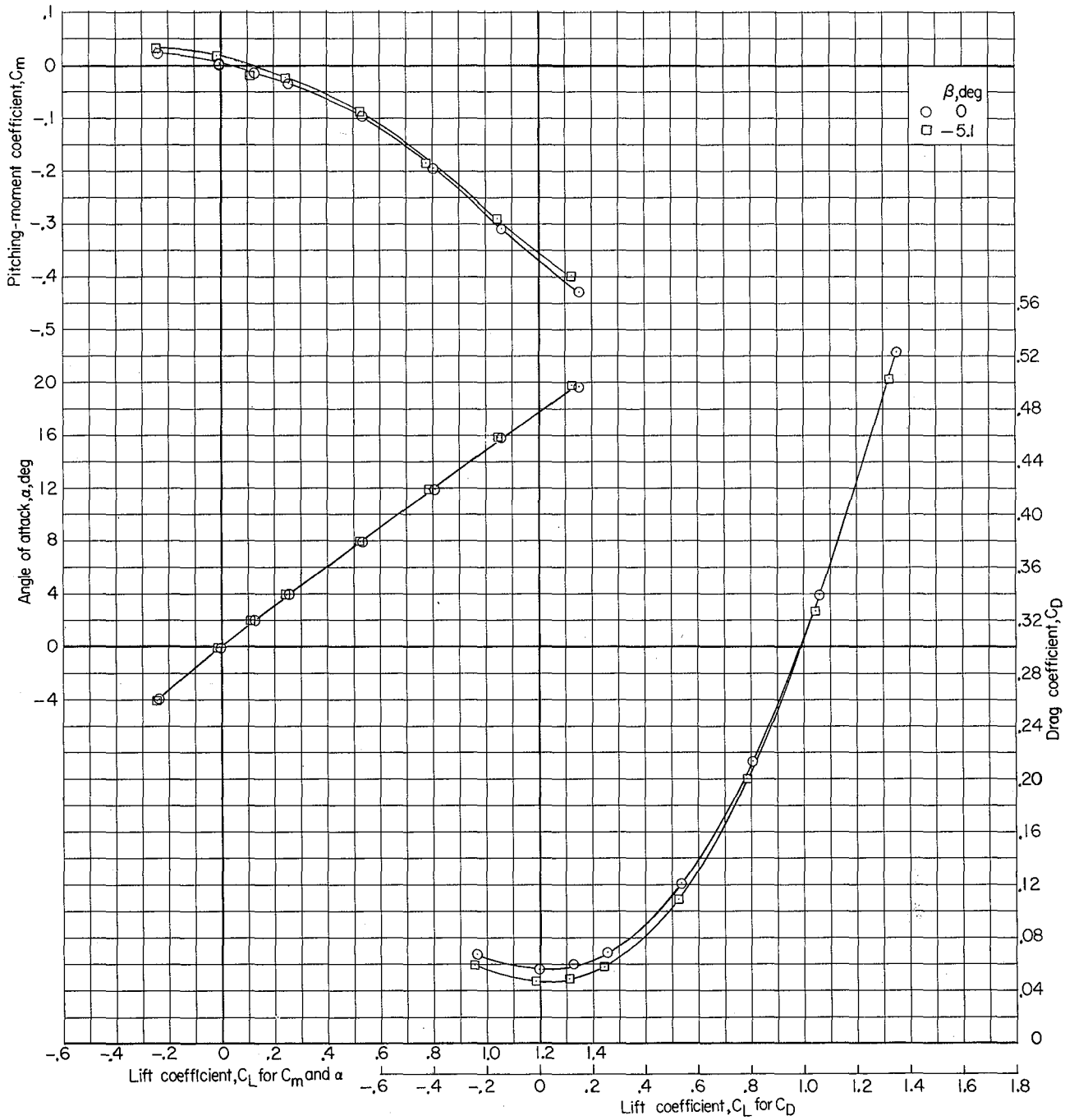

(a) M = 0.60.

Figure 15.- Longitudinal characteristics of complete model at $\beta = 0^\circ$ and -5.1°. $\delta_v = -7.5^\circ$; other surfaces undeflected.

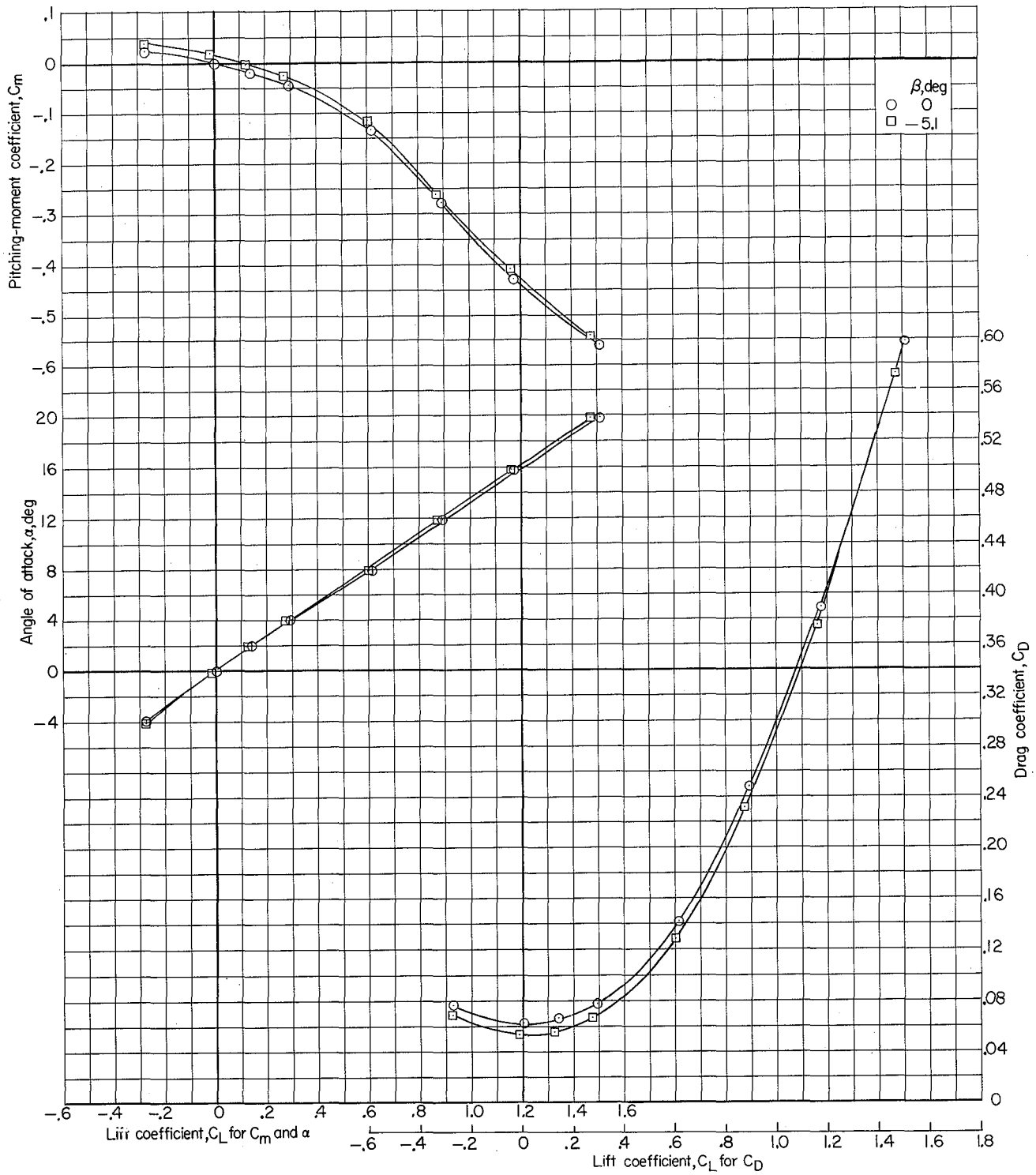

(b) M = 0.90.

Figure 15.- Continued.

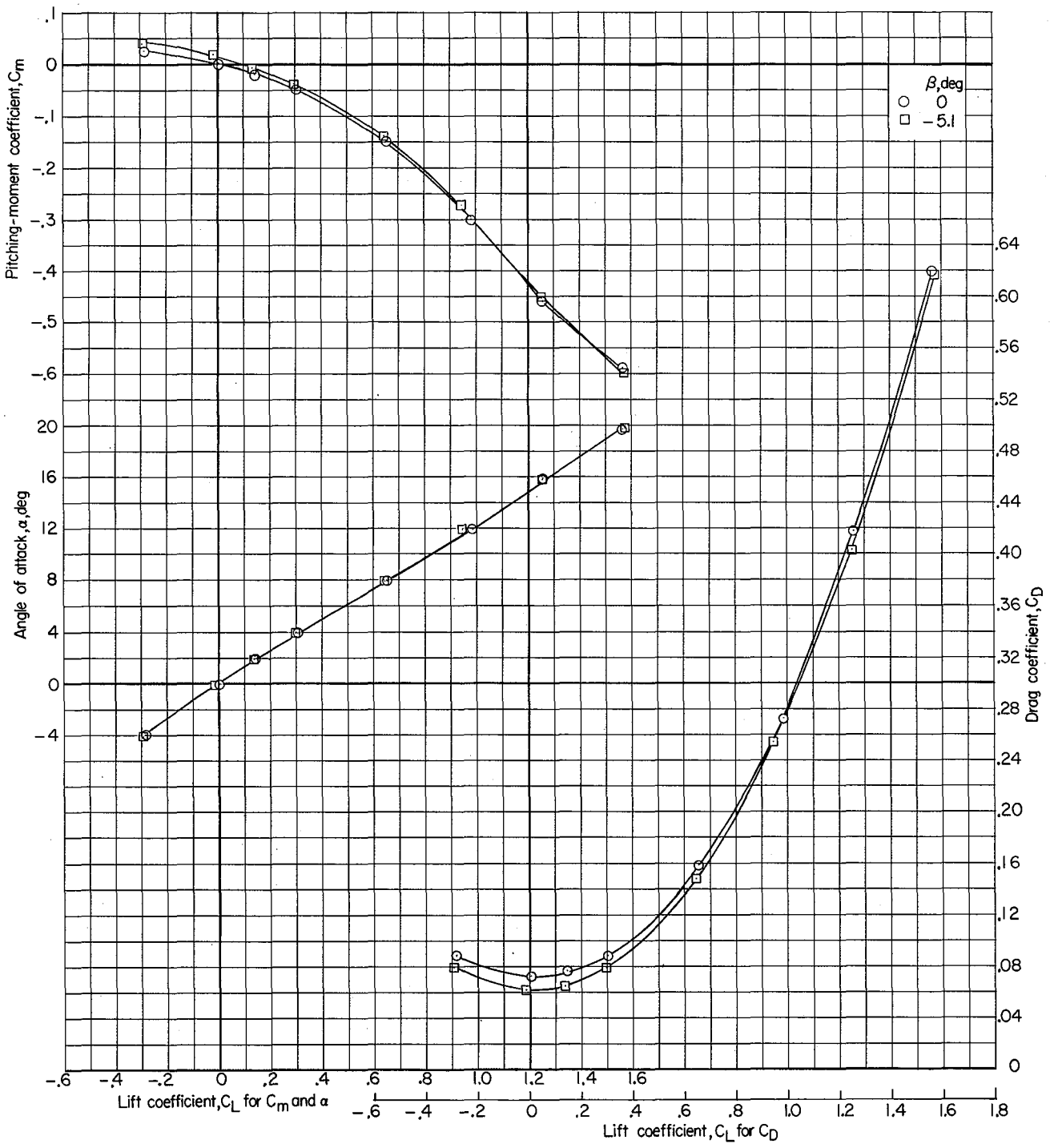

(c) M = 0.95.

Figure 15.- Continued.

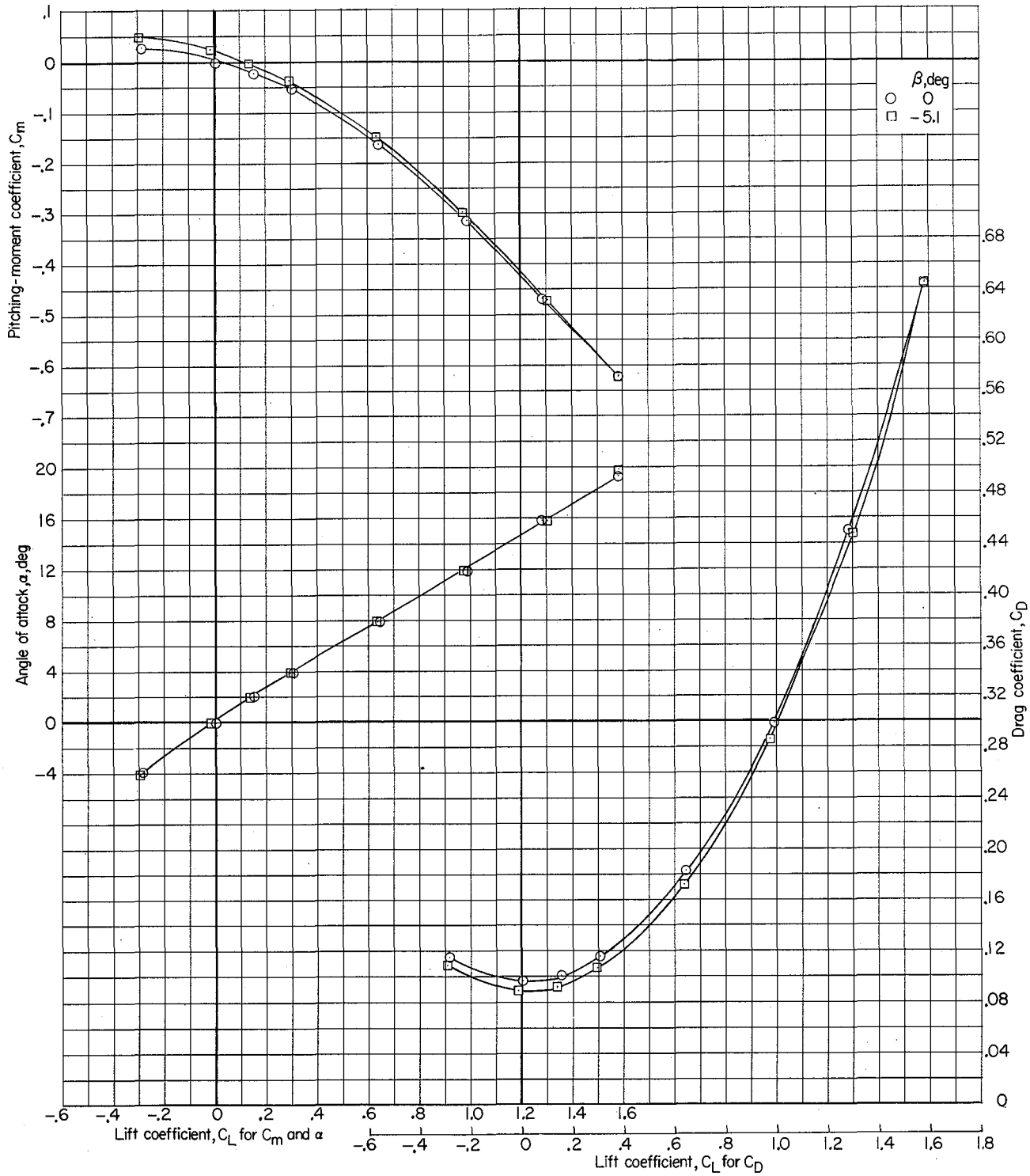

(d) M = 1.03.

Figure 15.- Continued.

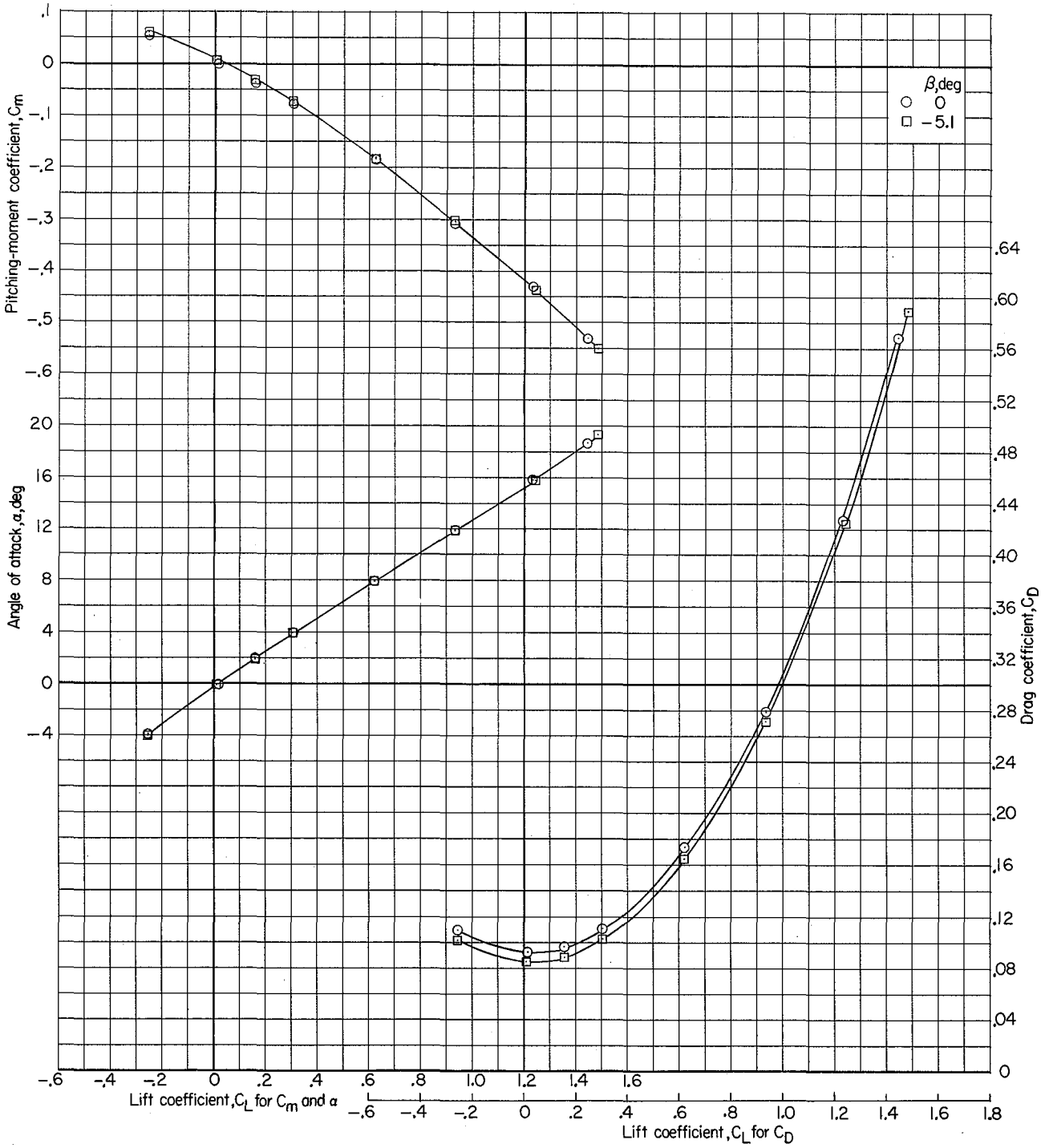

(e) M = 1.18.

Figure 15.- Concluded.

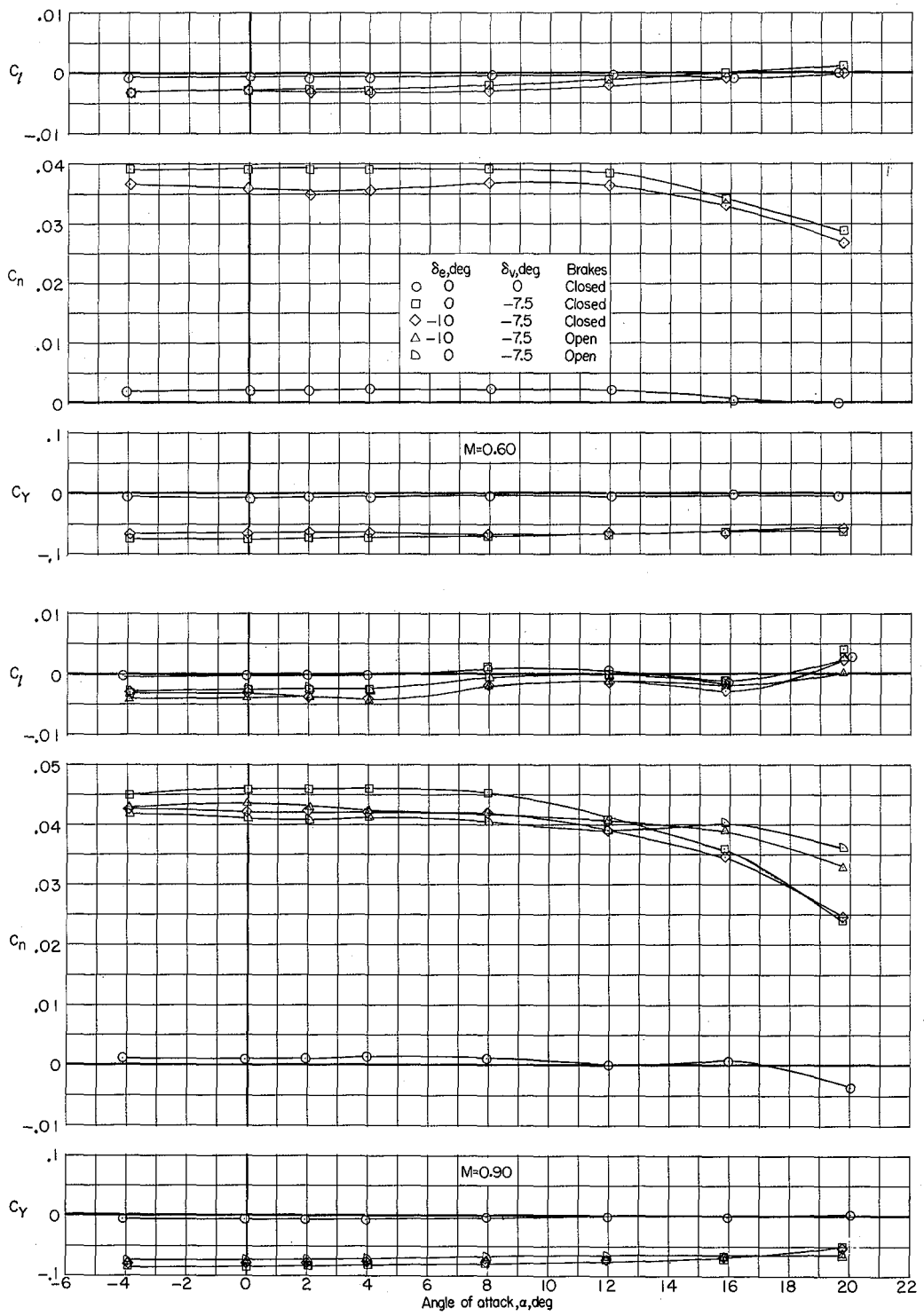

(a) M = 0.60 and 0.90.

Figure 16.- Lateral-directional characteristics of complete model with various δ_e and δ_v and with speed brakes open and closed. $\beta = 0^o$; $\delta_a = 0^o$.

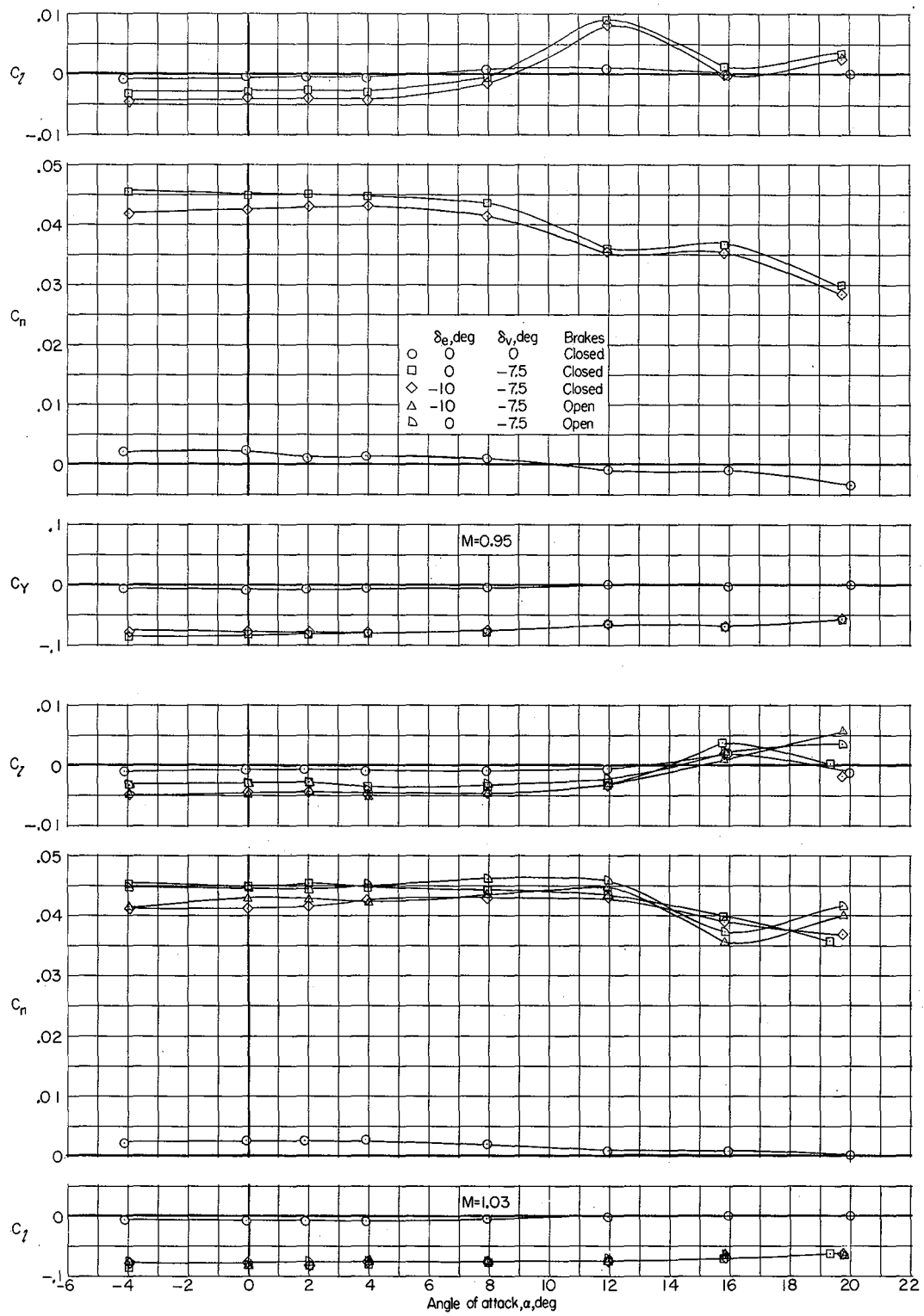

(b) M = 0.95 and 1.03.

Figure 16.- Continued.

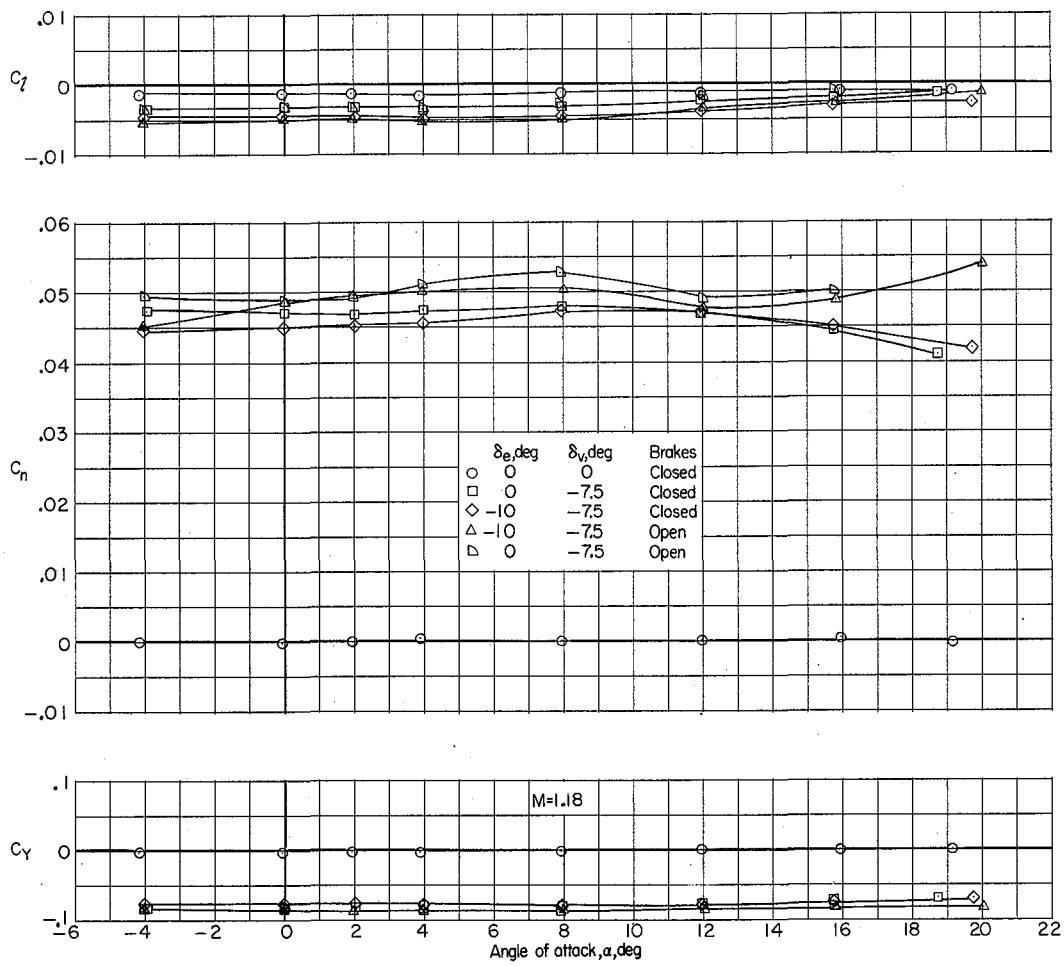

(c) M = 1.18.

Figure 16.- Concluded.

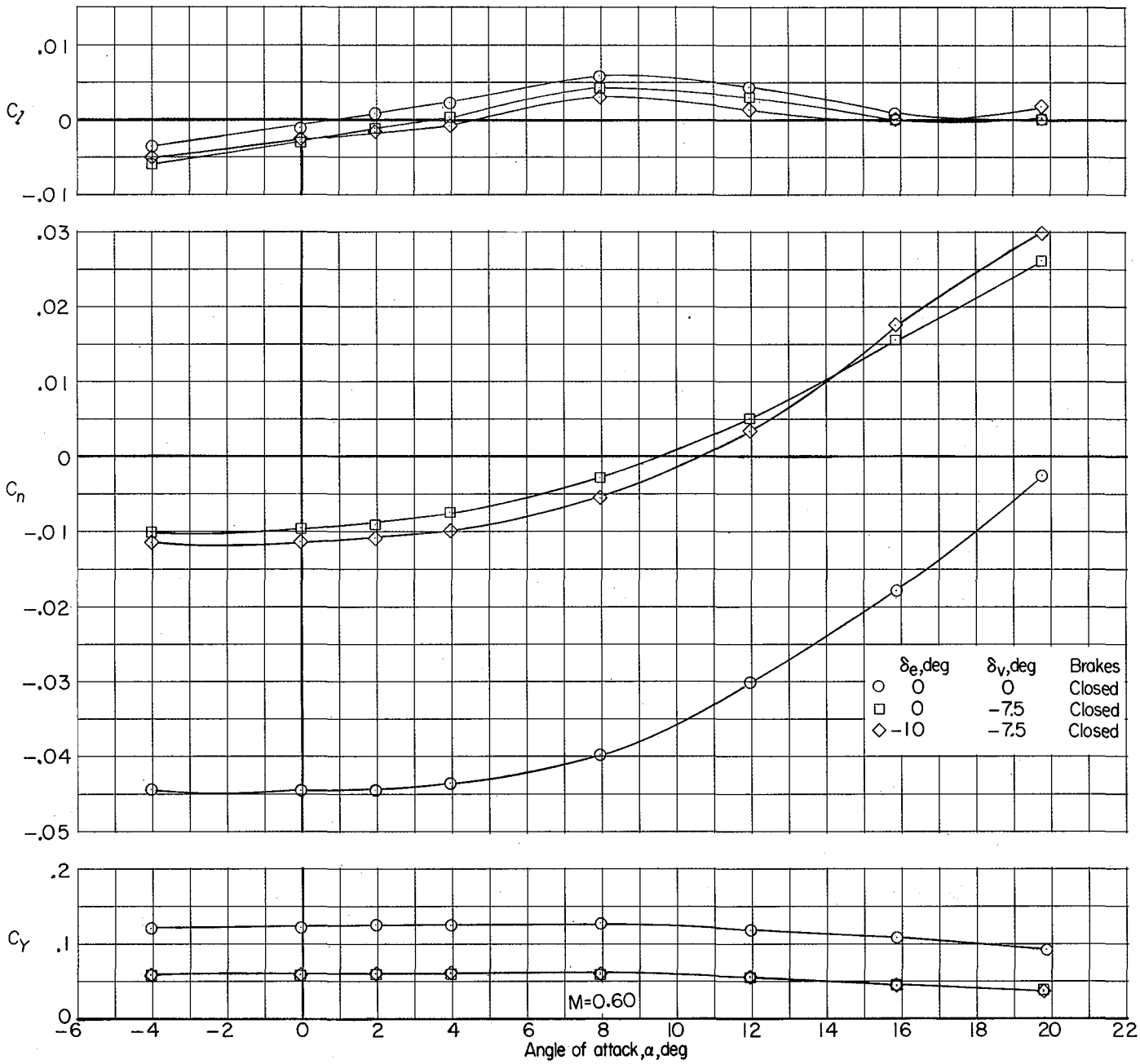

(a) M = 0.60.

Figure 17.- Lateral-directional characteristics of complete model with various δ_e and δ_v and with speed brakes open and closed. $\beta = -5.1^\circ$; $\delta_a = 0^\circ$.

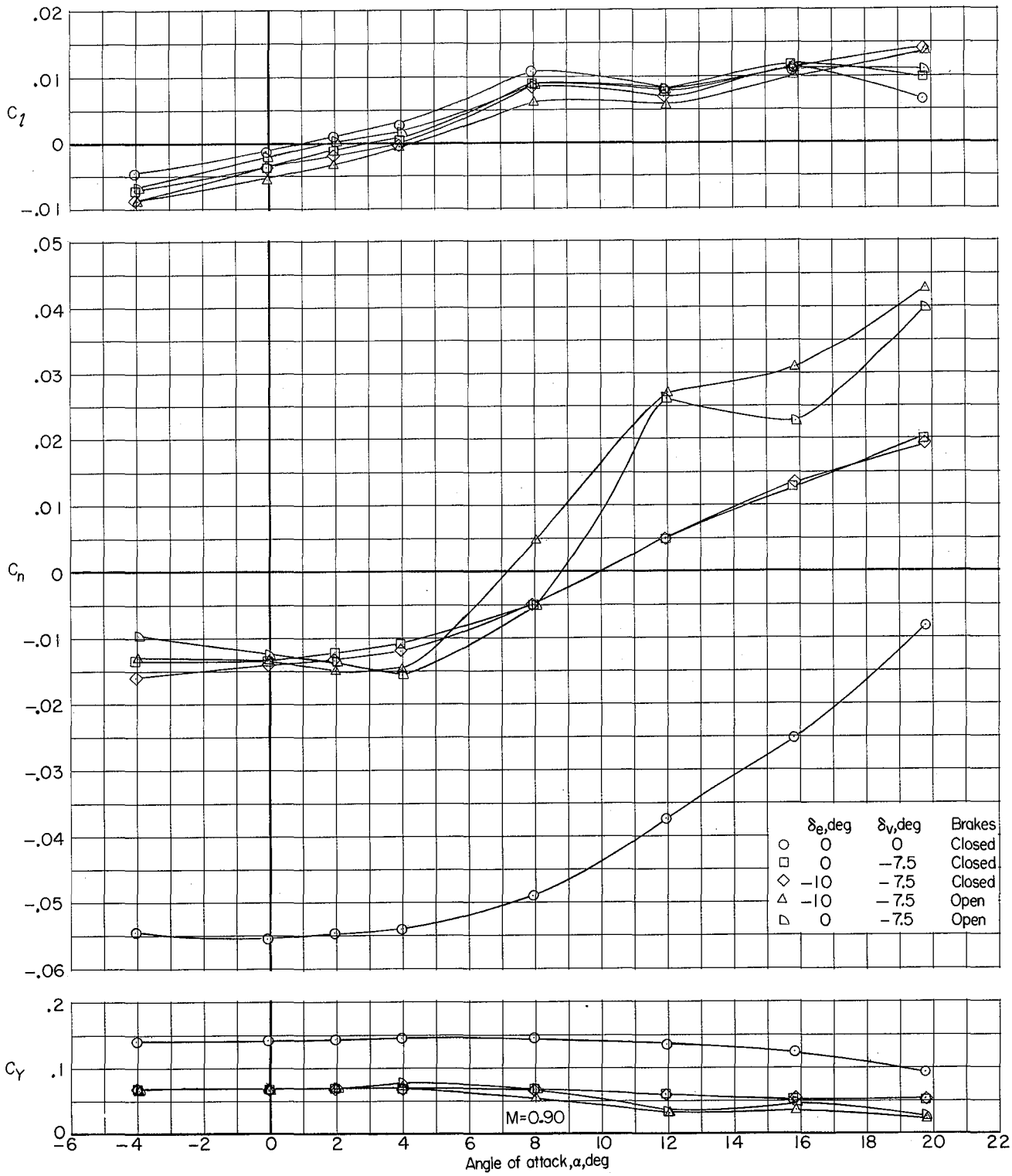

(b) M = 0.90.

Figure 17.- Continued.

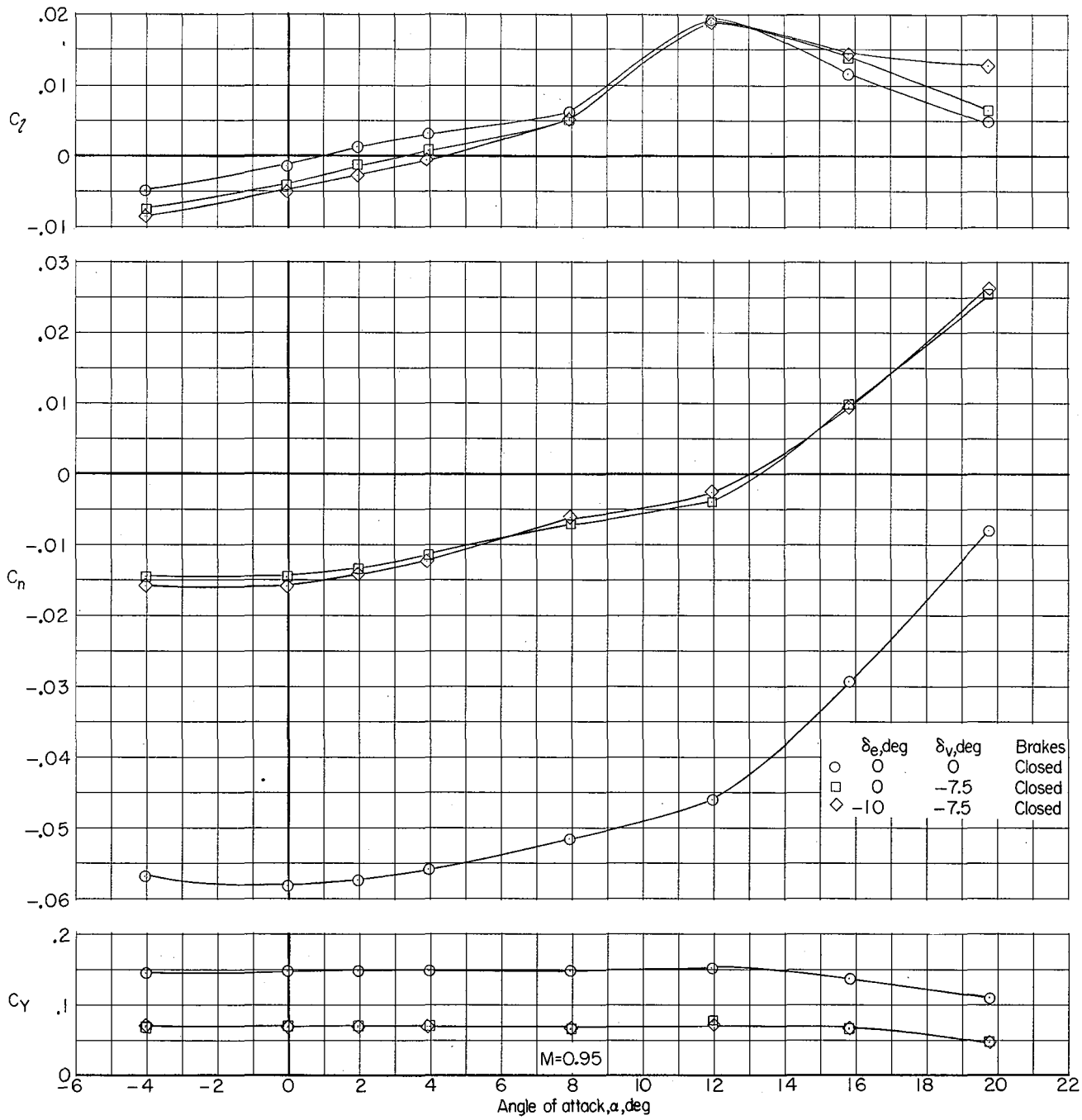

(c) M = 0.95.

Figure 17.- Continued.

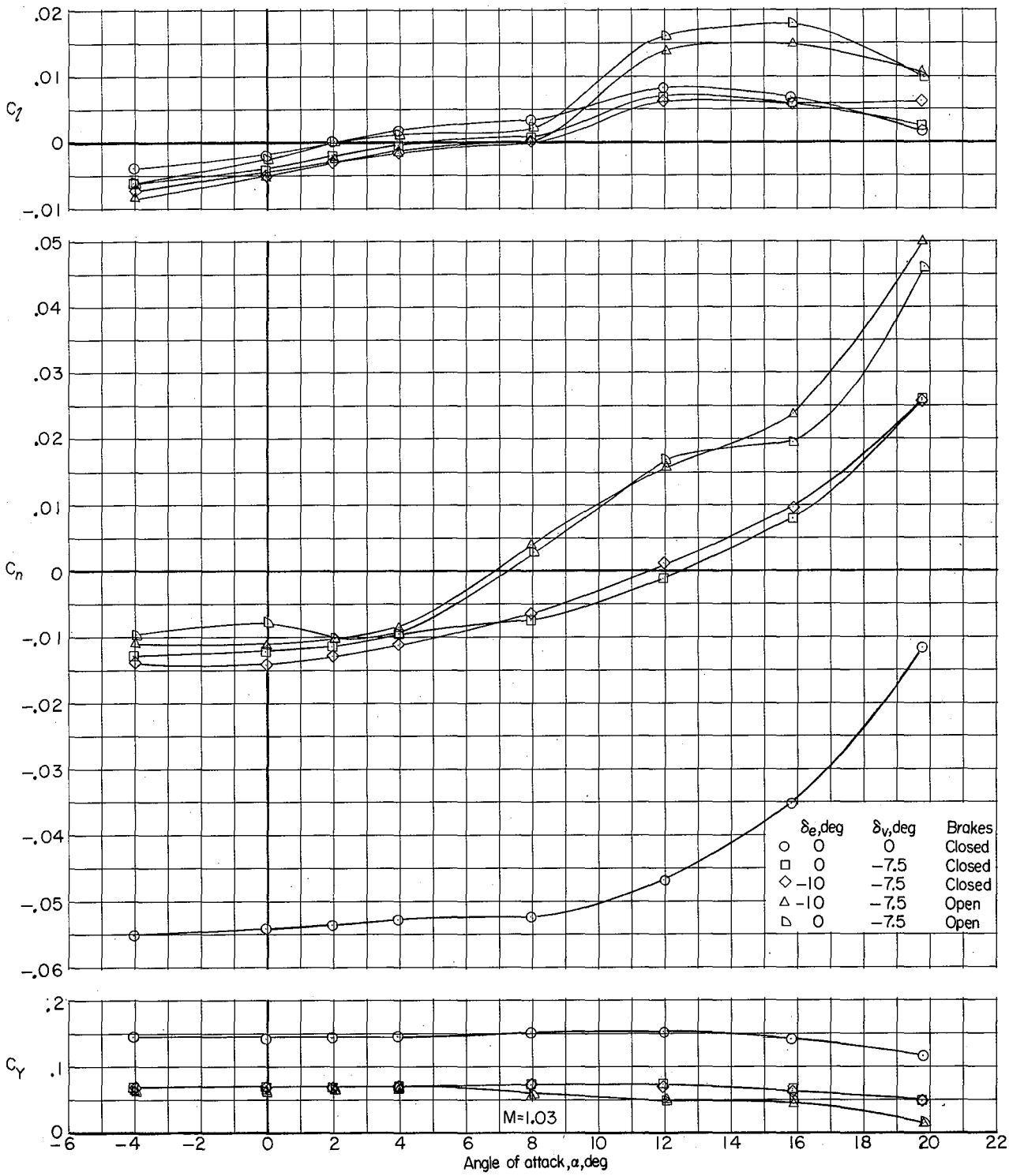

(d) M = 1.03.

Figure 17.- Continued.

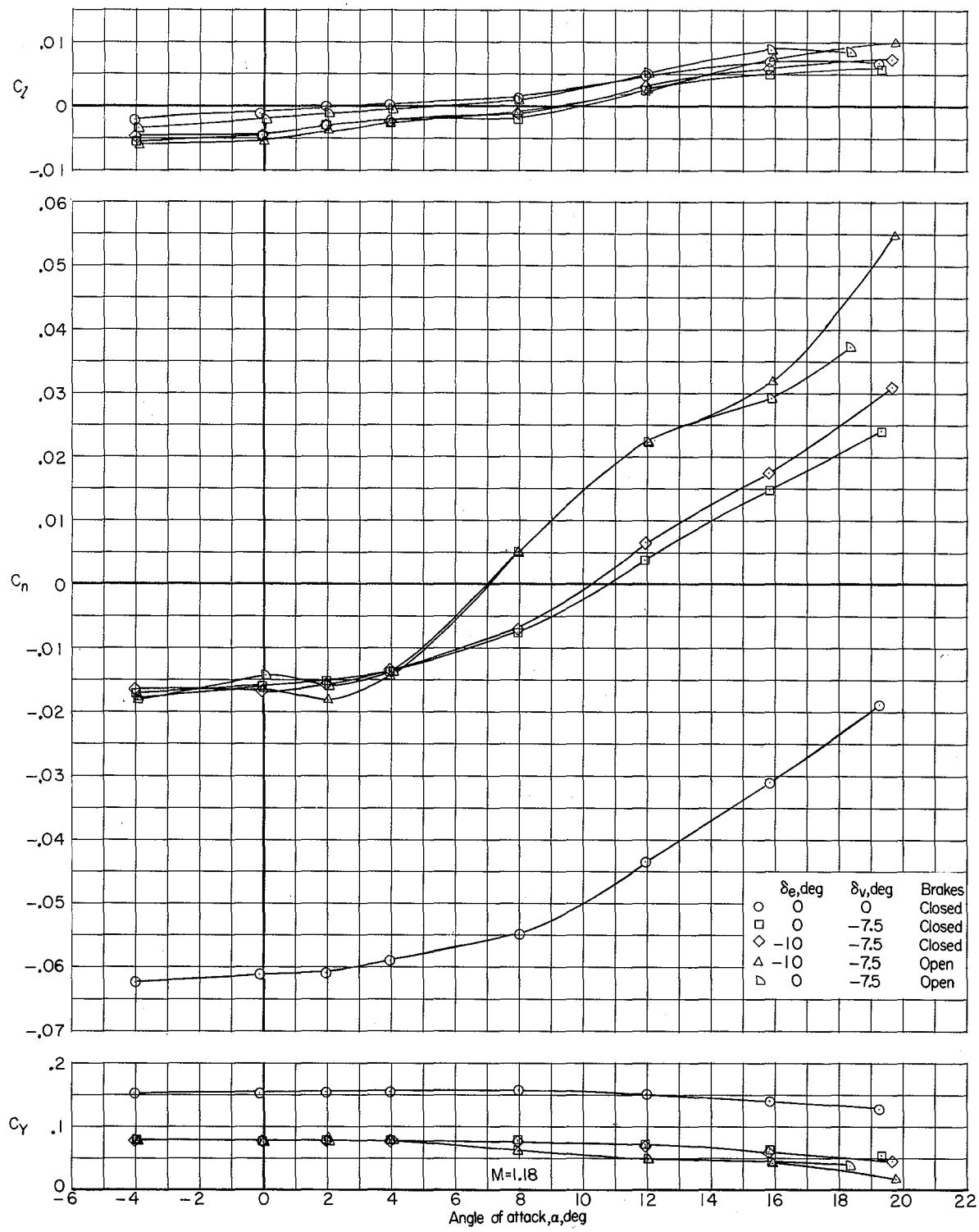

(e) M = 1.18.

Figure 17.- Concluded.

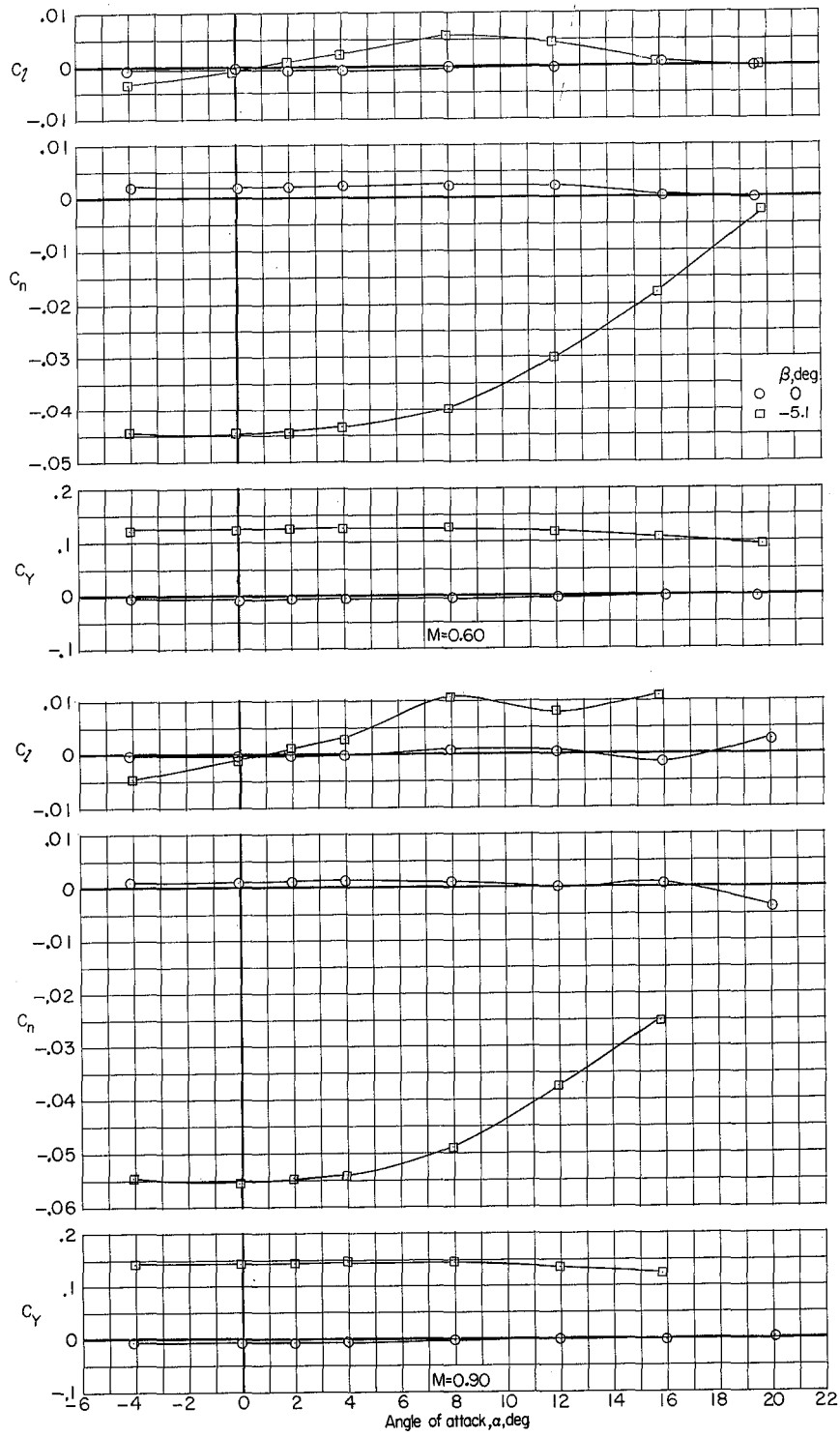

(a) M = 0.60 and 0.90.

Figure 18.- Lateral-directional characteristics of complete model with surfaces undeflected. $\beta = 0^{\circ}$ and -5.1°.

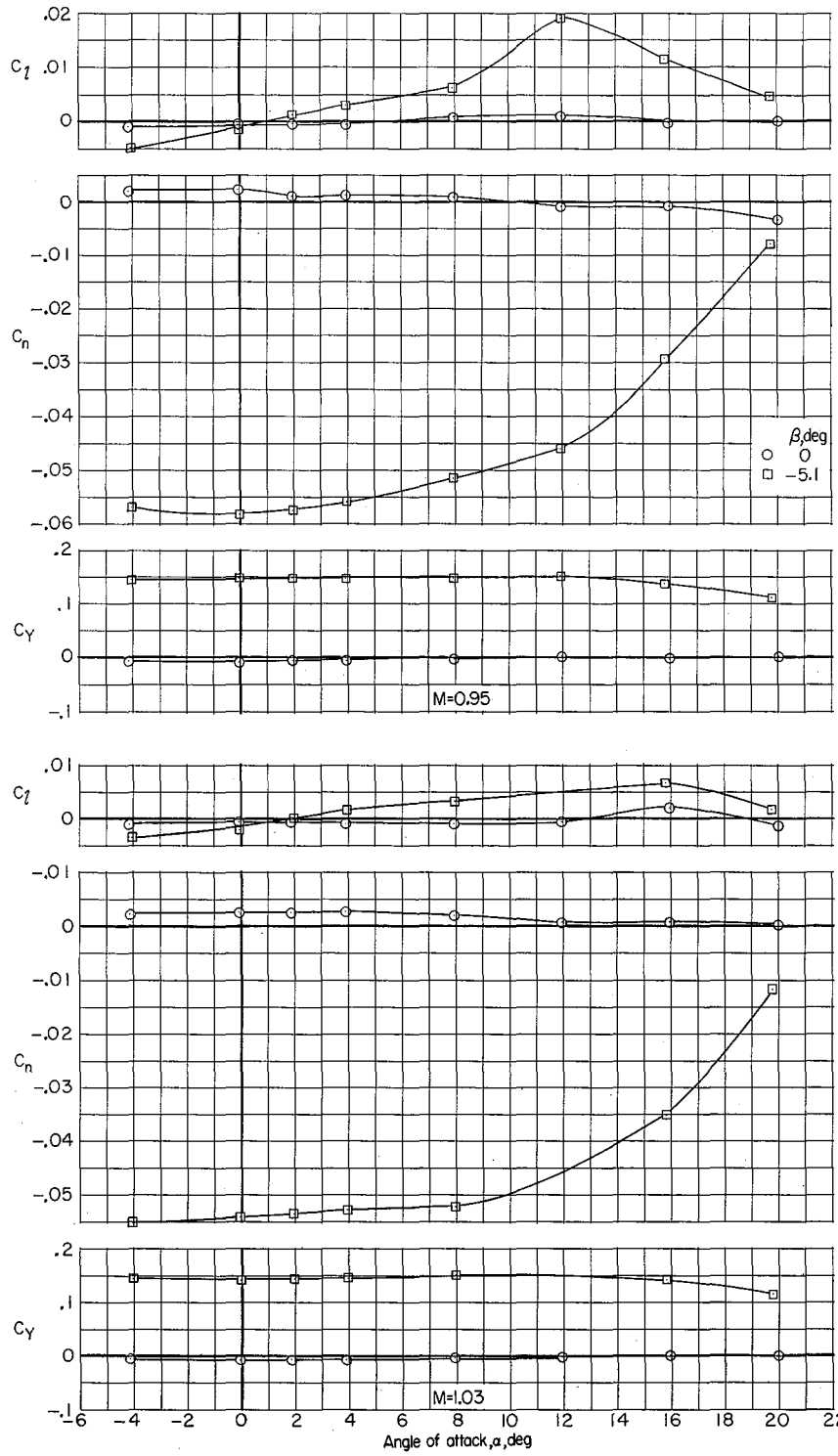

(b) M = 0.95 and 1.03.

Figure 18.- Continued.

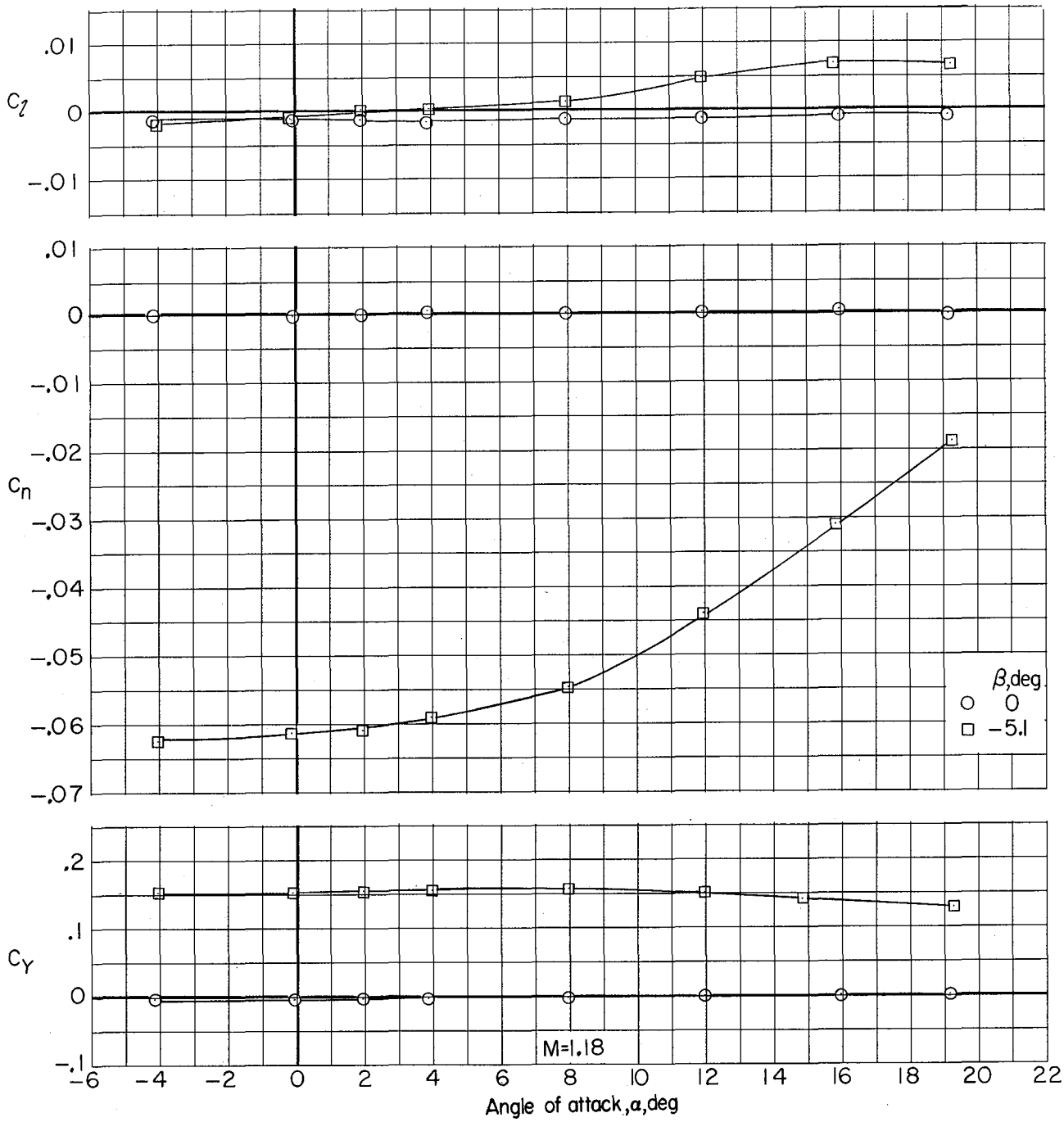

(c) M = 1.18.

Figure 18.- Concluded.

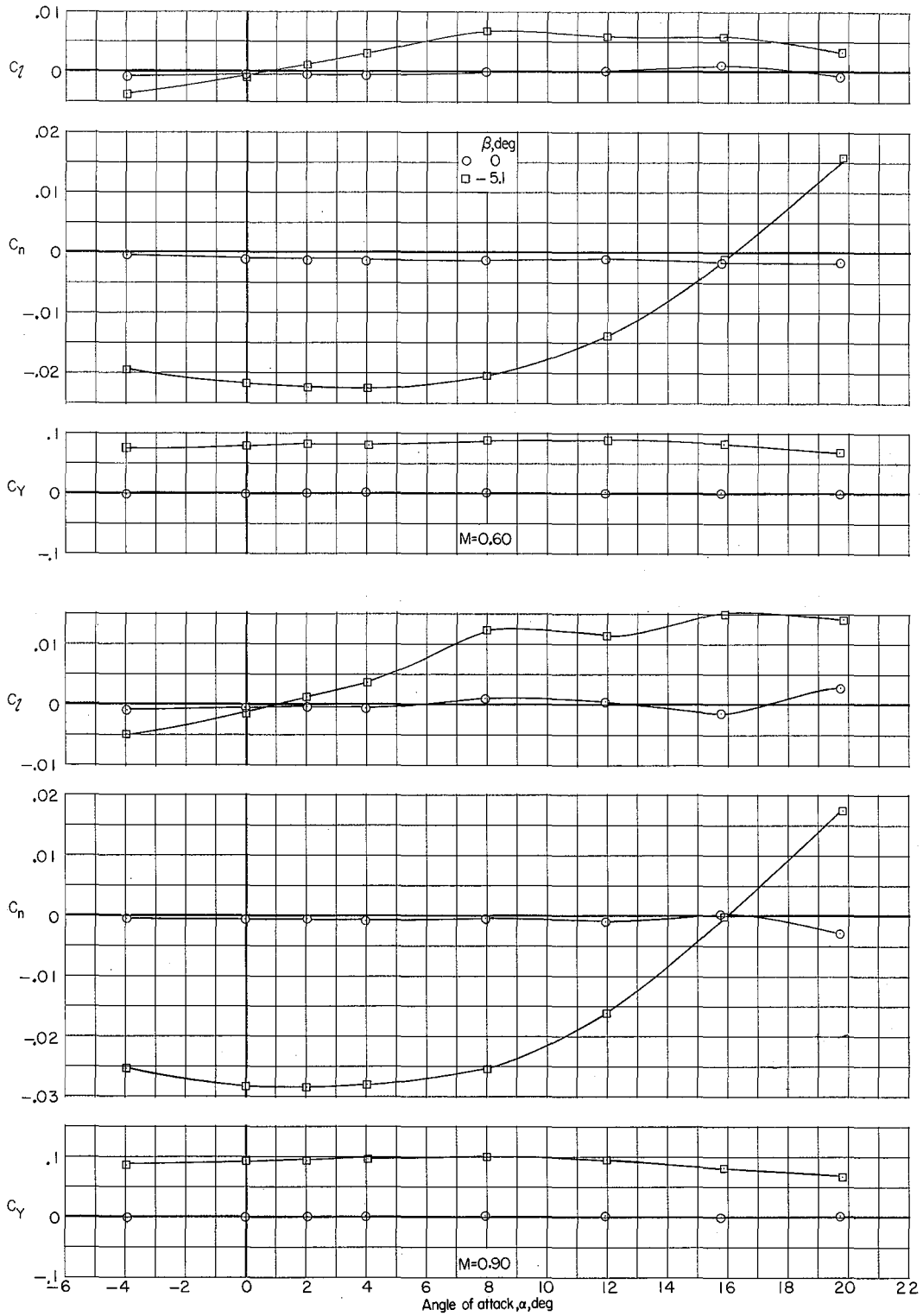

(a) M = 0.60 and 0.90.

Figure 19.- Lateral-directional characteristics of model without lower vertical tail and with other surfaces undeflected. $\beta = 0^{\circ}$ and -5.1°.

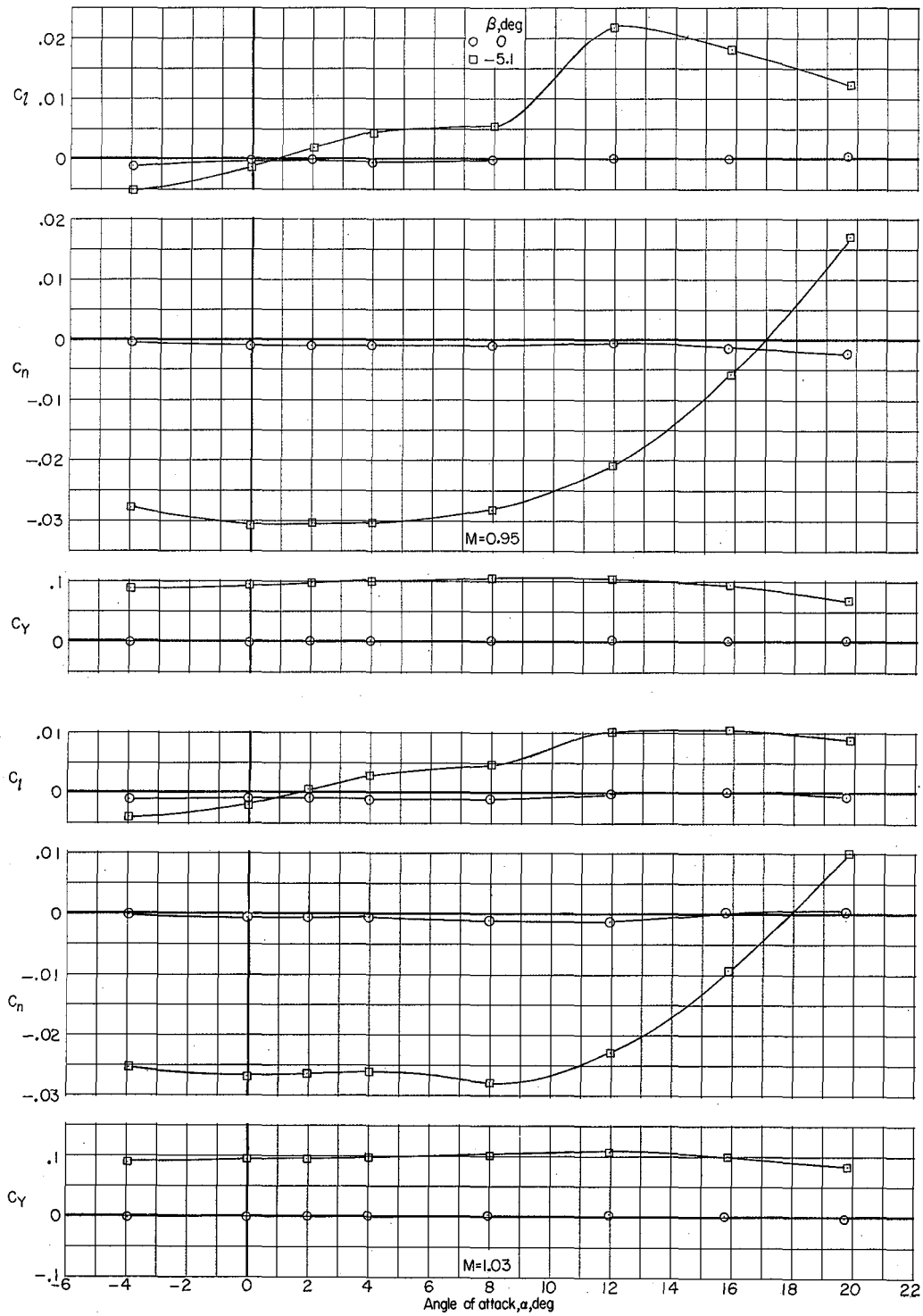

(b) M = 0.95 and 1.03.

Figure 19.- Continued.

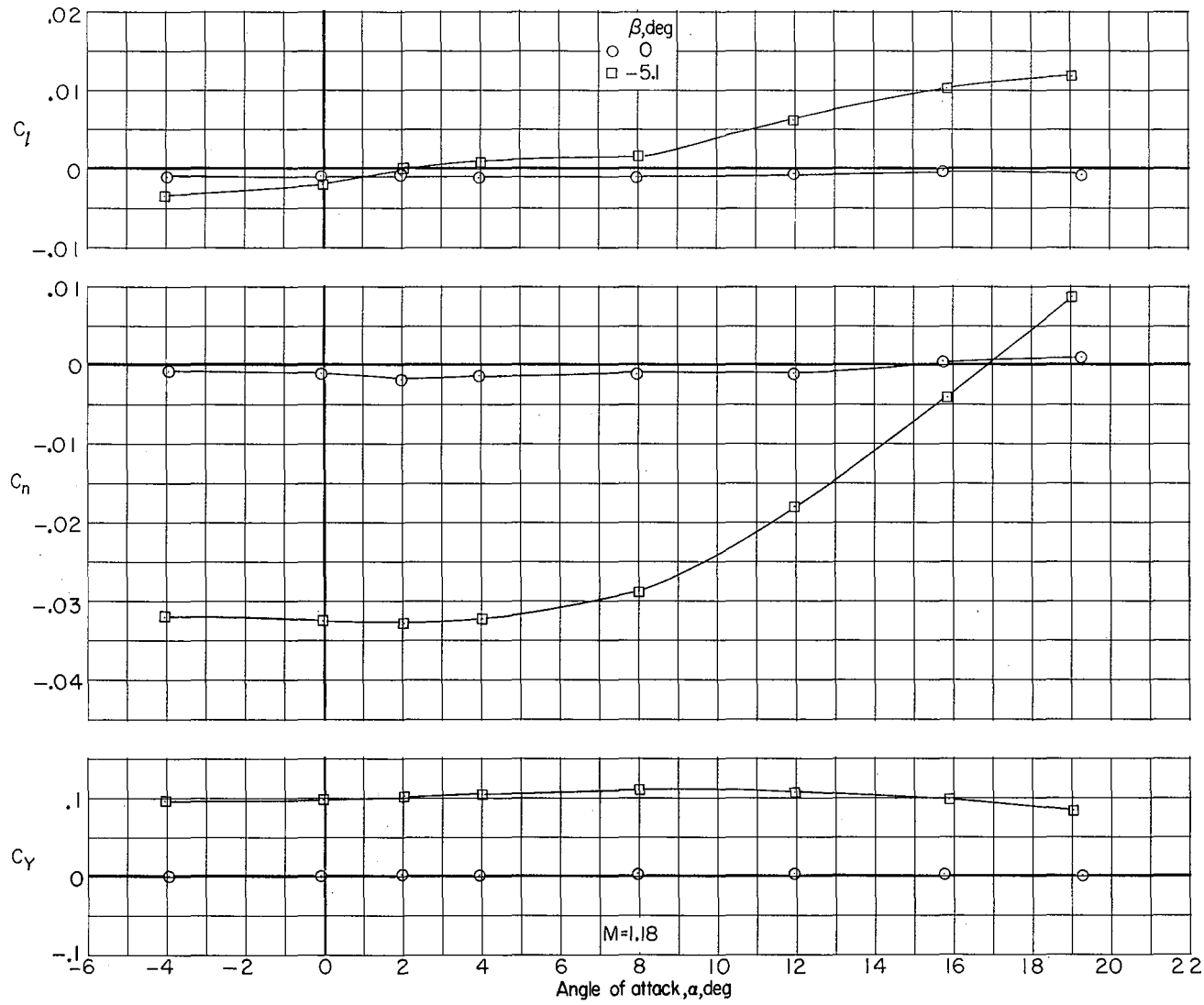

(c) M = 1.18.

Figure 19.- Concluded.

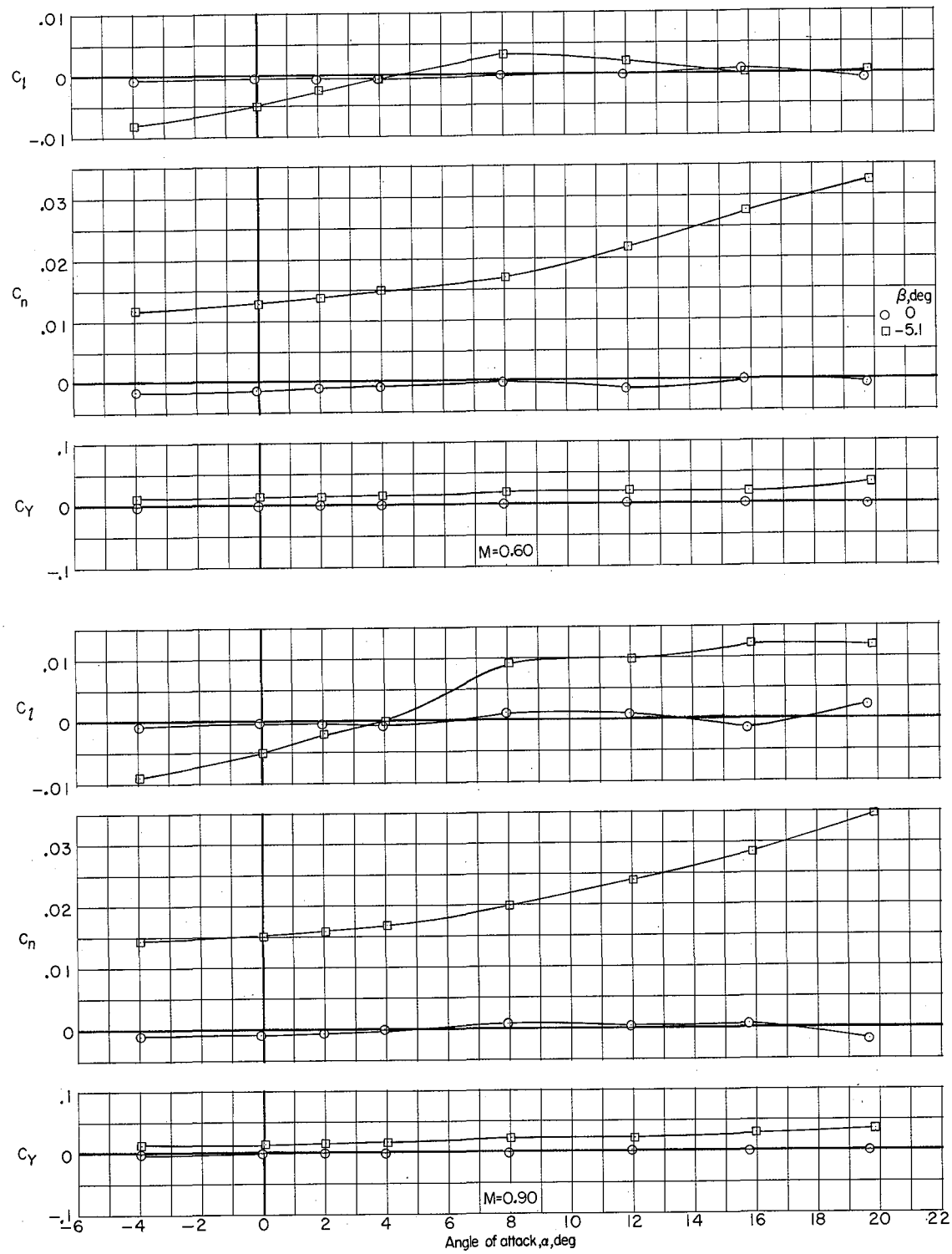

(a) M = 0.60 and 0.90.

Figure 20.- Lateral-directional characteristics of model without both vertical tails and with other surfaces undeflected. $\beta = 0^{\circ}$ and -5.1°.

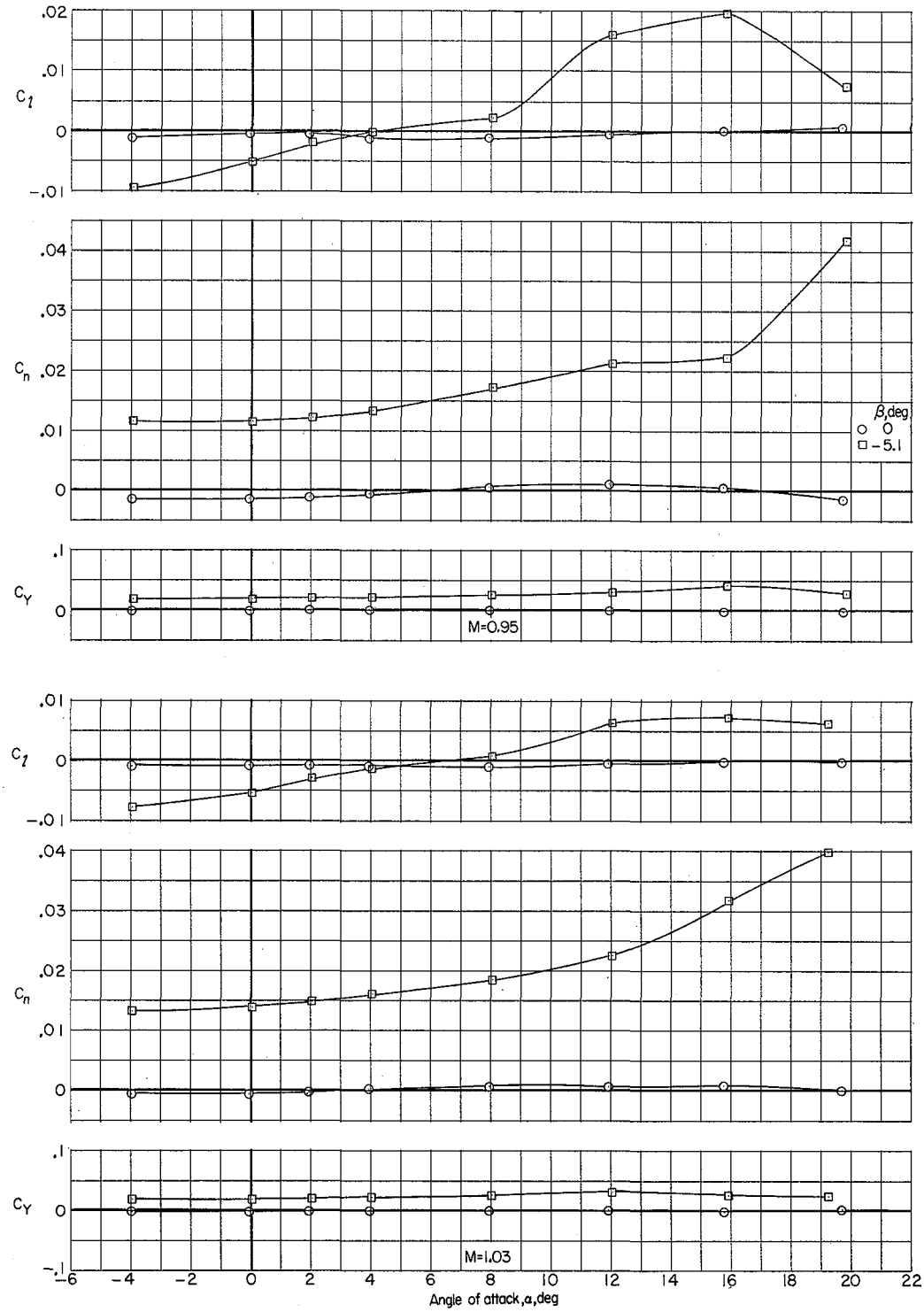

(b) M = 0.95 and 1.03.

Figure 20.- Continued.

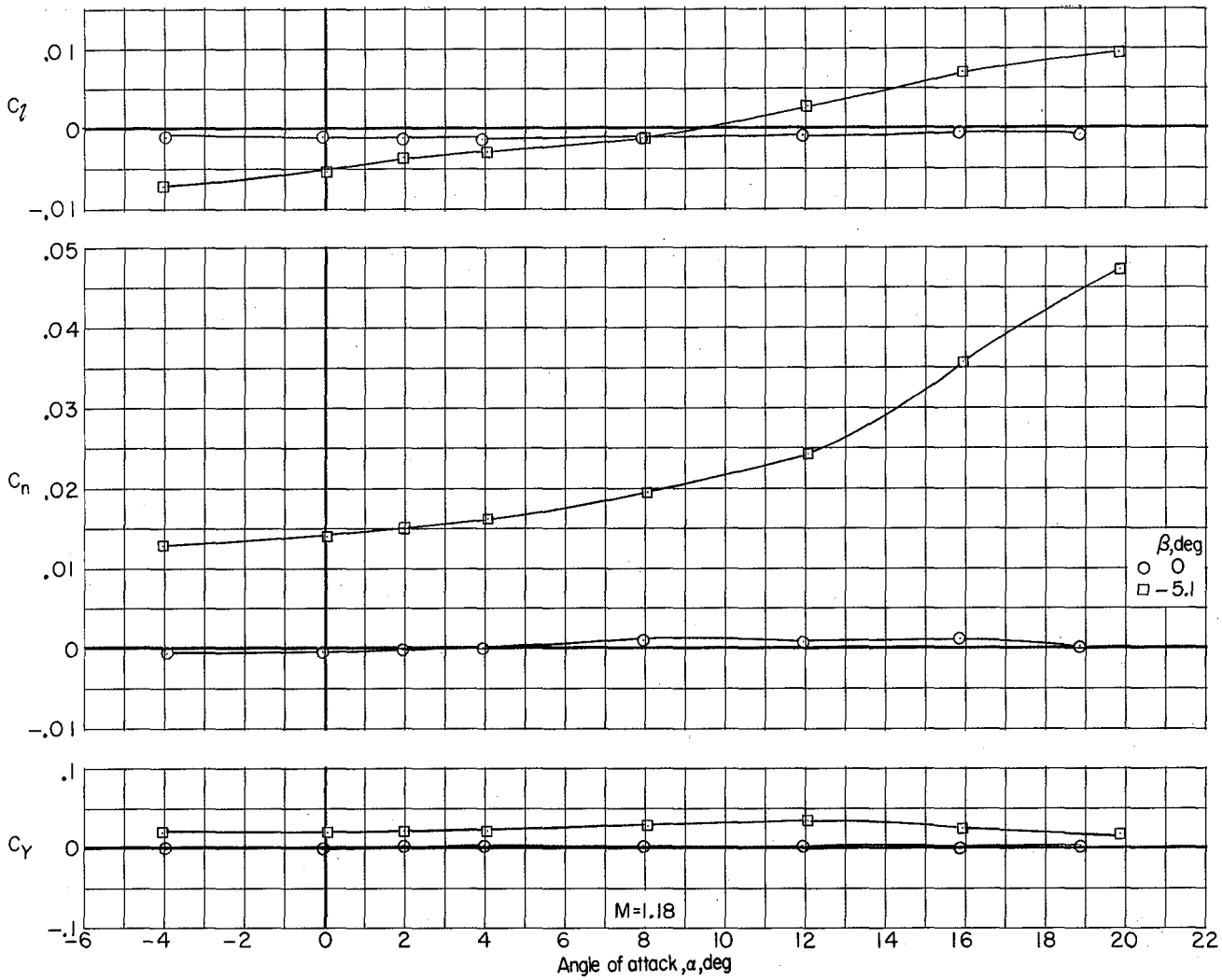

(c) M = 1.18.

Figure 20.- Concluded.

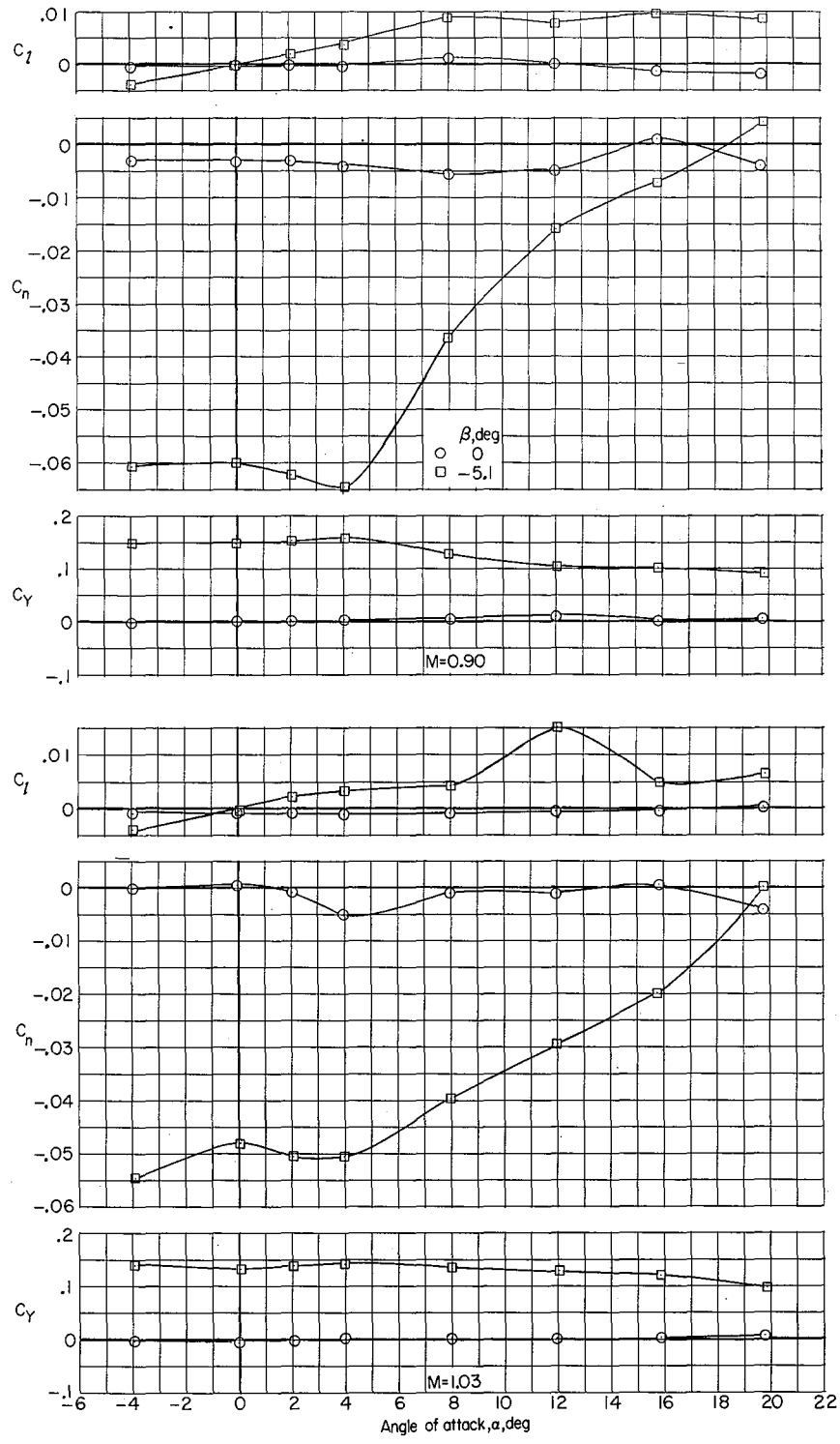

(a) M = 0.90 and 1.03.

Figure 21.- Lateral-directional characteristics of complete model with speed brakes open; other surfaces undeflected. $\beta_r = 0^\circ$ and -5.1°.

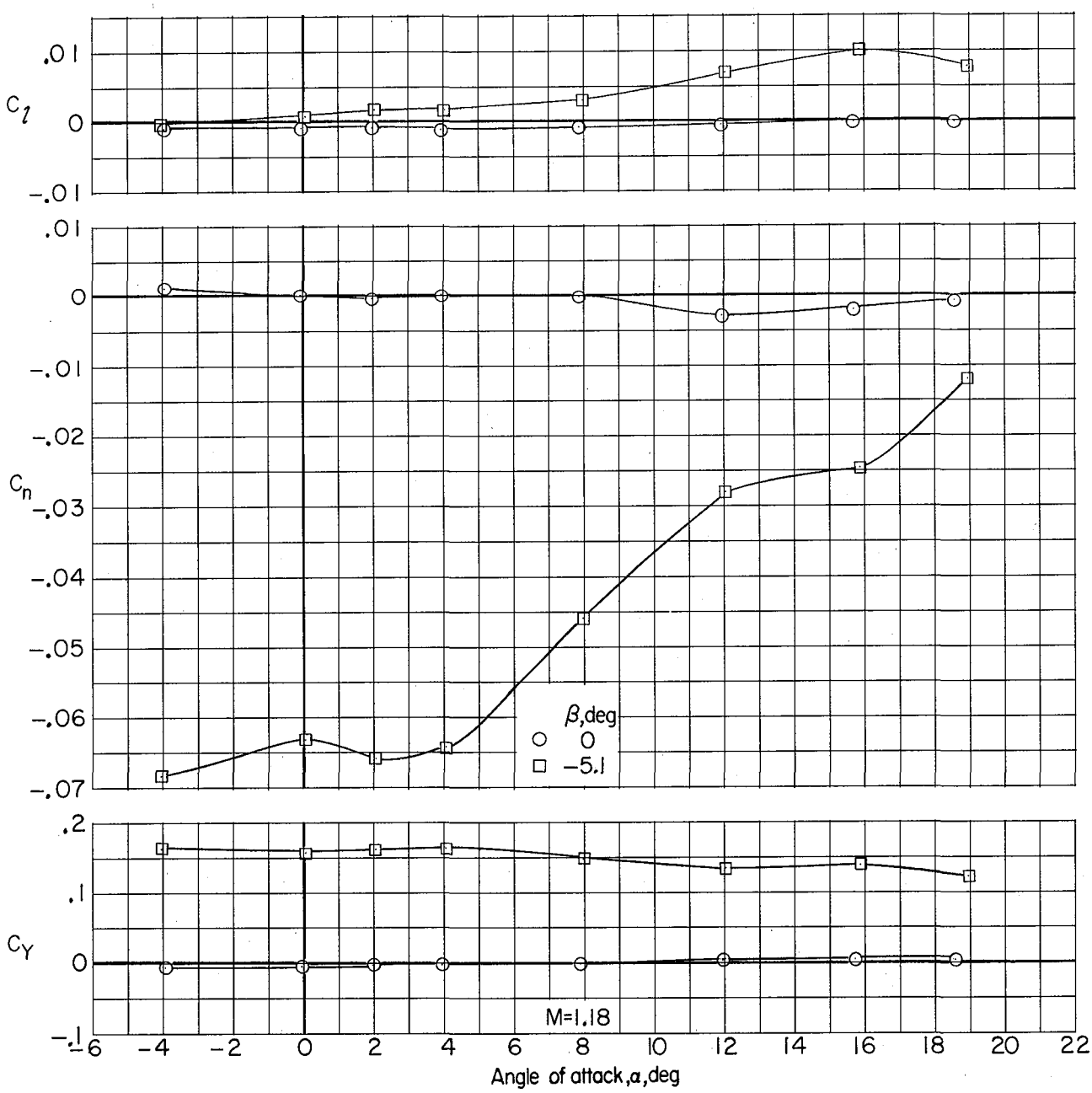

(b) M = 1.18.

Figure 21.- Concluded.

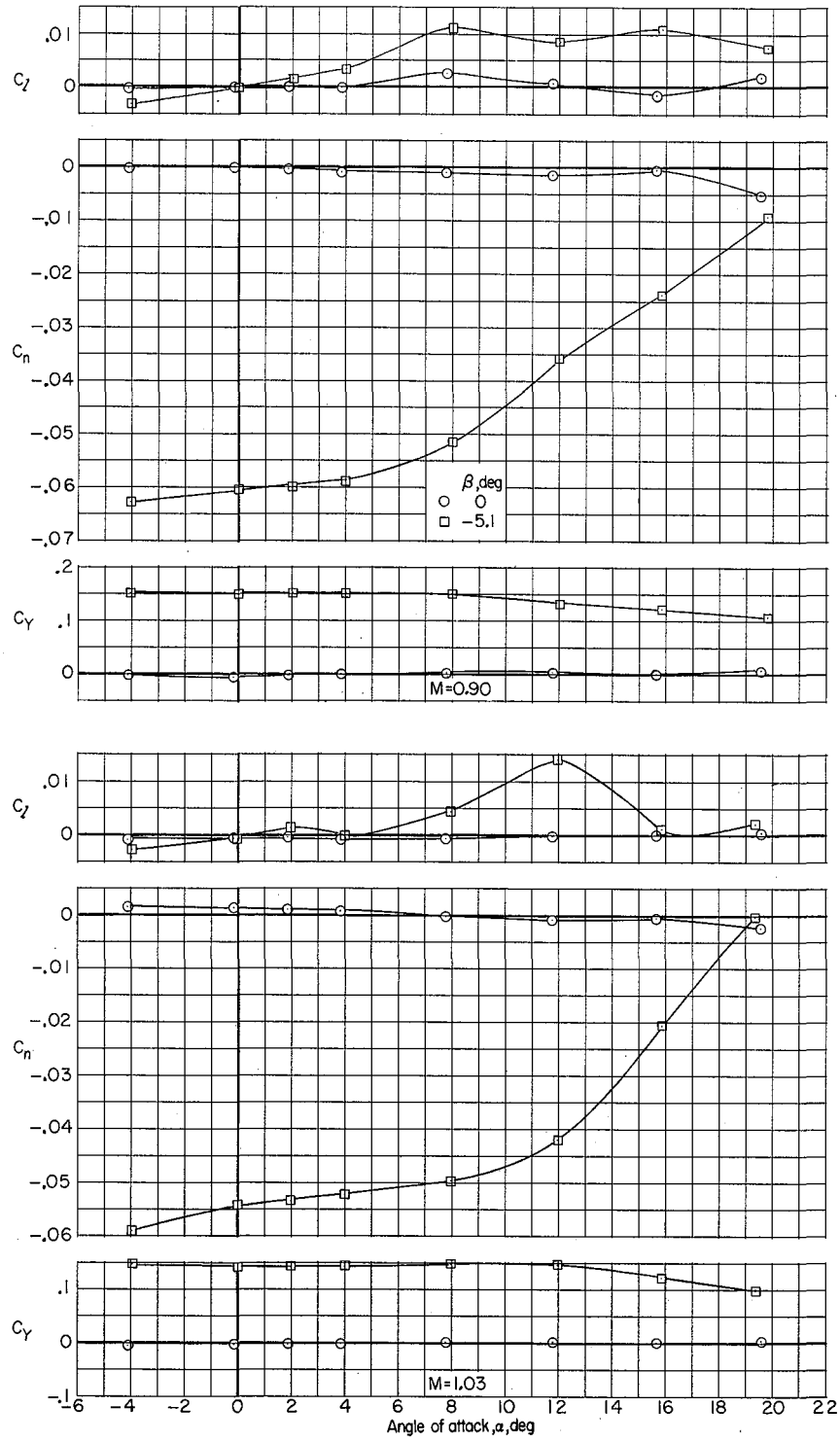

(a) M = 0.90 and 1.03.

Figure 22.- Lateral-directional characteristics of complete model with lower speed brakes open; other surfaces undeflected. $\beta = 0^{\circ}$ and -5.1°.

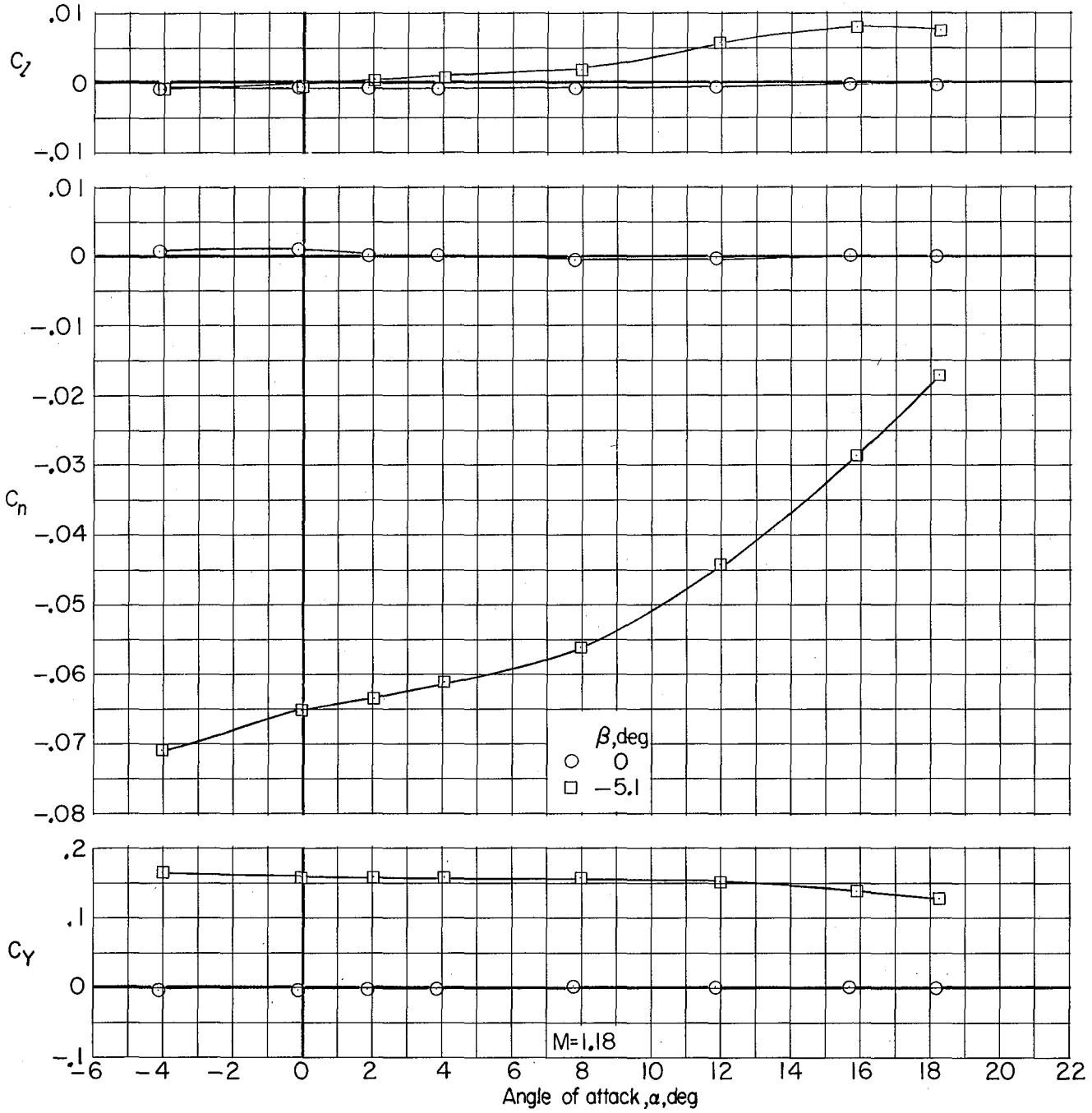

(b) M = 1.18.

Figure 22.- Concluded.

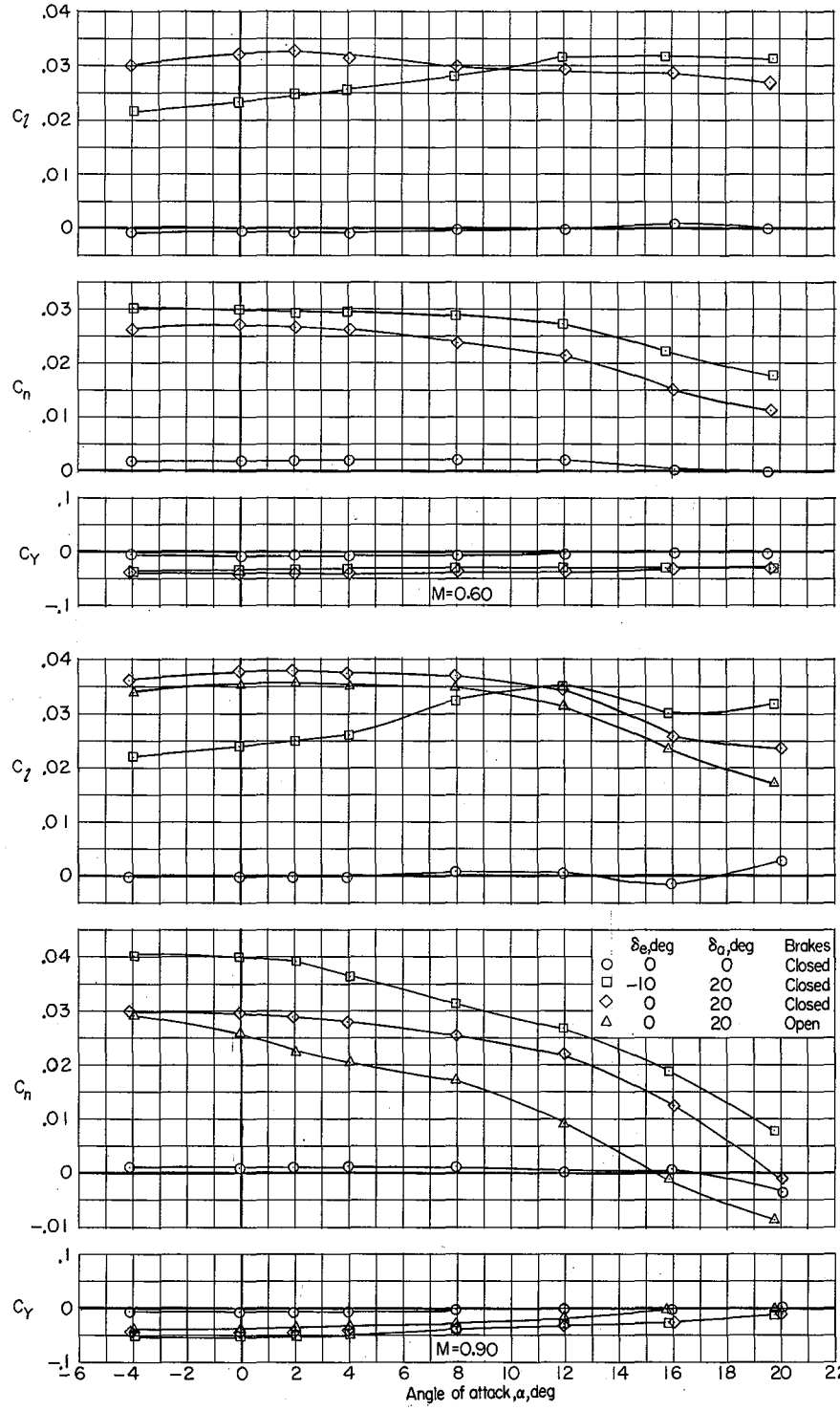

(a) M = 0.60 and 0.90.

Figure 23.- Lateral-directional characteristics of complete model with various δ_a and δ_e, and with speed brakes open and closed. $\beta = 0^o$; $\delta_r = 0^o$.

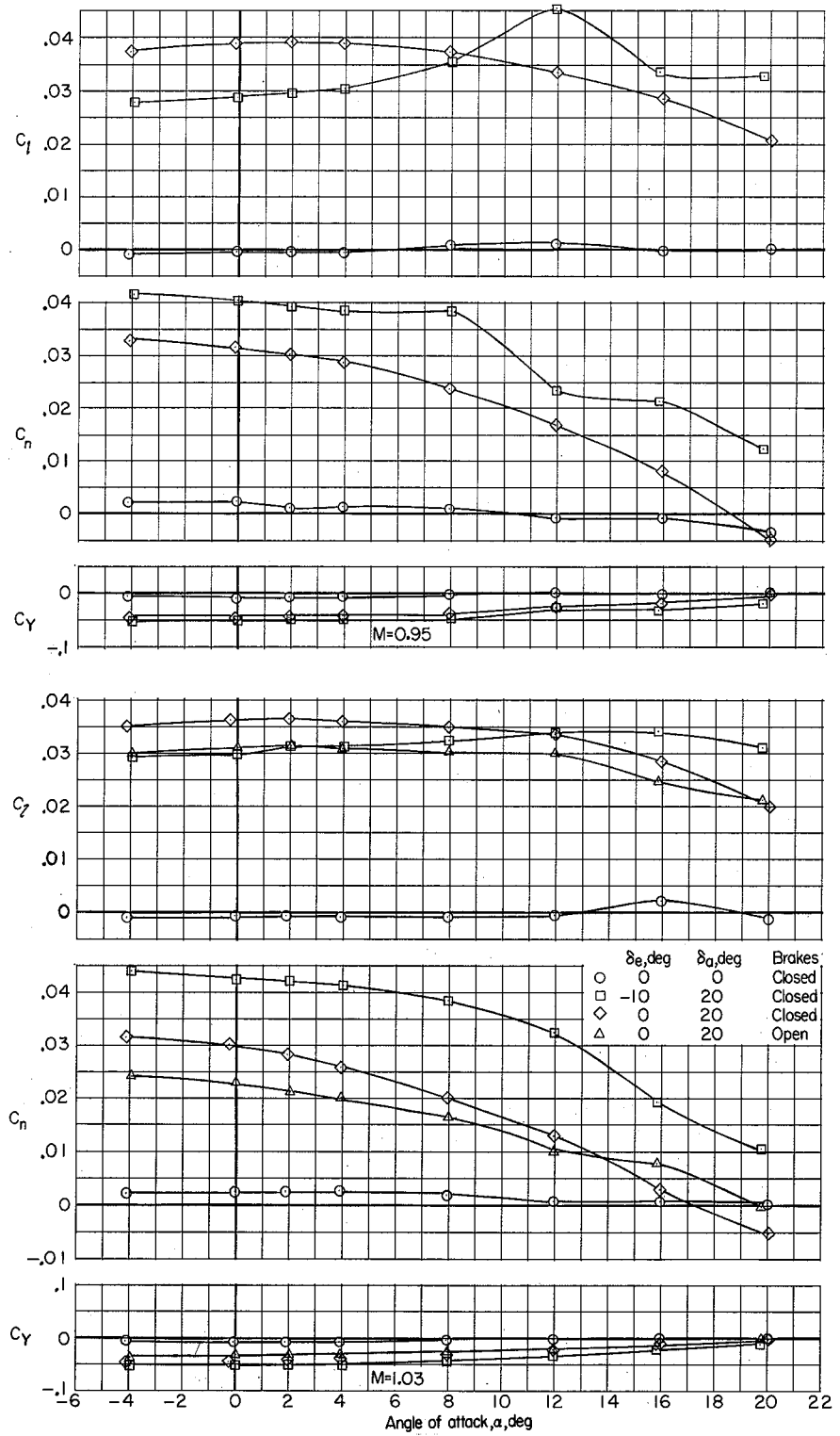

(b) M = 0.95 and 1.03.

Figure 23.- Continued.

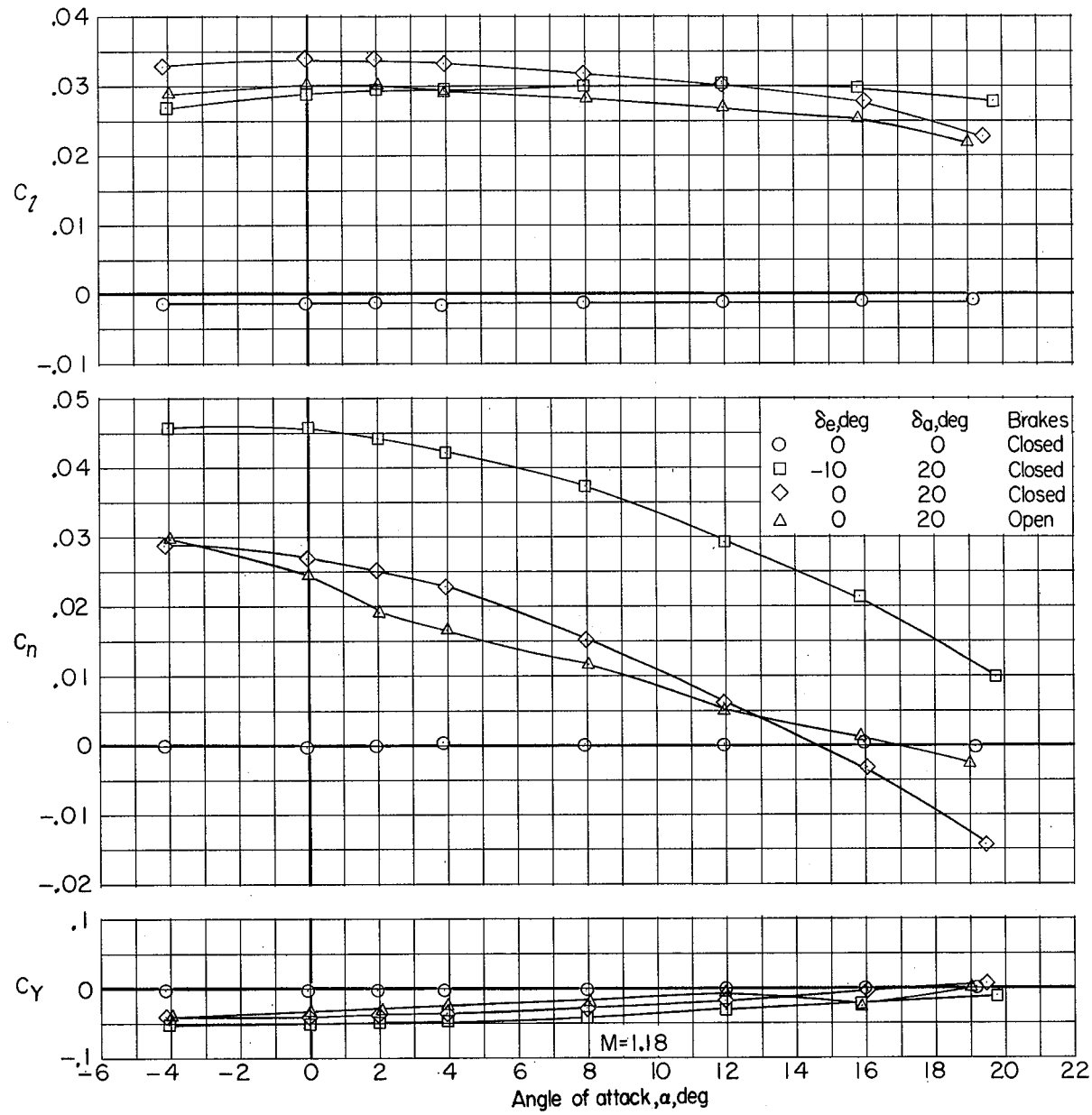

(c) M = 1.18.

Figure 23.- Concluded.

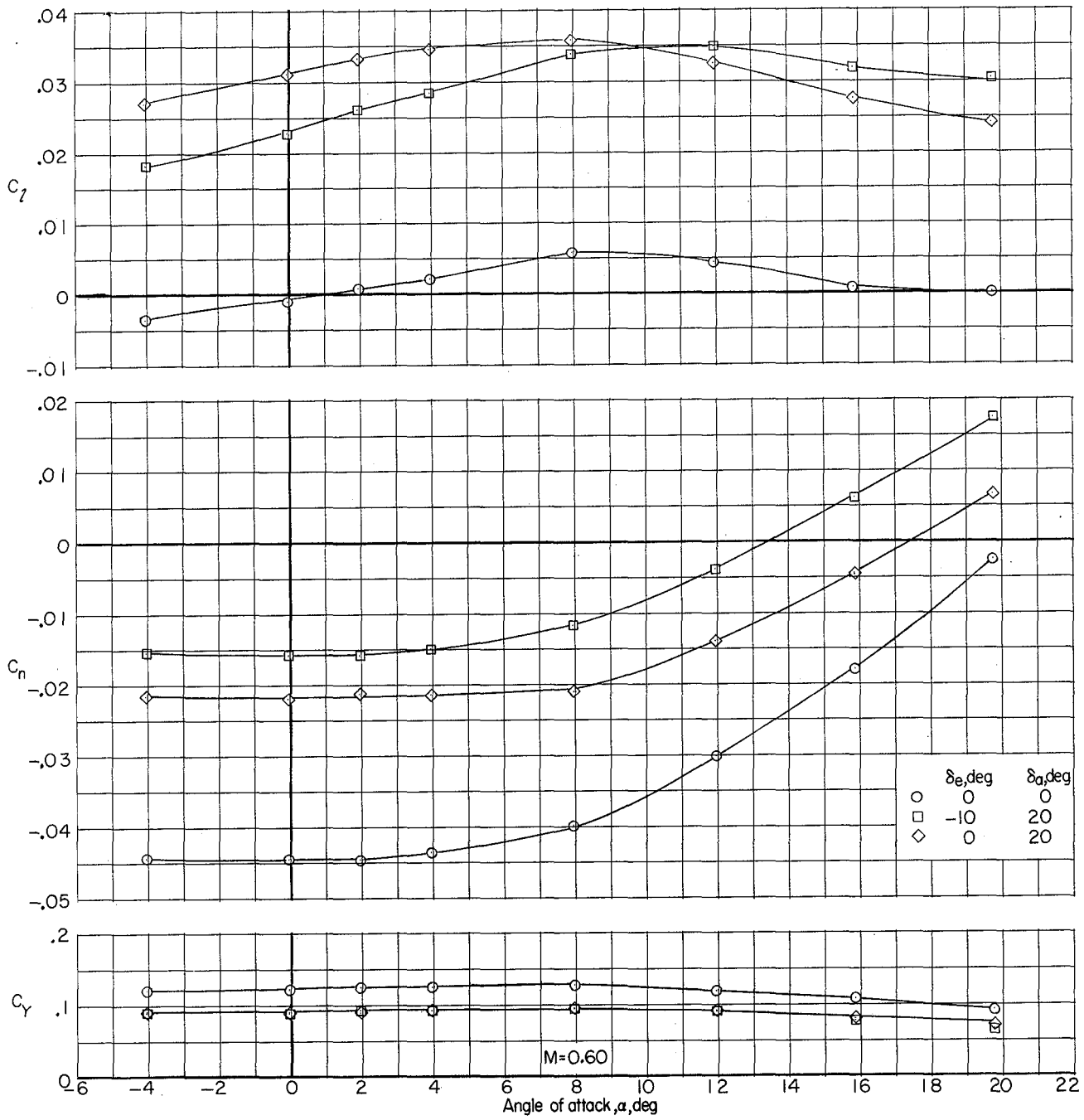

(a) M = 0.60.

Figure 24.- Lateral-directional characteristics of complete model with various δ_a and δ_e; other surfaces undeflected. $\beta = -5.1^\circ$.

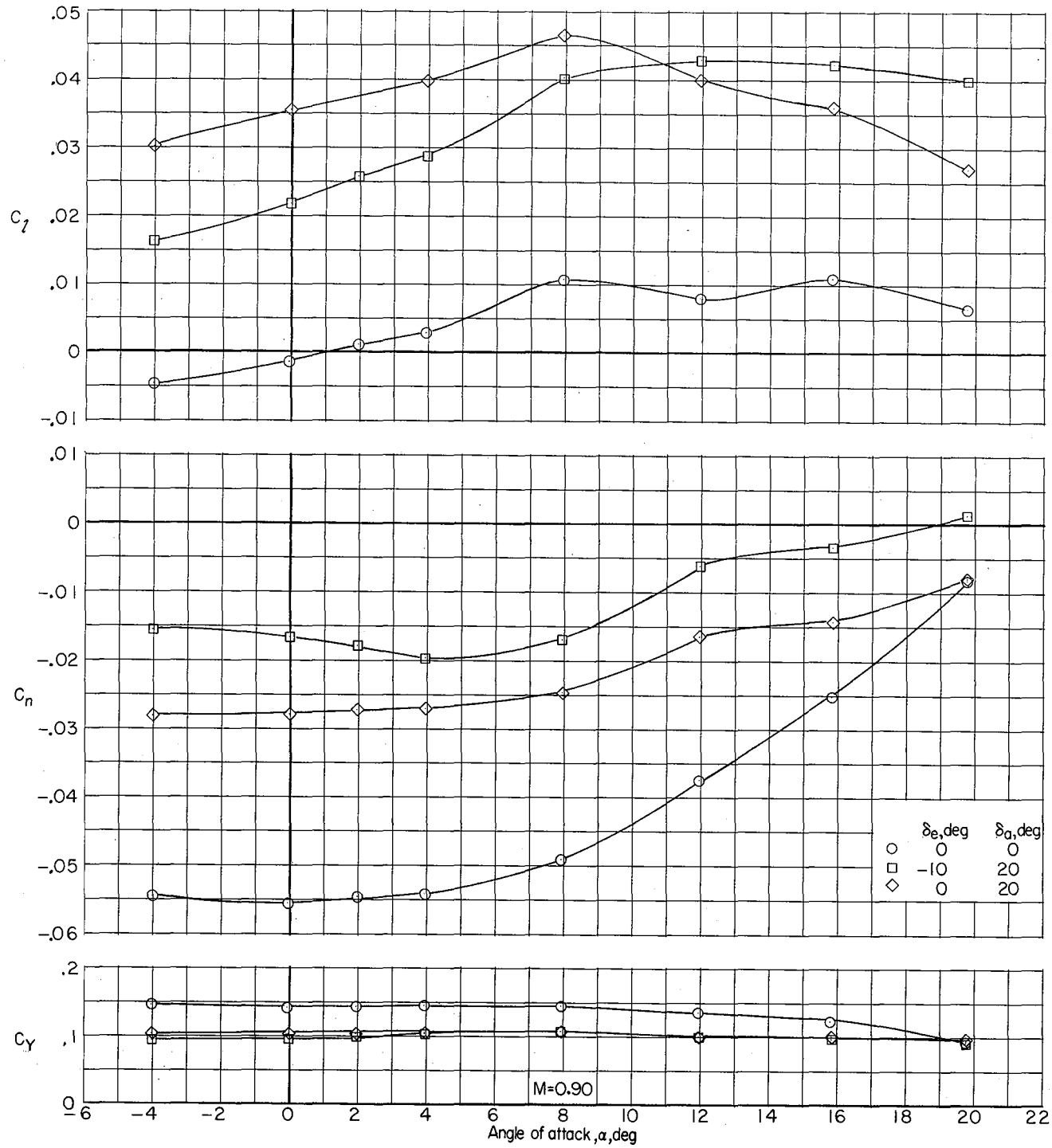

(b) M = 0.90.

Figure 24.- Continued.

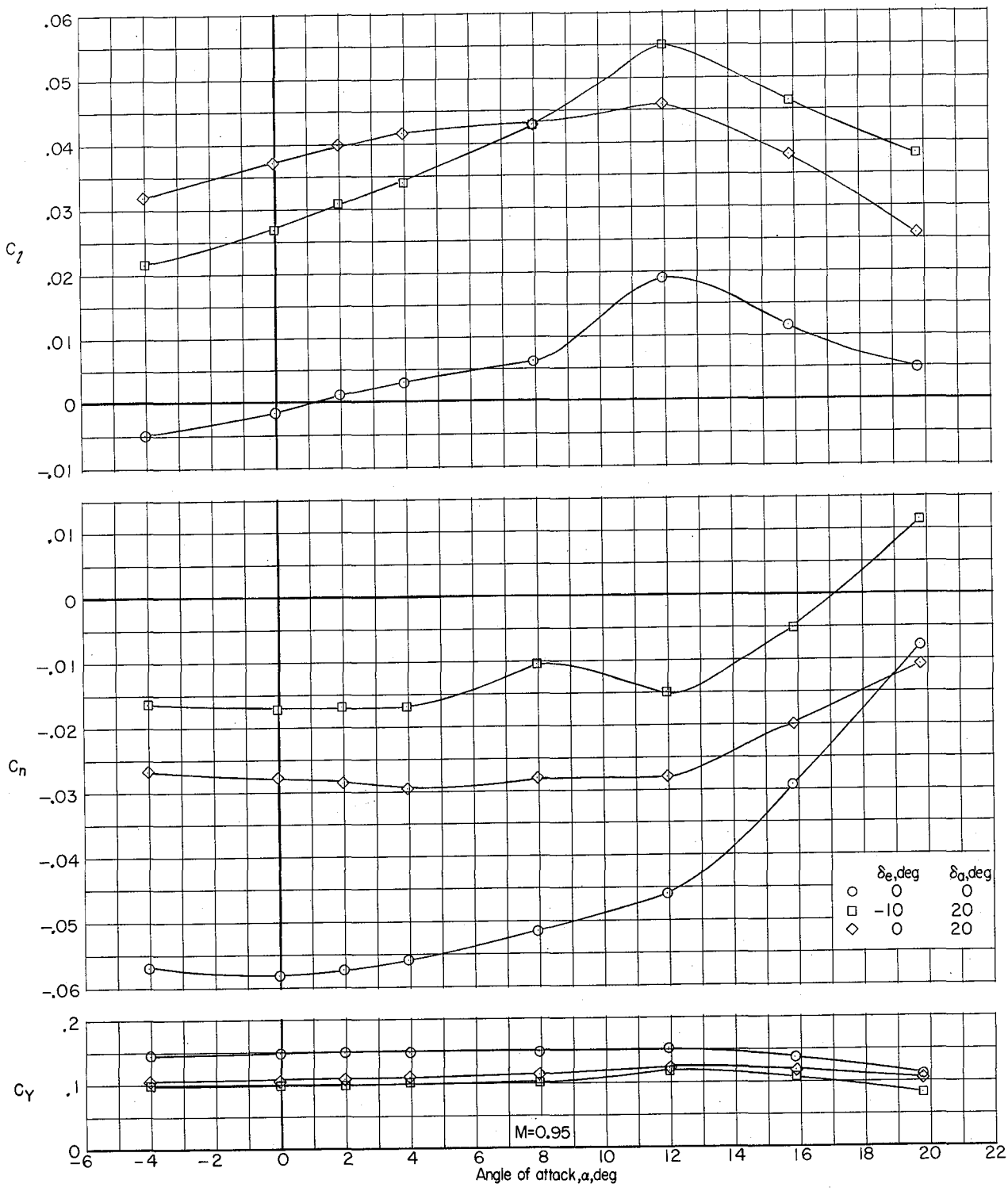

(c) M = 0.95.

Figure 24.- Continued.

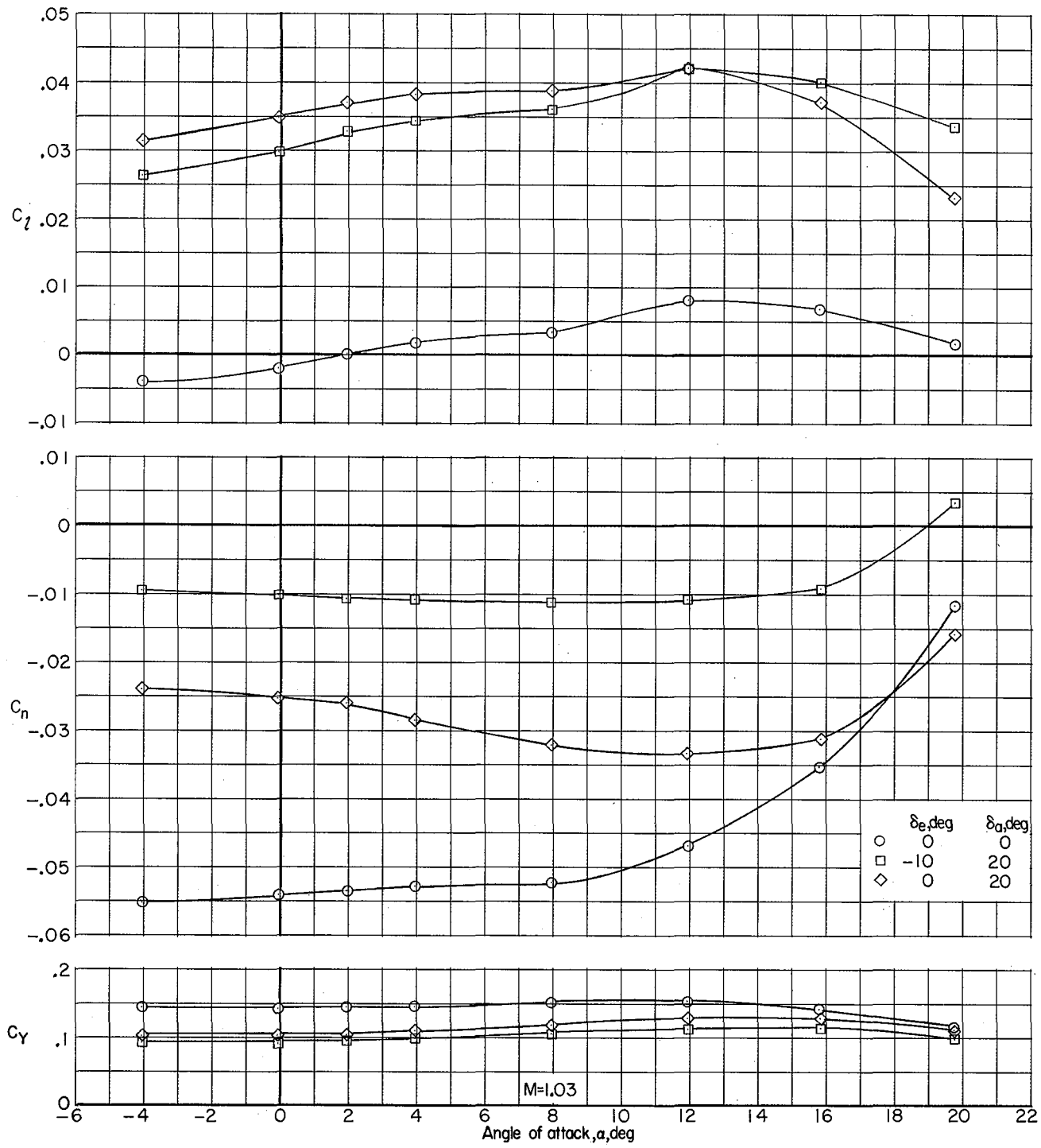

(d) M = 1.03.

Figure 24.- Continued.

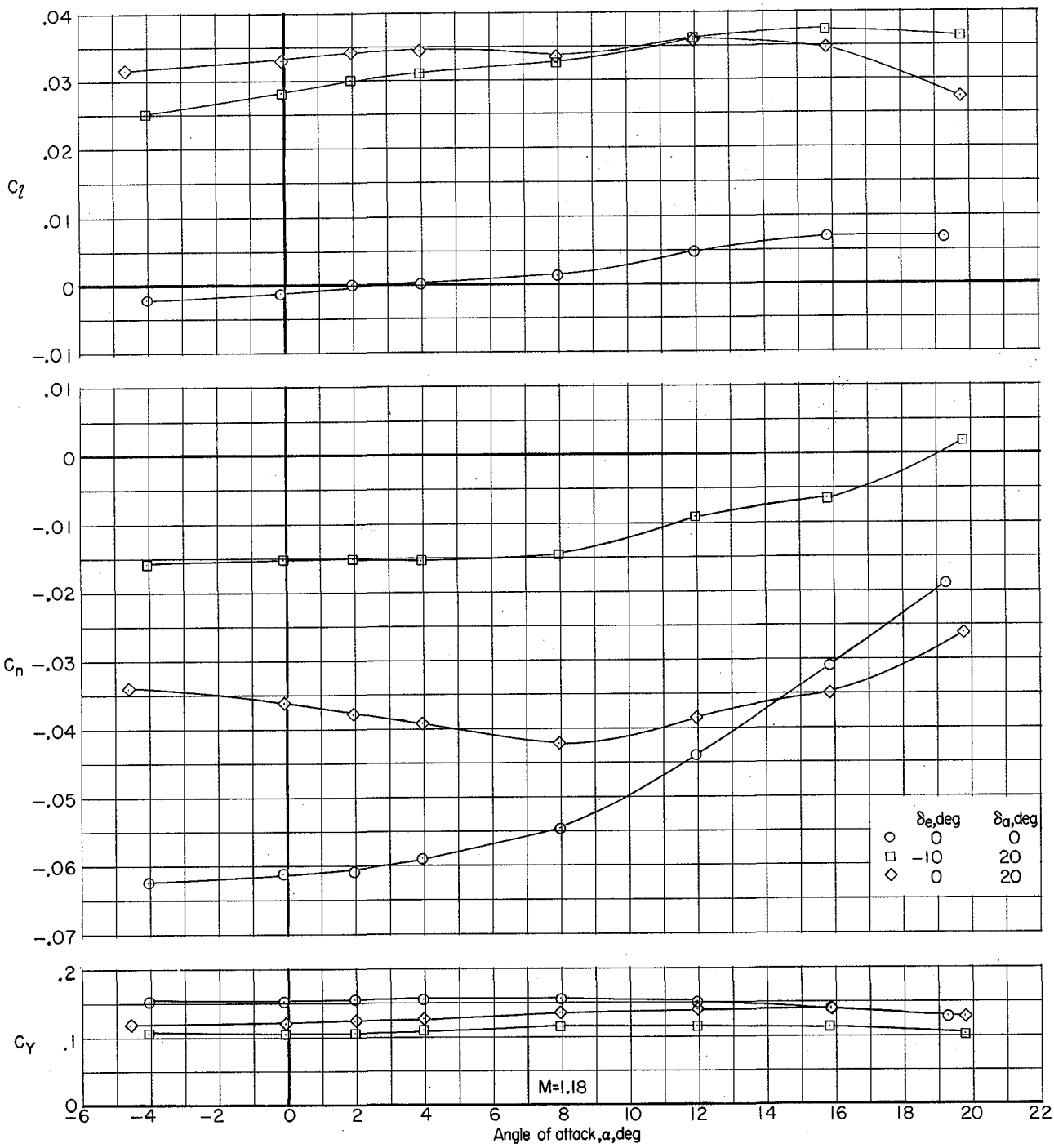

(e) M = 1.18.

Figure 24.- Concluded.

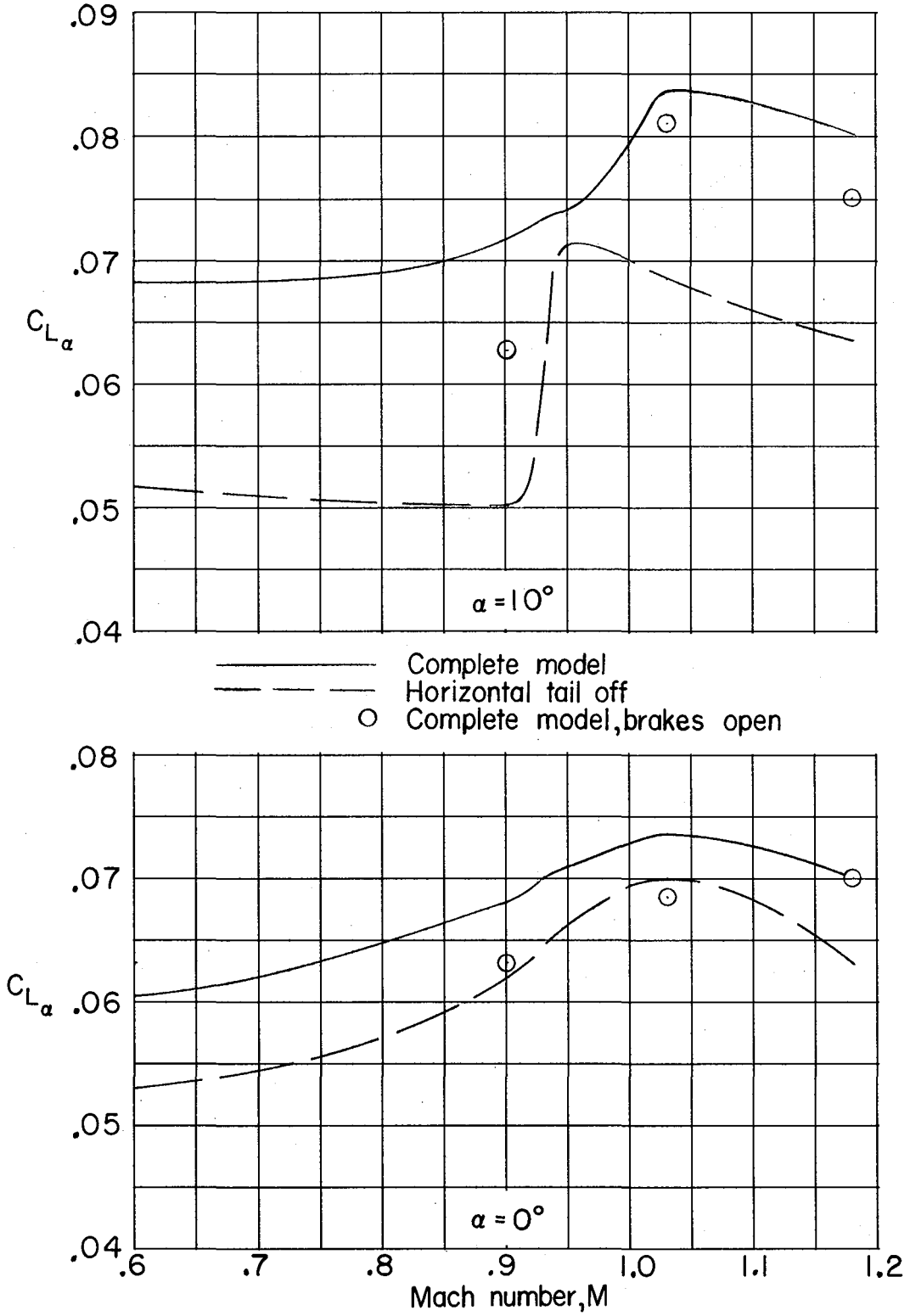

Figure 25.- Variation with Mach number of lift-curve slopes. Surfaces undeflected unless otherwise noted. $\beta = 0^\circ$.

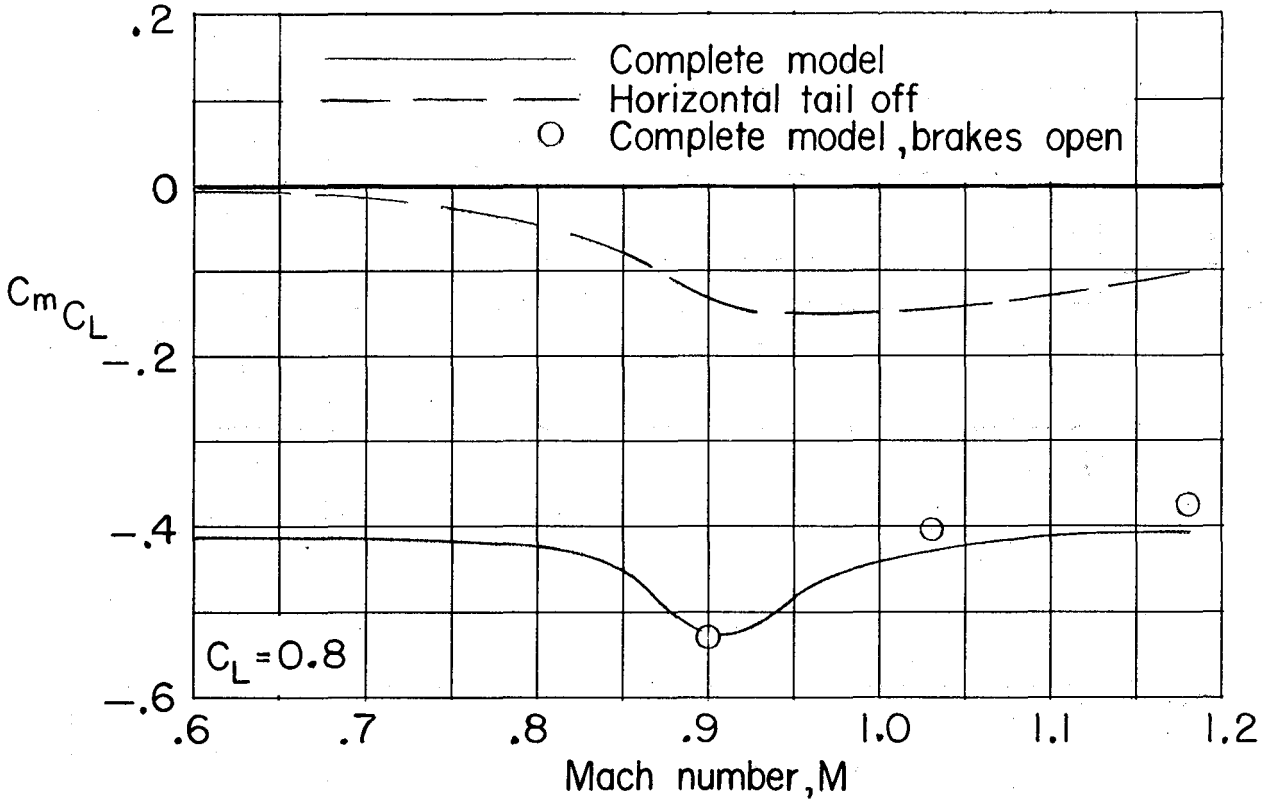

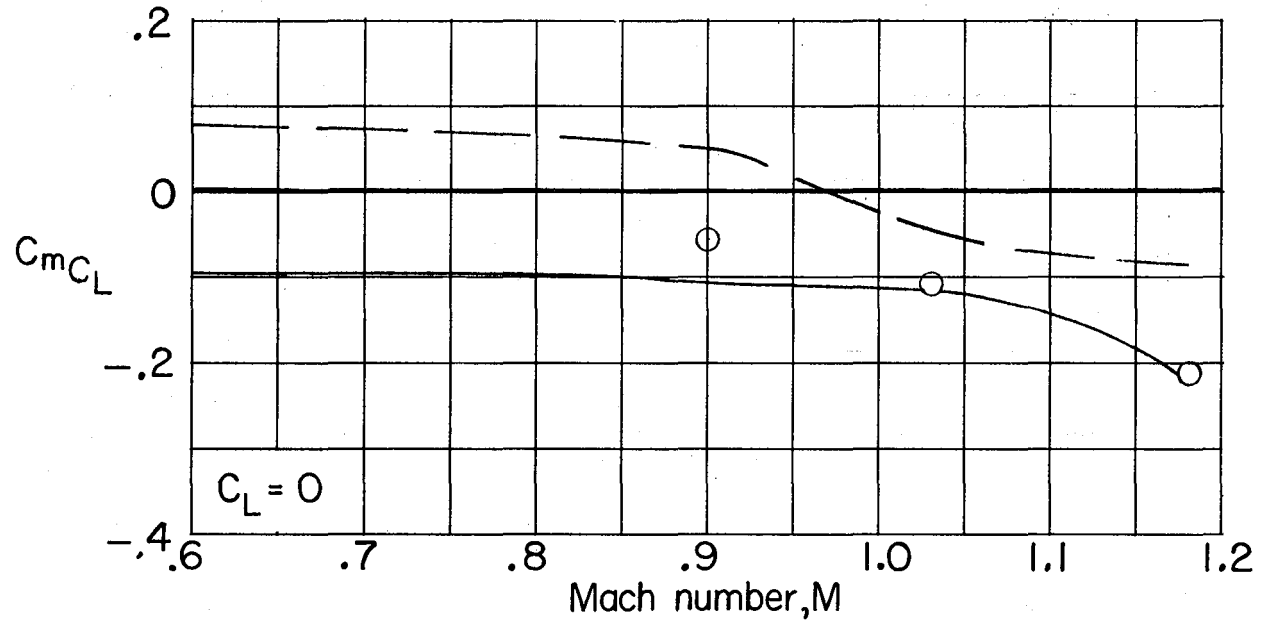

Figure 26.- Variation with Mach number of static longitudinal stability parameter. Surfaces undeflected unless otherwise noted. $\beta = 0^{\circ}$.

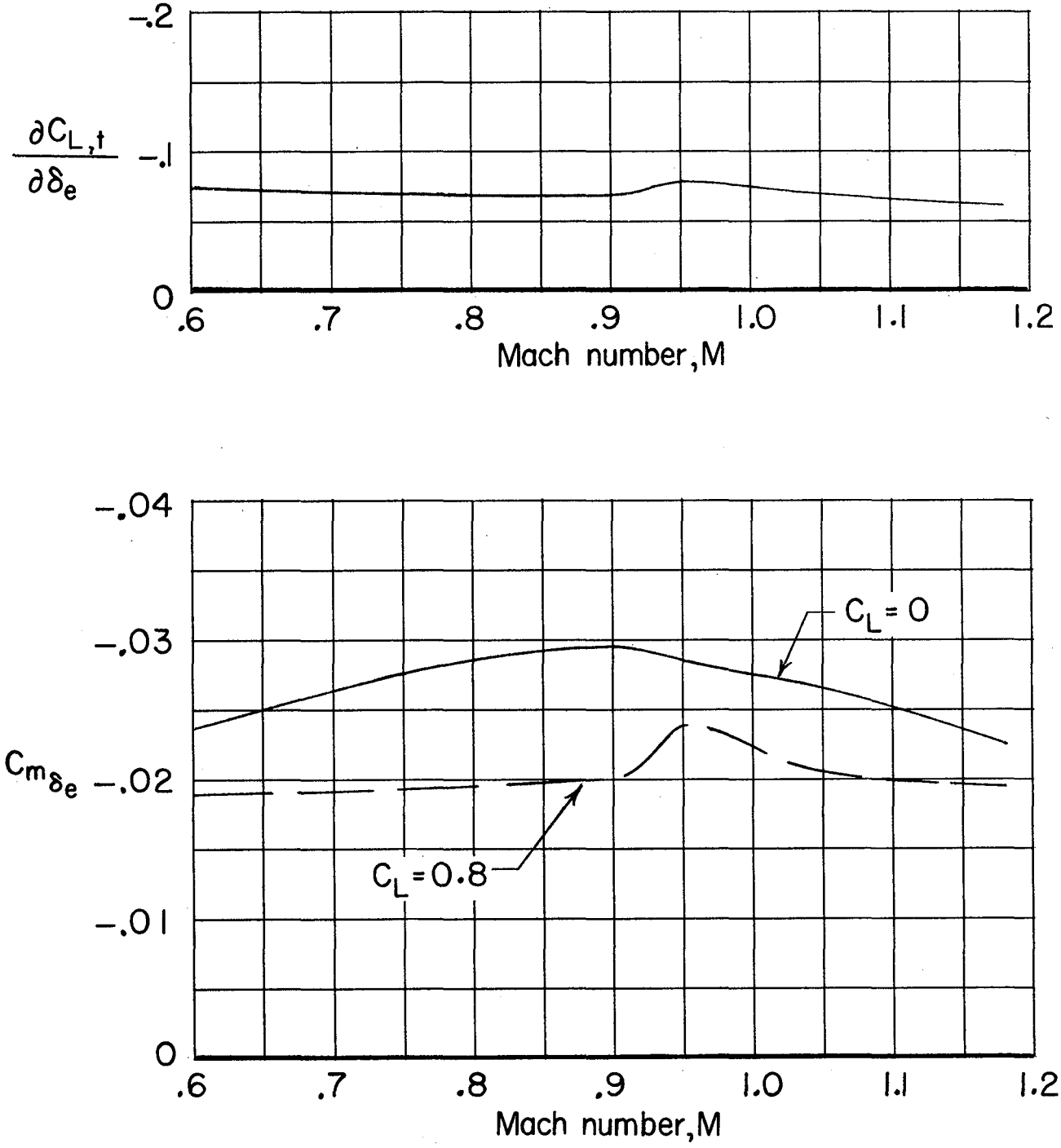

Figure 27.- Variation with Mach number of longitudinal control parameters for complete model at $\beta = 0^\circ$. Surfaces other than horizontal tail undeflected.

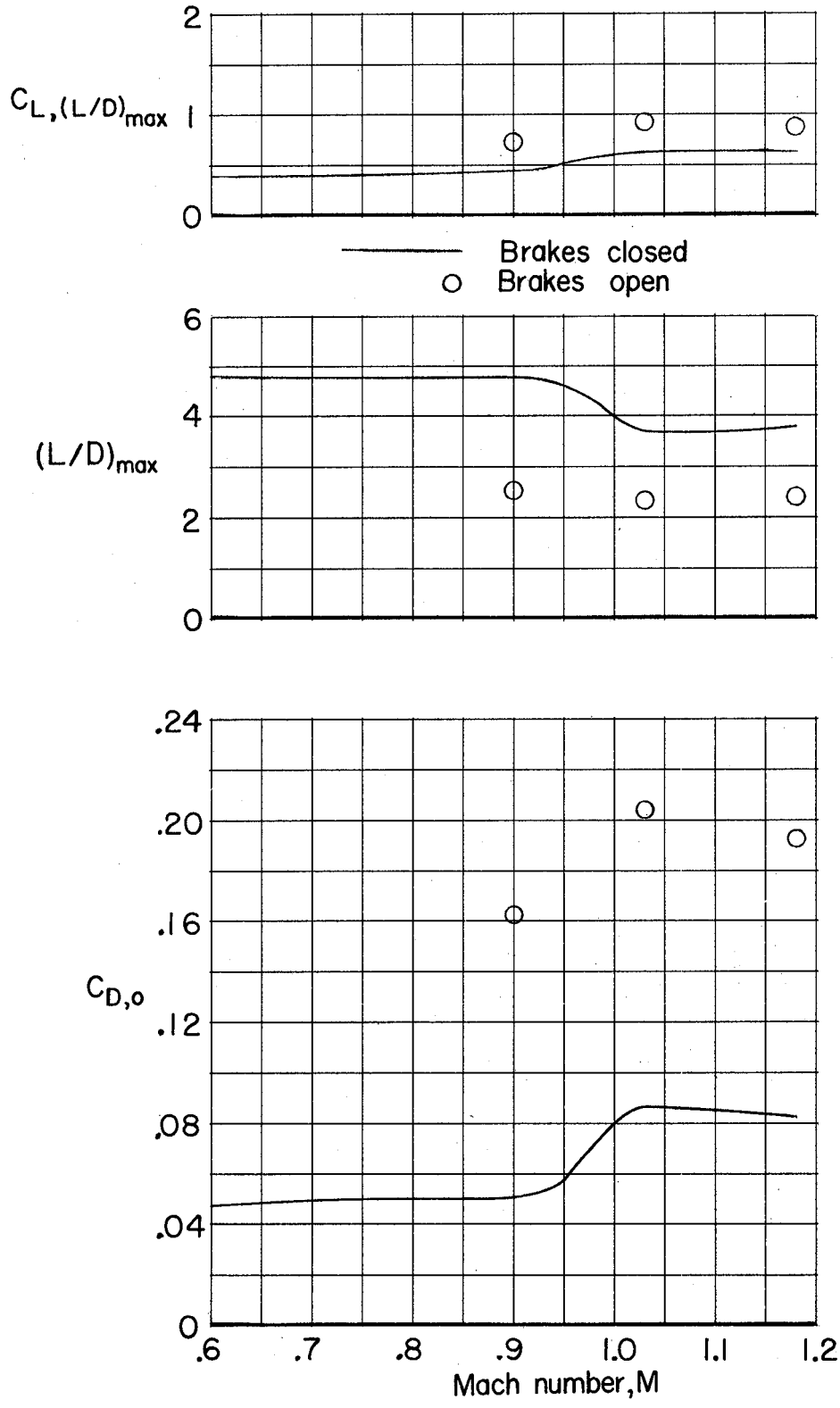

Figure 28.- Variation with Mach number of drag and maximum lift-drag-ratio parameters for complete model at $\beta = 0^{o}$. Surfaces undeflected unless otherwise noted.

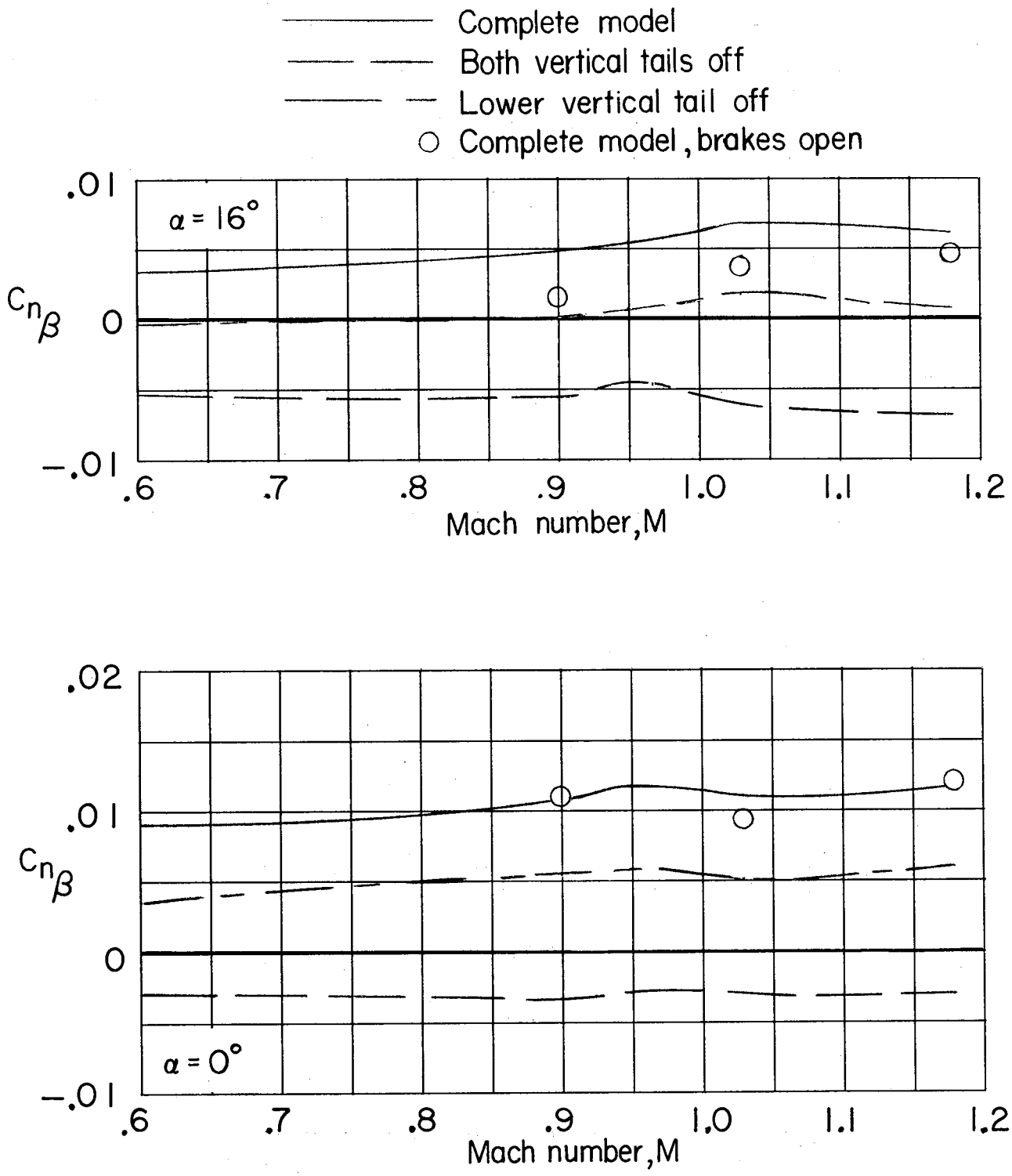

Figure 29.- Variation with Mach number of static directional stability parameter. Surfaces undeflected unless otherwise noted.

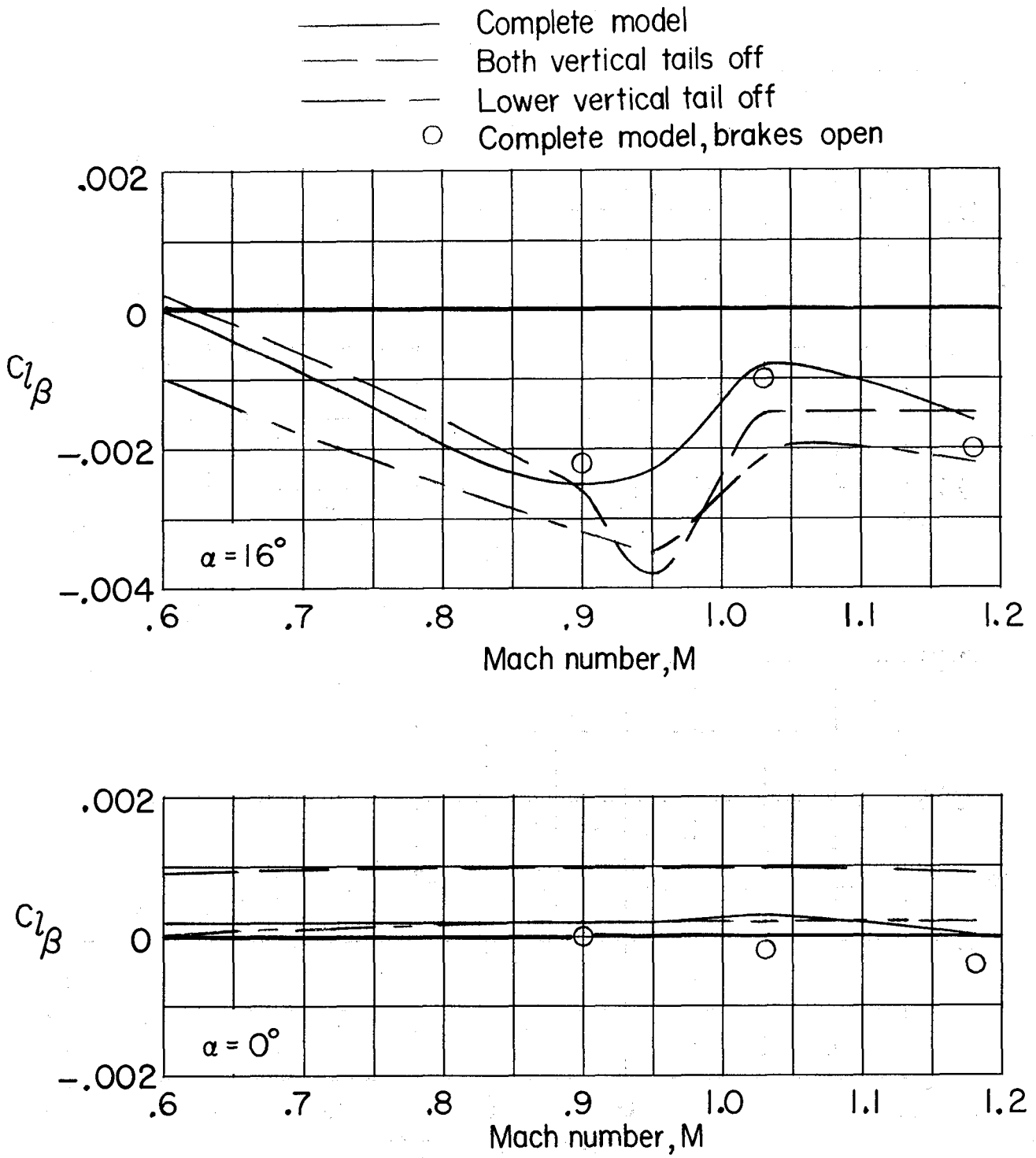

Figure 30.- Variation with Mach number of effective dihedral parameter. Surfaces undeflected unless otherwise noted.

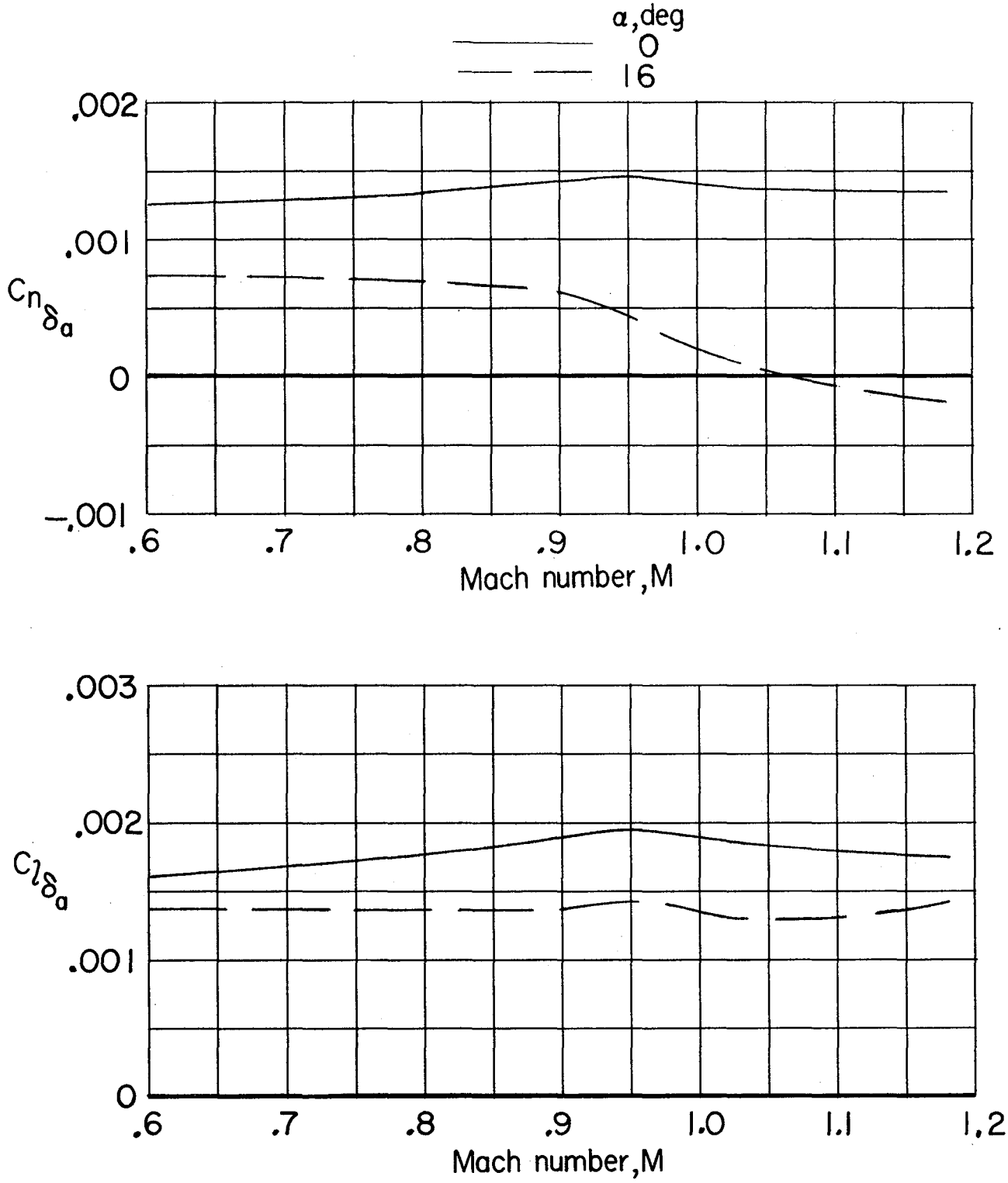

Figure 31.- Variation with Mach number of lateral control parameters for complete model at $\beta = 0^{\circ}$. Surfaces undeflected except for horizontal tail as a roll control.

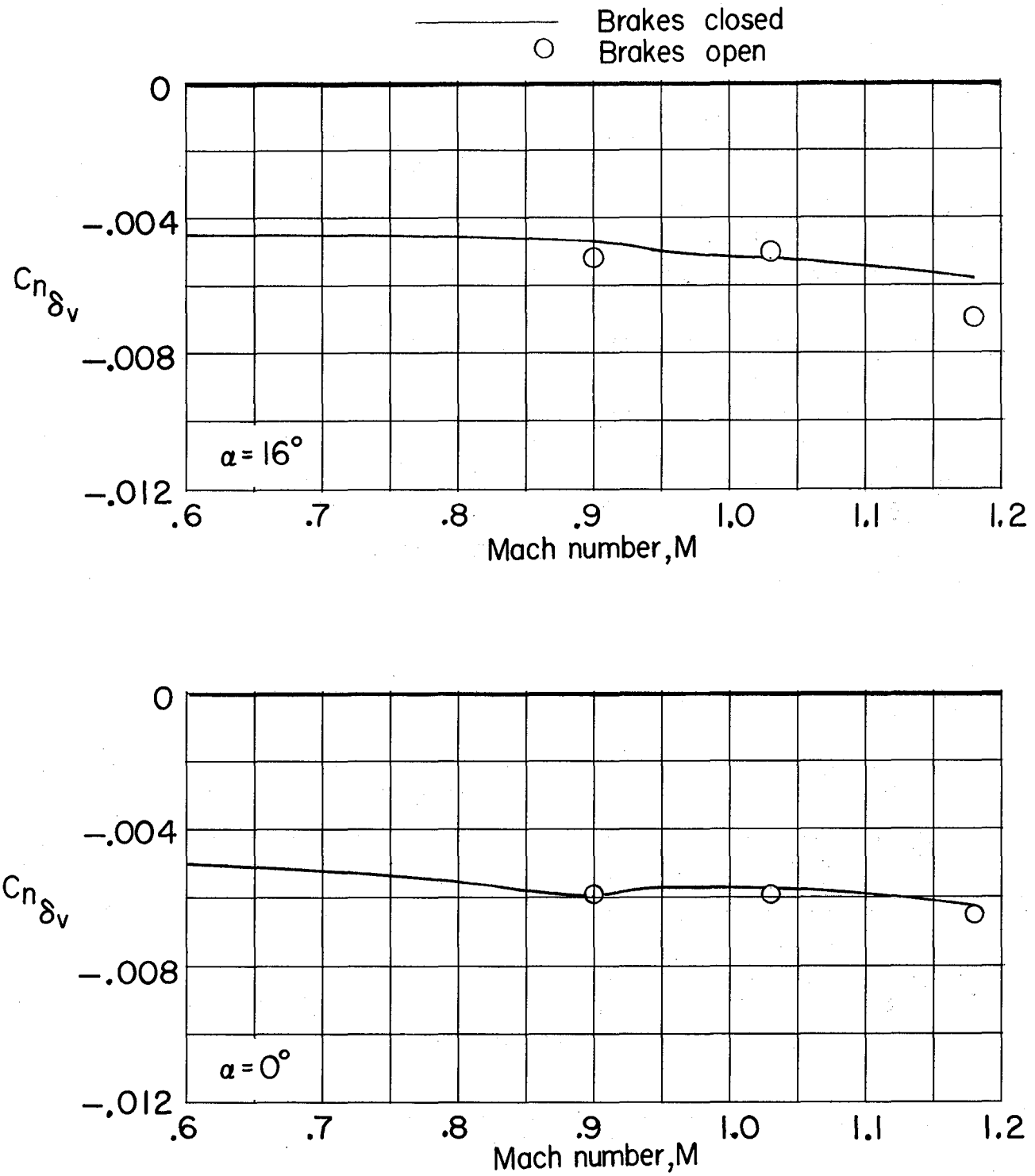

Figure 32.- Variation with Mach number of yawing moment due to vertical-tail deflection for complete model at $\beta = 0^{\circ}$. Horizontal surfaces undeflected.

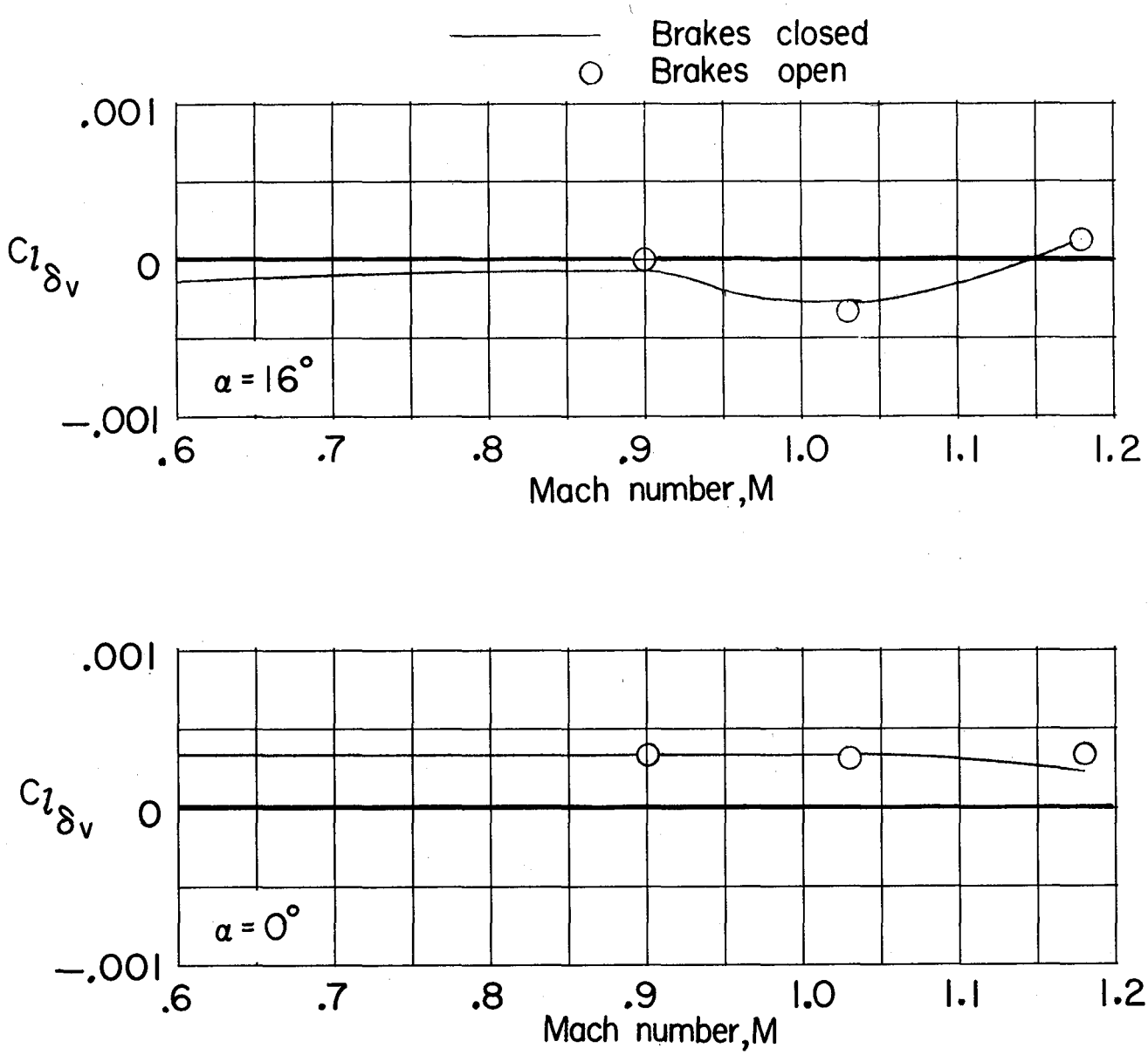

Figure 33.- Variation with Mach number of rolling moment due to vertical-tail deflection for complete model at $\beta = 0^\circ$. Horizontal surfaces undeflected.